

10-

Computationally Efficient Power Allocation and Equalization Schemes for Multi-Carrier Systems

Wladimir Bocquet

submitted to
Kyoto University
in partial fulfillment of the requirements
for the degree of
Doctor in Informatics

Supervisor: Professor Hideaki Sakai

Graduate School of Informatics
Kyoto University

December, 2008

Abstract

This thesis examines the benefit of using computationally efficient power allocation and equalization schemes for multi-carrier systems in terms of spectral and energy efficiency and probability of bit error.

The International Telecommunication Union (ITU) World Radiocommunication Conference in 2007 (WRC-07) adopted new spectrum allocations to the mobile service and new identifications for International Mobile Telecommunications (IMT) systems in a number of the frequency bands. Therefore, the Resolution has clarified what is meant by IMT-Advanced, at least for its initial vision, by referring to Recommendation ITU-R M.1645, which defines the new capabilities of systems Beyond 3G. All the new systems that will compose the new parts of Beyond 3G, would use, without any exception, multi-carrier (MC) technique as a fundamental basis.

In wireless communications systems, spectrum and power are most precious commodities. For many years, researchers in the field have been looking for ways to either conserve or exploit them for their most efficient use. Recent increase in demand for higher transmission rate beyond hundreds of Mbps with limited bandwidth and with limited size of handsets further puts greater importance on researches in that direction. The MC technique has been considered as one of ~~a~~ promising candidates for the solution, where power allocation to each subcarrier and frequency domain equalization using fast Fourier transform (FFT) play central role for full exploitation of the wireless resources.

In this thesis, power allocation algorithms and frequency domain equalizer structures are considered to improve the spectral and/or energy efficiency of MC systems. We propose a novel power allocation scheme for orthogonal frequency division multiplexing (OFDM) scheme using a heuristic evaluation of bit error rate (BER) for a given total transmission power. The proposed method consists of ordering subcarriers in terms of fading impact, grouping them into a certain number of subcarriers, and performing local power adaptation in each subcarrier group based on the mini-

mization of the heuristic BER with a closed form solution. The subcarrier grouping is performed in order to decrease the computational complexity, while the ordering is performed so as to even out the average channel condition of each subcarrier group, which mitigates the performance degradation due to the grouping. Moreover, we propose to extend the power allocation method to various MC systems, such as adaptation modulation OFDM systems, multi-input multi-output (MIMO) OFDM systems, and MIMO coded MC code division multiple access (MC-CDMA) systems.

As for the equalization scheme, we focus on ~~overlap~~^{five 2} frequency domain equalization (FDE) scheme, which does not require any insertion of guard interval (GI) at the expense of higher computational complexity. In order to bring down the computational cost, we propose a systematic design method to adaptively determine the block of the overlap FDE, where the block is defined as a set of symbols at the equalizer output with sufficiently low error rate. Finally, we provide the overall conclusions highlighting our contributions achieved in this thesis and presents some suggestions for future research.

Acknowledgments

At this key time, I would like to express my sincere gratitude to the following people.

My deepest gratitude goes first and foremost to Professor Hideaki Sakai, my supervisor, for his great help, constant encouragement and consistent guidance. He has walked me through all the stages of finishing my doctor course. Without his patient guidance, this thesis would not have been possible.

I am highly grateful to Professor Susumu Yoshida and Professor Toshiyuki Tanaka, as two members of my thesis committee, for their valuable insights and suggestions.

I would like to express my sincere gratitude to Assistant Professor Kazunori Hayashi for his unlimited encouragement, helpful discussions, suggestions, reviews and unconditional support of my research. The discussions with Assistant Professor Hayashi make my research progress continuously. The assistance from him made the three-year period an unique experience.

I would like to thank my sponsor FT Group - Orange Labs Tokyo. This opportunity of combining financial support and available time gave me the possibility to perform research in an unique industrial environment. Jerome Laudouar, President of Orange Labs Tokyo, has played a key role by supporting my application and encouraging me daily. I would like to personally thank two colleagues, Patrice Coupe and Francis Perrin for their unconditional support during all the doctor course period.

I would also like to thank the Broadband Access and Usage team, Asako Nakano, Hidenari Nozaki, Kenneth Wu, Kiyoshi Egawa, Nicolas Delacourcelle, Radim Zemek, Thomas Derham, Yaping Gong, for their real friendship and fresh vision about work and life.

I would like to acknowledge Professor Shinsuke Hara from Osaka City University for his help and discussions in my research.

Finally, I wish to acknowledge all my beloved family who has supported me throughout my PhD study. There is no way I would be where I am today without

iv

the immeasurable love and support of my family. My biggest thanks go to my wife and daughter, who are a constant source of support, help, and encouragement.

Contents

Abstract	i
Acknowledgments	iii
Abbreviations	xiii
1 Introduction	1
1.1 Background	1
1.2 Position of the Work	4
1.3 Outline of the Thesis	5
2 Background Material	7
2.1 Introduction to MC Systems	7
2.2 Signal Modeling of MC Based Systems	12
2.2.1 Signal Modeling for OFDM	13
2.2.2 Signal Modeling for MIMO-OFDM	15
2.2.3 Signal Modeling for MIMO MC-CDMA	17
2.2.4 Signal Modeling for SC-FDE	20
2.3 Heuristic Expression of BER	23
2.3.1 Approximated BER Expression	24
2.3.2 Convolutional Coded Case	25
2.3.3 Turbo Coded Case	27
3 Proposed Power Allocation Scheme for OFDM Systems	29
3.1 Introduction	30
3.2 Proposed Power Allocation Scheme	31

3.2.1	Subcarrier Ordering and Grouping	31
3.2.2	Closed Form Solution of Proposed Power Allocation	33
3.3	Optimal Power Allocation	34
3.4	Computational Complexity	35
3.5	Numerical Experimentation	37
3.5.1	Uncoded OFDM	39
3.5.2	Convolutional Coded OFDM	40
3.5.3	Turbo Coded OFDM	45
3.6	Conclusion	48
4	Extension of Proposed Power Allocation to Various MC Systems	51
4.1	Introduction	52
4.2	Proposed Power Allocation Scheme for Adaptive Modulation OFDM Systems	53
4.2.1	Subcarrier Adaptive Modulation	53
4.2.2	State-of-Art of Subcarrier Adaptive Modulation	54
4.2.3	Proposed Power Allocation Combined with Adaptive Modulation	55
4.3	Power Allocation Scheme for MIMO OFDM Systems	57
4.3.1	Combined Spatial and Frequency Domains Power Allocation	58
4.3.2	Spatial Domain Power Allocation Scheme	59
4.3.3	Frequency Domain Power Allocation Scheme	60
4.4	Power Allocation Scheme for MIMO MC-CDMA Systems	60
4.4.1	State-of-Art of MIMO MC-CDMA Systems	60
4.4.2	Proposed Power Allocation Scheme for MIMO MC-CDMA Systems	61
4.5	Numerical Experimentation	62
4.5.1	Power Allocation with Adaptive Modulation	62
4.5.2	Power Allocation Scheme for MIMO OFDM Systems	65
4.5.3	Power Allocation Scheme for MIMO MC-CDMA Systems	72
4.5.4	Impact of the Limited Feedback	77
4.6	Conclusion	80

CONTENTS	vii
5 Systematic Design of Overlap FDE Systems	83
5.1 Introduction	83
5.2 System Description	85
5.2.1 Signal Modeling and Channel Representation	85
5.2.2 SC Overlap FDE Receiver and Equalization	87
5.2.3 SINR Analysis of FDE Output	88
5.3 Proposed Systematic Design of the SC Overlap FDE	90
5.4 Numerical Simulation	93
5.4.1 Uncoded System	95
5.4.2 Coded System	97
5.5 Conclusion	97
6 Conclusions and Further Research	101
References	103
Publications	113

List of Figures

1.1 Main legacy radio access technologies	2
2.1 Beyond 3G and 4G definition	8
2.2 Example of multipath channel	9
2.3 Orthogonal multi-carrier principle	10
2.4 Example of frequency response	11
2.5 Example of impulse response	11
2.6 Guard interval principle	14
2.7 MIMO-OFDM transmitter scheme	15
2.8 MIMO-OFDM receiver scheme	16
2.9 MC-CDMA transmitter scheme	18
2.10 MC-CDMA receiver scheme	18
2.11 SC FDE transmitter scheme	21
2.12 SC FDE receiver scheme	22
2.13 BER for different modulations with channel coding $R = 1/2$ and $R = 3/4$ (solid lines denote exact BER and dashed lines are fitting curves to the exact BER)	26
2.14 BER for different frame size (i.e. number of OFDM symbol per frame) with channel coding $R = 1/2$ and QPSK modulation	26
3.1 Principle of subcarrier group selection	33
3.2 Complexity evaluation for $N = 64$ and $0 < N_s < 64$	37
3.3 BER performance for uncoded OFDM with QPSK modulation	39
3.4 BER performance for uncoded OFDM with 16-QAM	40

LIST OF FIGURES

3.5 BER performance for uncoded OFDM with 64-QAM	41
3.6 BER performance of coded OFDM with $R=1/2$ for QPSK and 64-QAM modulations	42
3.7 BER performance of coded OFDM with $R=3/4$ for QPSK and 64-QAM modulations	42
3.8 BER performance for coded OFDM with 16-QAM and $R = 1/2$	43
3.9 BER performance for coded OFDM with 16-QAM and $R = 3/4$	43
3.10 BER performance for coded OFDM with QPSK modulation using optimized and non-optimized a_m and b_m	45
3.11 BER performance for $R = 1/3$ and QPSK modulation	46
3.12 BER performance for $R = 1/2$ and QPSK modulation	46
3.13 BER performance for $R = 3/4$ and QPSK modulation	47
3.14 BER performance for 16-QAM modulation	48
4.1 BER performance for uncoded and coded OFDM with $\bar{B} = 3$	64
4.2 BER performance for uncoded and coded OFDM with $\bar{B} = 5$	65
4.3 BER performance for QPSK modulation and coding rate $R=1$	66
4.4 BER performance for 16-QAM modulation and coding rate $R=1$. .	66
4.5 BER performance for 64-QAM modulation and coding rate $R=1$. .	68
4.6 Layout of the room	70
4.7 BER performance for $N_t = N_r = 2$, $SF_f = SF_t = 4$ and $R = 1/2$. .	74
4.8 BER performance for $N_t = N_r = 4$, $SF_f = SF_t = 4$ and $R = 1/2$. .	75
4.9 BER performance for $N_t = N_r = 8$, $SF_f = SF_t = 4$ and $R = 1/2$. .	76
4.10 Required SNR at $\text{BER}=10^{-4}$ for $N_t = N_r = 4$, $SF_f = SF_t = 4$ and $R = 3/4$	76
4.11 BER performance for $N_t = N_r = 2$, $SF_f = SF_t = 4$ and QPSK modulation	77
4.12 BER performance for $N_t = N_r = 4$, $SF_f = SF_t = 4$ and QPSK modulation	78
4.13 BER performance for $N_t = N_r = 4$, 14 active users, and 16-QAM modulation	78

LIST OF FIGURES

xi

4.14 BER performance for $N_t = N_r = 4$, 14 active users, and 64-QAM modulation	79
4.15 BER performance for $N_t = N_r = 2$, 12 active users QPSK modulation and $R=1/3$	80
4.16 BER performance for $N_t = N_r = 2$, 12 active users 64-QAM modulation and $R=1/2$	81
5.1 Basic procedure of overlap FDE	88
5.2 Examples of SINR and interference power for the window size $N = 128$	91
5.3 M_{\inf} and M_{\sup} at the end of iterative process	93
5.4 BER performance for QPSK modulation, $R = 1$ and $N = 64$	95
5.5 BER performance for 16-QAM modulation, $R = 1$ and $N = 64$	96
5.6 BER performance for 64-QAM modulation, $R = 1$ and $N = 64$	96
5.7 Impact of SINR range on block size, $R = 1$ and $N = 64$	97
5.8 BER performance for QPSK modulation, $R = 1/2$ and $N = 64$	98
5.9 BER performance for 16-QAM modulation, $R = 1/2$ and $N = 64$	98
5.10 BER performance for 64-QAM modulation, $R = 1/2$ and $N = 64$	99
5.11 Impact of SINR range on block size, $R = 1/2$ and $N = 64$	99

Abbreviations

2G	Second Generation
3G	Third Generation
3GPP	Third Generation Partnership Program
4G	Fourth Generation
AMC	Adaptive Modulation and Coding
AWGN	Additive White Gaussian Noise
B3G	Beyond Third Generation
BER	Bit Error Rate
BS	Base Station
CDF	Cumulative Distribution Function
CDMA	Code Division Multiple Access
CP	Cyclic Prefix
CSI	Channel State Information
DAB	Digital Audio Broadcasting
DL	DownLink
DMB	Digital Multimedia Broadcasting
DS	Direct Sequence
DSL	Digital Subscriber Line
DSP	Digital Signal Processing
DVB	Digital Video Broadcasting
FDE	Frequency Domain Equalization
FFT	Fast Fourier Transform
FIR	Finite Impulse Response

GI	Guard Interval
HARQ	Hybrid Automatic Repeat Request
IBI	Inter-Block Interference
ICI	Inter-Carrier Interference
iid	Independent and Identically Distributed
IFFT	Inverse Fast Fourier Transform
IMT	International Mobile Telecommunication
ISI	Inter-Symbol Interference
ITU	International Telecommunication Union
LAN	Local Area Network
LDPC	Low Density Parity Check
LTE	Long-Term Evolution
MAC	Media Access Control ^{layer}
MAN	Metropolitan Area Network
MBWA	Mobile Broadband Wireless Access
MC-CDMA	Multi-Carrier Code Division Multiple Access
MIMO	Multi-Input Multi-Output
MLD	Maximum Likelihood Detection
MMSE	Minimum Mean-Square-Error
MT	Mobile Terminal
NLOS	Non Line Of Sight
OFDM	Orthogonal Frequency Division Multiplexing
OFDMA	Orthogonal Frequency Division Multiple Access
PHY	PHYSical ^{layer}
QAM	Quadrature Amplitude Modulation
QPSK	Quadrature Phase Shift Keying
RF	Radio Frequnecy
SC	Single Carrier
SC-FDMA	Single Carrier Frequency Division Multiple Access
SDM	Space Division Multiplexing
SINR	Signal-to-Interference-plus-Noise Ratio

SISO	Single Input Single Output
SNR	Signal-to-Noise Ratio
UL	UpLink
WCDMA	Wideband CDMA
WiMAX	Worldwide interoperability for Microwave Access
WLAN	Wireless Local Area Network
WRC	World Radiocommunication Conference
ZF	Zero Forcing
ZP	Zero Padding

Chapter 1

Introduction

1.1 Background

A radical change of vision recently appeared for wireless communications. Up to the end of the 90's, only voice calls were the main wireless applications. Since the beginning of this new century, data oriented applications through wireless transmissions have become more and more popular. The success of i-mode, a famous cellular service for data transfer proposed by NTT DoCoMo and the worldwide success of the wireless local area network (WLAN), created a huge demand for data transfer and a radical change of mentality in the usage of wireless devices. Before proceeding to an era of International Mobile Telecommunications - Advanced (IMT-Advanced), technical or operational aspects of broadband cellular systems will be investigated through implementation of the third generation (3G) Long-Term Evolution (LTE) or Worldwide Interoperability for Microwave Access (WiMAX), which are regarded as the ultimate applications of future development of International Mobile Telecommunications - 2000 (IMT-2000). Fig. 1.1 shows several legacy radio access technologies and their specificities [1]-[3]. In the International Telecommunication Union Radio-communication Sector (ITU-R) work [1] for IMT-Advanced, it has been recognized that in order to reach the full performance set of IMT-Advanced requirements, it is likely that a new radio interface will be needed. Frequency bandwidth of up to 100 MHz is anticipated, which would in most cases requires new allocations of spectrum (addressed in World Radiocommunication Conference in 2007 (WRC-07))

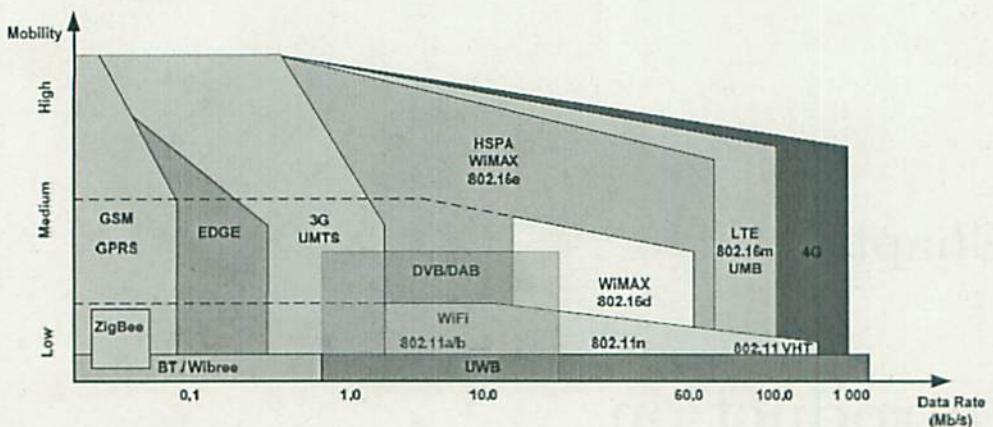


Figure 1.1: Main legacy radio access technologies

ies of

[2]-[3]. The requirement of having to obtain additional spectrum triggered an initiative within the 3G partnership project (3GPP) to define a radio interface that was based on the latest developments within the different fourth generation (4G) research activities, but with a bandwidth that would allow for deployments also in spectrum already identified and/or used for the second generation (2G) and the 3G systems. The overall target of the 3G LTE is to arrive at an evolved radio access technology that can provide service performance at reduced cost compared to current radio access technologies.

The 3G LTE radio access technology [4] is based on Multi-Carrier (MC) transmission in the downlink (DL) and single carrier frequency division multiple access (SC-FDMA) in the uplink (UL) providing peak data rates beyond 300 Mbps (DL) and 80 Mbps (UL). The 3G LTE makes extensive use of advanced multi-antenna transmission technologies, including both beam-forming for improved coverage and capacity and spatial multiplexing for higher data rates. Furthermore, the 3G LTE provides a very high flexibility in terms of system bandwidth, allowing for deployment in spectrum allocations as small as 1.25 MHz up to at least 20 MHz. The high bandwidth flexibility e.g. provides smooth migration from the current 3G system to the 3G LTE system. With a support of data rates beyond 300 Mbps, the current specification of the 3G LTE already today exceeds the anticipated requirements for IMT-Advanced wide area coverage bit rates. And by utilizing the inherent band-

width flexibility, the 3G LTE specification can in later releases be complemented with even wider bandwidths and corresponding even higher bit rates in order to fully comply also with the indoor hot-spot component of IMT-Advanced (1 Gbps). Another important aspect of the ITU-R recommendation for "Systems Beyond IMT-2000" is that it identifies the need for a packet-based core network that is common for the 2G, the 3G, and the 4G radio access systems.

The IEEE 802.16 Working Group [5] on Broadband Wireless Access Standards (established by IEEE Standards Board in 1999), aims to prepare formal specifications for the global deployment of broadband Wireless Metropolitan Area Networks (MANs). The Working Group is a unit of the IEEE 802 LAN/MAN Standards Committee. A related future technology Mobile Broadband Wireless Access (MBWA) is under development in IEEE 802.20. Although the IEEE 802.16 family of standards is officially called Wireless MAN, it has been dubbed "WiMAX" by an industry group called the WiMAX Forum. The IEEE 802.16 standard essentially standardizes two aspects of the air interface, the physical layer (PHY) and the Media Access Control layer (MAC). The IEEE 802.16e uses scalable Orthogonal Frequency Division Multiple Access (OFDMA) to carry data, supporting channel bandwidths of between 1.25 MHz and 20 MHz, with up to 2048 subcarriers. It supports adaptive modulation and coding. Other PHY features include support for Multi-Input Multi-Output (MIMO) system in order to provide good non-line-of-sight (NLOS) characteristics (or higher bandwidth) and Hybrid Automatic Repeat Request (HARQ) for good error correction performance.

Both WiMAX and 3G LTE use Orthogonal Frequency Division Multiplexing (OFDM) technique as a fundamental basis. This is because the MC communications have become attractive for providing multimedia services over multipath channels due to the flexibility in modulation scheme and multiple access with reasonable complexity. OFDM signal is composed by a large number of closely-spaced orthogonal subcarriers, over which conventional modulation schemes are adopted. Since 3G LTE, IEEE 802.16 and the future evolutions are designed to work on a wide bandwidth, the channel is therefore experience severe frequency-selective fading. By splitting a signal into several narrowband channels at different frequencies and using those slowly-modulated narrowband signals instead of one wideband sig-

nal with rapid modulation, OFDM based transmission is able to cope with severe channel conditions, contributing to spectral diversity gain. However, the demand for transmission rate of wireless communications systems has been increasing in an exponential manner, while the radio spectrum available for wireless systems is extremely scarce and the limitation on the size of mobile handsets restricts available power for communications. This motivates us to consider the key issues of MC communications systems, in other words, power allocation scheme and frequency domain equalization (FDE), in order to achieve further improvement in performance.

1.2 Position of the Work

The central problem, which has been processed in this industrial Doctor Course, is to define the way to efficiently allocate power to each subcarrier and perform equalization in frequency domain to improve the spectral and/or energy efficiency of MC systems. The water-filling approach [37] is a famous technique for the power allocation of MC systems. This approach is attractive since it can achieve optimum allocation in terms of system capacity. However, in practice, the capacity cannot be achieved due to the limitation of available modulation levels and/or coding rates. On the other hand, Chow's algorithm [36] is another typical solution of the power allocation, where the criterion is a minimization of error rate. However, the method requires complex iterative process in order to achieve optimum allocation because of the complex cost function. In this thesis, attaching greater importance to implementation issue, we will take latter approach for the performance criterion, but with much simpler cost function due to the employment ^{the} ~~considering~~ ^{use} of an heuristic expression of the error rate. Moreover, we propose a specific subcarrier ordering and grouping in order to further decrease the computational complexity required by the power allocation. Then, we will extend the study to different MC systems including multiple antennas, adaptive modulation, and MC-CDMA systems. As for the equalization scheme, in order to improve the spectral efficiency, we focus on ^{an} overlap FDE scheme [76]-[78], which does not require any insertion of guard interval (GI) at the expense of higher computational complexity. Based on the analysis of Signal-to-Interference-plus-Noise Ratio (SINR) of the equalizer output, we propose a systematic design

method to adaptively determine the block of the overlap FDE, where the block is defined as a set of symbols at the equalizer output with sufficiently low error rate, in order to reduce the computational cost as well.

1.3 Outline of the Thesis

This thesis consists of six chapters. In this section, we provide a chapter by chapter overview of the thesis and summarize the main contributions that this research achieved.

In **Chapter 2**, we gather together most of the background material needed for the rest of the thesis. It includes a description of the OFDM scheme, the SC-FDE, the MC-CDMA systems and the extension to multiple antennas. Furthermore, we summarize a simple and heuristic expression of an approximated BER and then show the validity of the expression.

In **Chapter 3**, we propose a framework to evaluate algorithm to allocate power for uncoded and coded OFDM transmission with fixed modulation. The proposed scheme consists of adapting the transmit power for OFDM transmission in the frequency domain using the heuristic expression of the BER for each subcarrier. The proposed method consists of ordering in terms of fading impact, grouping a certain number of subcarriers and performing local power adaptation in each subcarrier group. Grouping and local power adaptation allow us to reduce the computational complexity of the proposed power distribution scheme, while avoiding the performance degradation due to the suboptimum power adaptation as much as possible.

In **Chapter 4**, we propose to extend the power allocation scheme developed in the previous Chapter to different MC systems. First, we apply the proposed power allocation scheme to the OFDM scheme with adaptive modulation. Then, we propose several power allocation schemes for MIMO OFDM transmission based on minimization of the approximated BER expression and we evaluate the different solutions via field trial experimentations. The methods illustrated in this Chapter serve to allocate power among the different transmit antennas and the different subcarriers which compose the MIMO OFDM transmitted signal. Frequency domain power allocation, spatial domain power allocation and combined spatial and

frequency power allocation are evaluated. Finally, we propose to extend the power allocation scheme for MIMO MC-CDMA systems with two dimensional spreading where the optimum power allocation for different transmit antennas and different active users is obtained based on the minimization of the approximated^P average BER expression.

In **Chapter 5**, we propose a systematic design method of overlap FDE for SC transmission without a GI. Based on the analysis of the SINR of the equalizer output for each symbol, we adaptively determine the block of the overlap FDE, where the block is defined as a set of symbols at the equalizer output with sufficiently low error rate, for a certain fixed sliding window size, which corresponds to a fast Fourier transform (FFT) window size. The proposed method takes advantage of the fact that the utility part of the equalized signal is localized around the center of the FFT window. In addition, we also propose to adjust the block size in order to control the computational complexity of the equalization per processed sample associating with the average BER of the system.

Finally, **Chapter 6** provides the overall conclusions highlighting our contributions achieved in this thesis and presents some suggestions for future research.

Chapter 2

Background Material

In this chapter, we introduce the background material, including a simple description of the basic OFDM transmission and the different derivative access schemes such as MC-CDMA and SC-FDE. In addition, we develop in this chapter the basic description of the multiple antenna schemes. Finally, using ~~the~~ mathematical tools, we propose a simple and heuristic expression of the BER. Then, we show the range of validity of the heuristic expression of the BER.

2.1 Introduction to MC Systems

The 3G mobile communication systems are already in deployment in several countries and this has enabled whole new ways to communicate, access information, conduct business and be entertained, liberating users from slow, cumbersome equipment and immovable points of access. In a way the 3G has been the right bridge for mobile telephony and the internet. 3G services enable users to make video calls to the office and surf the internet simultaneously, or play interactive games wherever they may be. Second and third generation systems like the wideband CDMA (WCDMA) can provide nominal data rates of about 384 kbps. While the 3G and the 3G evolution are just transforming itself into a reality from an engineers' dream, research efforts are already on to look into systems that can provide even higher data rates and seamless connectivity. Such systems are categorized under the 4G and are predicted to provide packet data transmission rates of 100 Mbps in outdoor macro-

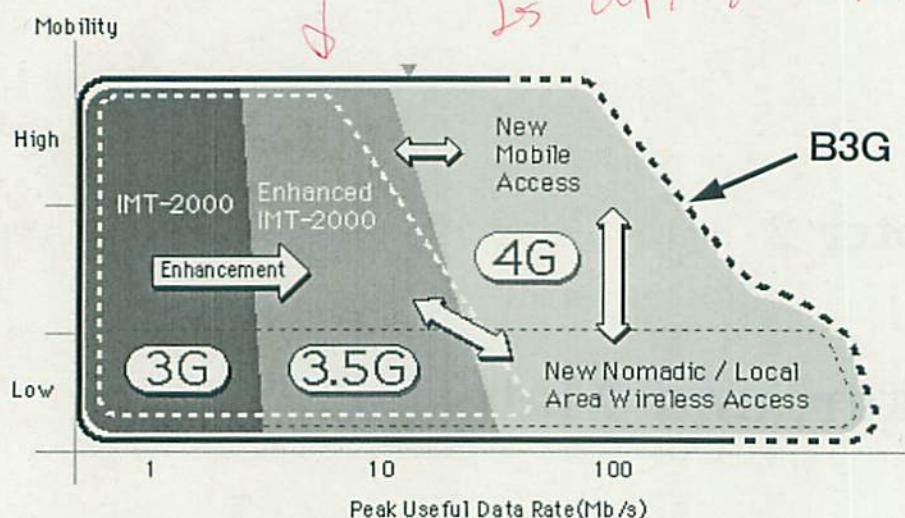


Figure 2.1: Beyond 3G and 4G definition

cellular environments and up to 1 Gbps in indoor and micro-cellular environments as defined in [1]-[2] and shown in Fig. 2.1.

While wideband systems could be a natural choice to provide high data rates, service providers have to pay dearly for the spectrum necessary. Hence, spectrum efficiency is always a factor on the choice of any wireless technology. Very wideband systems usually require complex receivers as the channel is frequency selective due to the presence of large number of resolvable multipaths. OFDM based transmission has recently gained a lot of attention and is a potential candidate for the 4G systems. OFDM is very efficient in spectrum usage and is very effective in a frequency selective channel. By taking advantage of recent improvements in Digital Signal Processing (DSP) and Radio Frequency (RF) technologies, OFDM can provide higher data rates and is a very good choice for service providers to compete with wire-line carriers. A variation of OFDM which allows multiple accesses is MC-CDMA which is essentially an OFDM technique where the individual data symbols are spread using a spreading code in the time and frequency domains.

In order to consider realistic radio propagation channels, studying the performance of the algorithms in additive white Gaussian noise (AWGN) alone is not sufficient. We must also include the effects of multipath propagation. To do so we

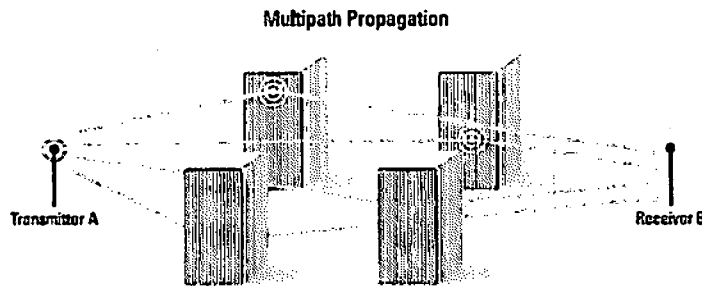


Figure 2.2: Example of multipath channel

must understand the effect of multipath on the received signal and how to emulate these effects in base band. The received signal is composed of several time delayed versions of the transmitted signal as illustrated in Fig. 2.2. These signals add at the receiver with different phases as a result of different propagation delays. It has been shown that the envelope of this follows a Rayleigh distribution [6]. Additionally the rate at which the signal varies is inversely proportional to the Doppler spread of the channel. A simple way to model the fading effect is the quasi-static assumption wherein the channel is assumed to be constant over a block period of time.

Mobile radio channels introduce severe multipath propagation due to multiple scattering from objects in the vicinity of the mobile. This scattering introduces rapid fluctuation of the received signal envelope as well as phase variations. Measurements and theoretical analysis have shown that the envelope of the signal received is typically Rayleigh distributed. Also the motion of the mobile unit introduces a Doppler shift which causes a broadening of the signal spectrum [6]. The multipath channel can also be frequency selective in which case the fading envelope of the received signal at one frequency might not be correlated with the envelope at another frequency. This is due to the fact that the symbol duration might be less than (or on the order of) the maximum delay spread. As a result, the received signal consists of overlapping versions of the transmitted symbols or Inter-Symbol Interference (ISI). Also, if we consider a cellular environment or military applications, there is the effect of co-channel interference due to the frequency reuse of the available spectrum. In addition to this, the received signal is subjected to large scale fading also called

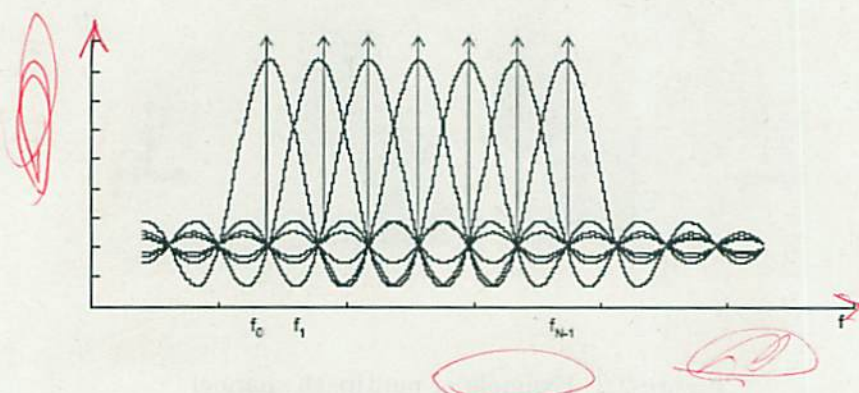


Figure 2.3: Orthogonal multi-carrier principle

shadow fading due to the propagation effects. Given these adverse mobile environments it is necessary to look for intelligent transmission and reception techniques. In a conventional serial data transmission, the symbols are transmitted sequentially with the frequency spectrum of each transmitted symbol occupying the entire bandwidth available. The delay spread due to the channel dictates the symbol duration or alternatively the data rate that can be achieved to prevent the effects of the ISI. The idea behind multicarrier modulation is that it is a technique where multiple low data rate carriers are combined by a transmitter to form a composite high data rate transmission. In a parallel transmission system several sequential streams of data are transmitted simultaneously. In a classical parallel transmission system, the available spectrum is split into several non-overlapping frequency sub channels. The individual data elements are modulated into these sub channels and are thus frequency multiplexed. The main advantage is that the parallel transmission increases the symbol time by modulating the symbols into narrow sub channels, as shown in Fig. 2.3. This increase in symbol time makes it more robust to the channel delay spread effects. The Figs 2.4 and 2.5 show the channel frequency response for multi carrier system and the response in the time domain.

Such parallel data transmission techniques were in vogue even during the early 1960's. To implement the multiple carrier scheme using a bank of parallel modulators would not be very efficient in analog hardware. However, in the digital domain, MC modulation can be done efficiently with currently available DSP hardware and

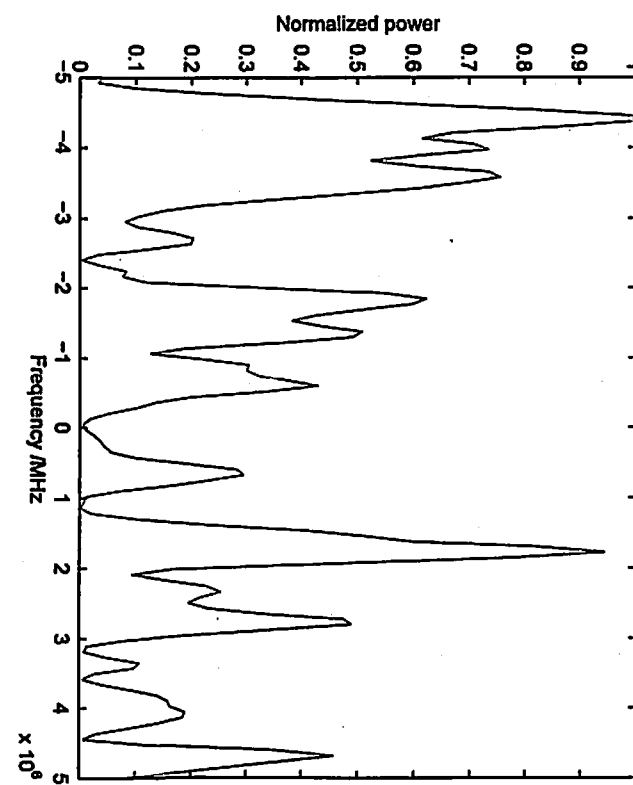


Figure 2.4: Example of frequency response

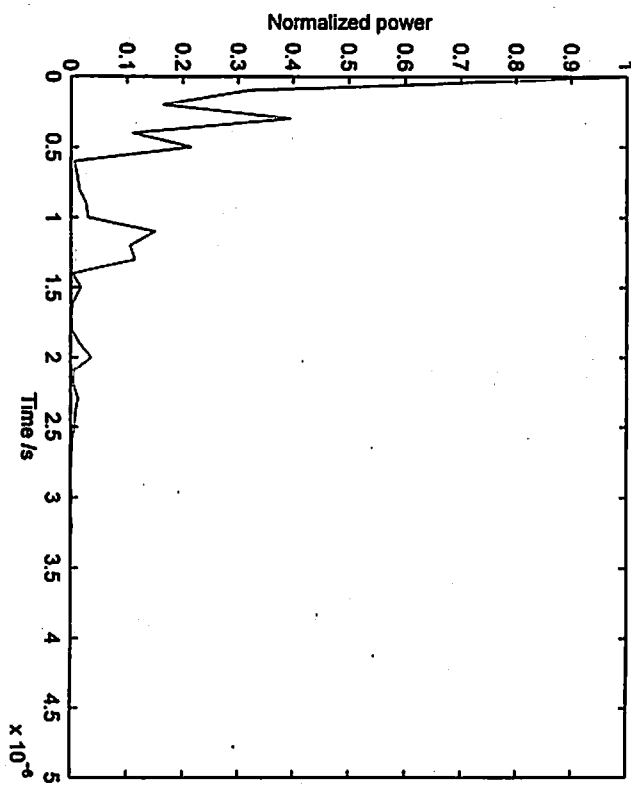


Figure 2.5: Example of impulse response

software. Hence MC modulation is a very attractive technique for commercial applications as high power Digital Signal Processors are available for affordable prices in recent times.

2.2 Signal Modeling of MC Based Systems

Recent advances in multimedia mobile communications have sparked much research in techniques that can deliver very high data rates. Data rate is really what broadband is all about. Traditional single carrier (SC) modulation techniques can achieve only limited data rates due to the restrictions imposed by the multipath channel and the receiver complexity. MC techniques can provide high data rates at reasonable receiver complexities and are increasingly becoming popular in audio/video broadcasting, mobile local area networks and future generation wideband cellular systems.

OFDM has been proven as an efficient MC modulation technique to transmit at high data rate over the hostile multipath wireless channel [7]. The MC modulation divides the frequency-selective wideband channel into multiple non-interfering narrowband, each modulated on a separate subcarrier. Equivalently, in the time domain, the high data rate stream is converted into multiple lower rate streams that are sent in parallel. OFDM is an efficient version of MC modulation because it utilizes the available spectrum more efficiently by allowing subcarriers to overlap without causing Inter-Carrier Interference (ICI). This is due to the orthogonality of its subcarriers. Finally, OFDM provides an efficient implementation through inverse FFT (IFFT) and FFT at the transmitter and receiver respectively. The first OFDM wireless system was the European digital audio broadcasting (DAB). Later, it was used in the European digital video broadcasting (DVB)-T (Terrestrial), DVB-H (Handheld) and digital multimedia broadcasting (DMB). Today, many of the high data rate wireless standards have adopted OFDM as the preferred technology of choice, including Wireless LAN (i.e. IEEE 802.11a and 802.11n in the U.S., and High Performance LAN (HIPERLAN)/2 in Europe), Broadband Wireless Access Networks (i.e. IEEE 802.16-2004 and 802.16e-2005), which are adopted by Fixed and Mobile WiMAX respectively and 3G LTE DL system.

Recent studies by researchers have combined the principle of CDMA with OFDM which allows one to use the available spectrum in an efficient way and retain the many advantages of a CDMA system. If the number and spacing between the subcarriers are chosen appropriately, it is unlikely that all the subcarriers will be in deep fade and thus provides frequency diversity. This combination of OFDM-CDMA is a useful technique for 4G systems where we need variable data rates as well as provide reliable communication systems. In [8] this form of OFDM-CDMA or multi-carrier CDMA (MC-CDMA) was first proposed and the performance of MMSE detection was studied for MC-CDMA. [9] also proposed the same idea at the same time and analyzed the performance of maximum likelihood detection (MLD) for MC-CDMA systems. A MCCDMA system basically applies the OFDM type of transmission to a direct sequence (DS) - CDMA signal. In conventional DS-CDMA each user symbol is transmitted in the form of sequential chips, each of which is narrow in time and hence wide in bandwidth. In contrast to this, in MC-CDMA due to the FFT transform along with OFDM the chips are longer in time duration and hence narrow in bandwidth. The multiple chips for a data symbol are not sequential but instead transmitted in parallel over many subcarriers. An interesting feature of MC-CDMA is that the modulation and demodulation can be easily implemented using simple FFT and IFFT operators. Although OFDM is robust to frequency selective fading, it has severe disadvantages in subcarrier synchronization and sensitivity to frequency offset estimation. The other main issue with respect to OFDM is the presence of a large number of subcarriers which exhibits a non-constant nature in its envelope. The combining of OFDM and CDMA has one major advantage though. It can lower the symbol rate in each subcarrier compared to OFDM so that longer symbol duration makes it easier to synchronize [10].

2.2.1 Signal Modeling for OFDM

When there is sufficient bandwidth available for data transmission, a classical parallel system can be used where the entire bandwidth available is split into narrow sub channels and data can be modulated into each of these sub channels. In such a system there is usually sufficient guard space in between the adjacent sub channels to effectively isolate them at the receiver using filters of appropriate cut-off frequencies.

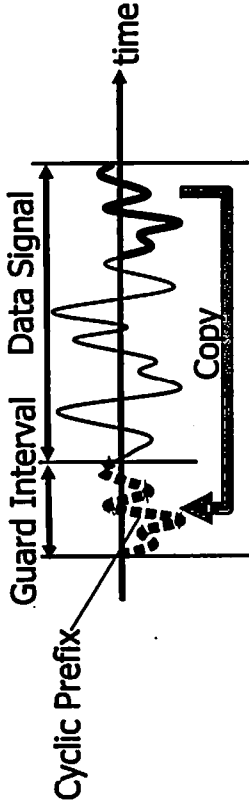


Figure 2.6: Guard interval principle

cies. A better and more efficient use of the bandwidth is possible if the spectra of individual sub-channels are allowed to overlap. By allowing the subcarrier tones to be separated by the inverse of the signaling symbol duration, independent separation of the frequency multiplexed tones is possible. This ensures that the spectra of individual sub channels are zeros at other subcarrier frequencies. This is the fundamental concept of OFDM.

We consider the OFDM system that transmits N modulated data symbols in an OFDM symbol period through N subcarriers. For the i -th OFDM symbol, the k -th sample of the OFDM signal is expressed as [7]

$$s_{i,k} = \frac{1}{\sqrt{N}} \cdot \sum_{m=0}^{N-1} \sqrt{p_m} \cdot x_{i,m} \cdot \exp \left\{ j \frac{2\pi km}{N} \right\}, \quad (2.1)$$

where $x_{i,m}$ is the modulated data symbol of the i -th OFDM symbol on the m -th subcarrier and p_m is the allocated power of the m -th subcarrier.

To combat ISI and ICI, a GI [11], such as the cyclic prefix (CP) or the zero padding (ZP), is added to each OFDM symbol. In the case of the CP, the last N_g samples of every OFDM symbol are copied and added to the heading part as shown in Fig. 2.6. The transmitted signal can be expressed as

$$\tilde{s}_{i,k} = \begin{cases} s_{i,N-N_g+k} & \text{for } 0 \leq k < N_g \\ s_{i,k-N_g} & \text{for } N_g \leq k < N + N_g \end{cases}. \quad (2.2)$$

We suppose that the fading channel can be modeled by a finite impulse response (FIR) filter. When the maximum delay spread does not exceed the GI, in the discrete

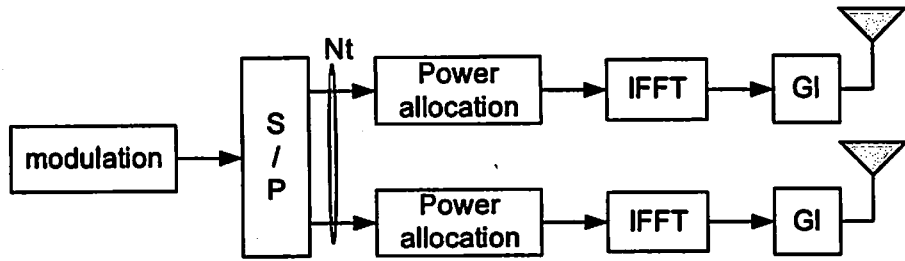


Figure 2.7: MIMO-OFDM transmitter scheme

frequency domain, the i -th received OFDM symbol for m -th subcarrier is given by

$$y_{i,m} = h_m \cdot \sqrt{p_m} \cdot x_{i,m} + n_{i,m}, \quad (2.3)$$

where h_m is a channel coefficient for the m -th subcarrier and $n_{i,m}$ denotes a zero mean AWGN of variance σ_n^2 . Thus it results in a frequency-flat-fading signal model per subcarrier. Channel correction is simply achieved by multiplying on each subcarrier the inverse of the channel coefficient in the ZF linear detector. The channel equalizer can be expressed as

$$G_m = \frac{h_m^*}{|h_m|^2}. \quad (2.4)$$

2.2.2 Signal Modeling for MIMO-OFDM

The principle of the OFDM transmission scheme [7] is to reduce the bit rate of each subcarrier and also to provide high bit rate transmission by using multiple low bit rate subcarriers. An OFDM system can provide immunity against frequency selective fading because each carrier goes through non-frequency selective fading. Suppose that a communication system consists of N_t transmit and N_r receive antennas, as illustrated in Fig. 2.7, denoted as an $N_t \times N_r$ system, where the transmitter sends an N_t -dimensional complex vector and the receiver receives an N_r -dimensional complex vector.

The transmitted baseband MIMO-OFDM signal for the i -th block symbol, is expressed as [12]

$$s_{i,k}^{(l)} = \frac{1}{\sqrt{N}} \cdot \sum_{m=0}^{N-1} \sqrt{p_{i,m}} \cdot x_{i,m}^{(l)} \cdot \exp \left\{ j \frac{2\pi m k}{N} \right\} \quad (2.5)$$

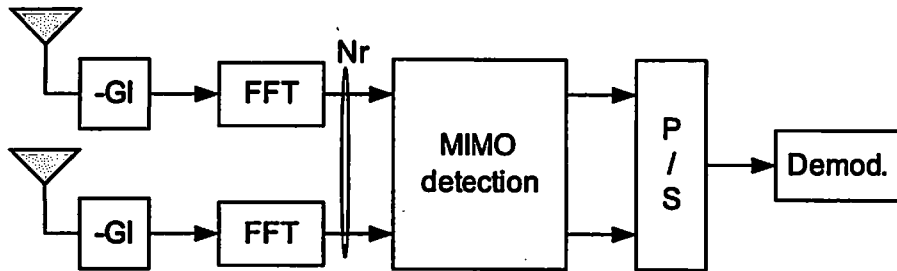


Figure 2.8: MIMO-OFDM receiver scheme

where k is the time domain index, $x_{i,m}^{(l)}$ and $p_{l,m}$ are respectively the modulated data symbol and the transmit power on the l -th transmit antenna for the i -th OFDM symbol on the m -th subcarrier. Similar to the OFDM transmission, to combat ISI and ICI, a GI [11] is added to the OFDM symbols among the transmit antenna. In the case of CP, the last N_g samples of every OFDM symbol are copied and added to the heading part.

We assume that the system is operating in a frequency selective Rayleigh fading environment [6] and the communication channel remains constant during transmission of one data frame. One data frame is composed of several MIMO-OFDM symbols and is assumed to be transmitted within the coherence time of the wireless system. In this case, channel characteristics remain constant during one frame transmission and may change between consecutive frame transmissions. We suppose that the fading channel can be modeled by a discrete-time baseband equivalent $(L-1)$ -th order finite impulse response (FIR) filter where L represents time samples corresponding to the maximum delay spread. Fig. 2.8 shows the receiver scheme of MIMO-OFDM systems.

When the maximum delay spread does not exceed the GI, ISI does not occur on the MIMO-OFDM symbols, so the frequency domain MIMO-OFDM received signal after removal of GI is described by

$$y_{i,m}^{(n)} = \sum_{l=0}^{N_t-1} h_m^{(n,l)} \cdot \sqrt{p_{l,m}} \cdot x_{i,m}^{(l)} + n_{i,m}^{(n)} \quad (2.6)$$

where $y_{i,m}^{(n)}$ is the received signal at the n -th received antenna for the i -th OFDM symbol and the m -th subcarrier and $h_m^{(n,l)}$ is the channel frequency response on the

m -th subcarrier from the l -th transmitting antenna to the n -th receiving antenna which composes a MIMO channel matrix. In addition, $n_{i,m}^{(n)}$ denotes the zero mean AWGN with N_r independent and identically distributed (iid), complex elements for the n -th received antenna [6]-[13].

In this thesis, we focus on the linear detection scheme. Thus, the output of the compensation scheme can be described by

$$\mathbf{z}_{i,m} = \mathbf{G}_m \cdot \mathbf{y}_{i,m} \quad (2.7)$$

where $\mathbf{z}_{i,m} = [z_{i,m}^{(0)}, \dots, z_{i,m}^{(N_t-1)}]^T$ and $\mathbf{y}_{i,m} = [y_{i,m}^{(0)}, \dots, y_{i,m}^{(N_r-1)}]^T$ respectively denote the output of the equalizer and the received signal. In the case of ZF detection [12], the equalizer matrix is calculated as

$$\mathbf{G}_m = (\mathbf{H}_m^H \mathbf{H}_m)^{-1} \cdot \mathbf{H}_m^H \quad (2.8)$$

with

$$\mathbf{G}_m = \begin{bmatrix} g_m^{(0,0)} & \dots & g_m^{(0,N_r-1)} \\ \vdots & & \vdots \\ g_m^{(N_t-1,0)} & \dots & g_m^{(N_t-1,N_r-1)} \end{bmatrix}, \quad (2.9)$$

and

$$\mathbf{H}_m = \begin{bmatrix} h_m^{(0,0)} & \dots & h_m^{(0,N_t-1)} \\ \vdots & & \vdots \\ h_m^{(N_r-1,0)} & \dots & h_m^{(N_r-1,N_t-1)} \end{bmatrix}. \quad (2.10)$$

2.2.3 Signal Modeling for MIMO MC-CDMA

The generation of a two-dimensional spreading MC-CDMA signal [14]-[15] with multiple antennas can be described as follows for the specific spreading configuration $SF = SF_f \cdot SF_t$ where SF , SF_t , and SF_f are respectively the total spreading factor, the time domain spreading factor and the frequency domain spreading factor. Figs. 2.9 and 2.10 show the conventional transmitter and receiver schemes for single antenna MC-CDMA modulation.

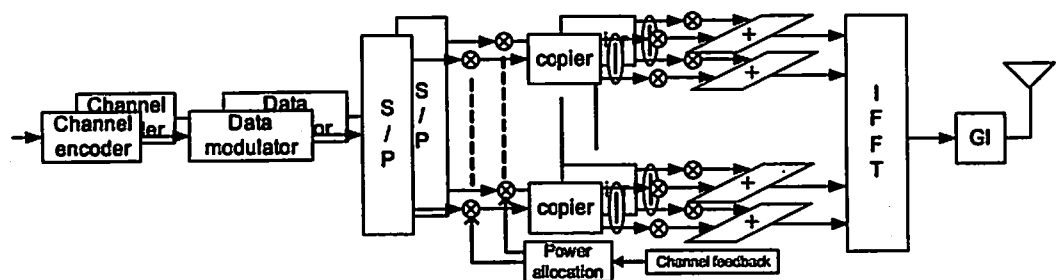


Figure 2.9: MC-CDMA transmitter scheme

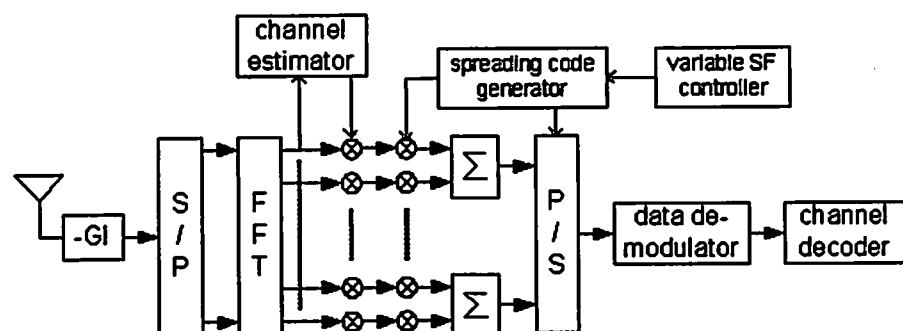


Figure 2.10: MC-CDMA receiver scheme

When the number of MC-CDMA elements in a packet frame and the number of subcarriers are represented by N_d and N , respectively, the resultant two-dimensional spreading sequence of the v -th MC-CDMA symbol ($v = 0, 1, \dots, N_d - 1$) at the w -th subcarrier ($w = 0, 1, \dots, N - 1$) for the l -th transmit antenna ($l = 0, \dots, N_t - 1$) is expressed as

$$x_{u,v,w}^{(l)} = \sqrt{p_{u,\lfloor w/SF_f \rfloor}^l} \cdot d_{u,\lfloor v/SF_t \rfloor, \lfloor w/SF_f \rfloor}^{(l)} \cdot c_{(v \bmod SF_t), (w \bmod SF_f)}^{(u)}, \quad (2.11)$$

where $d_{u,i,j}^{(l)}$ ($i = 0, 1, \dots, N_d/SF_t, j = 0, 1, \dots, N/SF_f$) is the data modulated symbol on the l -th transmit antenna for the k -th active user, $c_{i,j}^{(u)}$ ($i = 0, 1, \dots, SF_t, j = 0, 1, \dots, SF_f$) is the two-dimensional spreading code sequence for the u -th active user and $p_{u,j}^l$ is the allocated power of the u -th active user for the j -th modulated symbol on the l -th transmit antenna. In the case of equal power distribution, the term $p_{u,j}^l$ becomes equal to the constant average transmit power which is denoted \overline{P} in the rest of the Chapter. Furthermore, $\lfloor z \rfloor$ denotes the greatest integer that does not exceed z . Note that the number of data modulated symbols within a packet frame is represented by $(N_t \cdot N \cdot N_d)/(SF_f \cdot SF_t)$. For each transmit antenna, the spreading sequence of the v -th MC-CDMA symbol at the w -th subcarrier for the l -th transmitted antenna is given by

$$z_{v,w}^{(l)} = \sum_{u=0}^{N_u-1} x_{u,v,w}^{(l)}, \quad (2.12)$$

where N_u is the number of active users. The modulated signals are frequency-division multiplexed by an inverse FFT [16]. For the v -th OFDM symbol, the n -th sample of the MC-CDMA signal is expressed as [17]-[18]

$$s_{v,k}^{(l)} = \frac{1}{\sqrt{N}} \cdot \sum_{w=0}^{N-1} z_{v,w}^{(l)} \cdot \exp \left\{ j \frac{2\pi kw}{N} \right\}. \quad (2.13)$$

To combat ISI and ICI, similar to the OFDM scheme, the GI [6] such as a CP or a ZP is employed for the OFDM symbols. In the case of the CP, the last N_g samples of every MC symbol are copied and added to the heading part [19]. We suppose that the fading channel can be modeled by a FIR filter. At the receiving part for each user on each receive antenna, after removing the GI part, the received MIMO MC-CDMA signal is sampled into N orthogonal subcarriers by applying the FFT.

Including the channel response, we obtain for the specific k -th active user [12]

$$Y_{u,v,w}^{(n)} = \sum_{l=0}^{N_t-1} \xi_{u,w}^{(n,l)} \cdot z_{v,w}^{(l)} + e_{u,v,w}^{(n)}, \quad (2.14)$$

where $\xi_{u,w}^{(n,l)}$ and $e_{u,v,w}^{(n)}$ respectively denote the frequency response for the w -th sub-carrier between the l -th transmit and the n -th receive antenna and the AWGN of variance σ_n^2 on the n -th received antenna for the u -th active user. Because of the channel fading, the channel frequency response is not constant over the transmit bandwidth and the orthogonality between the different users may be destroyed. To mitigate the effect of the channel distortion, frequency domain equalization schemes such as ZF or minimum mean square error (MMSE), can be applied on the received signal. Finally, to extract data of the specific user from the received signal, despreading is performed over the interval of chips and the signals are coherently accumulated in both frequency and time domains. The despread data sequence of the u -th code channel (i.e. active user), $\hat{d}_{u,i,m}^{(l,k)}$ ($i = 0, \dots, N_d/SF_t, m = 0, \dots, N/SF_f$) is represented as

$$\hat{d}_{u,i,m}^{(l)} = \frac{1}{SF} \cdot \sum_{v=0}^{SF_t-1} \sum_{w=0}^{SF_f-1} \sum_{n=0}^{N_r-1} G_{u,w+SF_f \cdot m}^{(l,n)} \cdot Y_{u,i,SF_t+v,w+SF_f \cdot m}^{(n)} \cdot c_{v,w}^{(u)}, \quad (2.15)$$

where $G_{u,w+SF_f \cdot m}^{(l,n)}$ is the channel equalizer coefficient for the u -th active user on the $(w + SF_f \cdot m)$ -th subcarrier between the l -th transmit and the m -th receive antennas.

In the case of ZF compensation, the linear equalizer is equal to (for $0 \leq u < N_d/SF_t$ and $0 \leq m < N$)

$$\mathbf{G}_{u,m} = (\Psi_{u,m}^H \cdot \Psi_{u,m})^{-1} \cdot \Psi_{u,m}^H \quad (2.16)$$

2.2.4 Signal Modeling for SC-FDE

SC modulations are known to be suitable for CP-assisted block transmission within broadband wireless systems, since a low-complexity, linear FDE technique, involving simple FFT computations, can then be employed to solve the severe interference problem [20]. As with current OFDM-based schemes, the CP length is long enough to cope with the maximum relative channel delay. Therefore, in what concerns the useful part of each received burst, any inter-block interference (IBI) is avoided; moreover, the linear convolutions, in the time domain, which are inherent to the

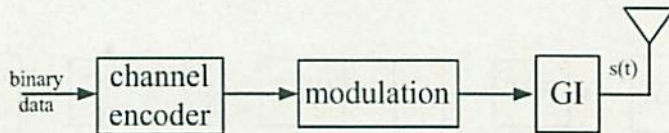


Figure 2.11: SC FDE transmitter scheme

time-dispersive channels, become equivalent to circular convolutions, corresponding to multiplications in the frequency domain. In recent papers [21], [22], [23], the authors considered both an OFDM option and an SC-FDE option for broadband wireless communications. These papers provided overall comparisons of the two options, with the help of selected performance results, which were used to support the suggestion of a mixed solution for future broadband systems: an OFDM option for the DL and an SC-FDE option for the UL. Especially when space diversity is adopted in the base station (BS) but not in the mobile terminal (MT), the implementation complexity becomes concentrated at the BS (where increased power consumption and cost are not so critical), concerning both the signal processing effort and, due to the strong envelope fluctuation of OFDM signals, the power amplification difficulties. For conventional CP-assisted block transmission implementations, either MC based, or SC based, the CP length is selected on the basis of the expected maximum delay spread, so as to ensure that it is always greater than the channel memory order. Next, the data block size can be selected to be large enough to make the channel variation over the block negligible. The operations on this block are a short ^{FFT}, channel compensation and an inverse FFT. In order to perform efficient equalization, a GI is added between each data block. Fig. 2.11 summarizes the main steps of the transmit scheme. Transmit data are first encoded and modulated. Then symbols are organized in blocks of length \underline{N} . A CP which is a copy of the last part of the transmitted block is included as a header part of each transmit block. The length of the CP has to be longer than the maximum delay spread in order to completely avoid the IBI. The CP at the beginning of each block has two main functions, it prevents contamination of a block by IBI from the previous block and it makes the received block appear to be periodic with period \underline{N} . The conventional receiving scheme is presented in Fig. 2.12. At the receiving part, the CP is discarded and FFT

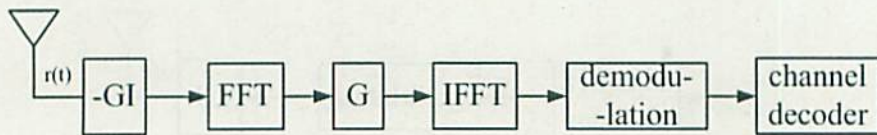


Figure 2.12: SC FDE receiver scheme

processing is done one each block of N data symbols. This produces the appearance of circular convolution which is important for the FDE implementation.

We assume that the system is operating in a frequency selective Rayleigh fading environment [6] and the communication channel remains constant during a packet transmission. The data frame duration is assumed to be within the coherence time of the wireless channel. In this case, channel variations remain constant during one frame transmission and may change between consecutive frame transmissions. We suppose that the fading channel can be modeled by a discrete-time baseband equivalent $(L - 1)$ -th order finite impulse response (FIR) filter where L represents time samples corresponding to the maximum delay spread. In addition, a zero-mean AWGN with iid is assumed.

The signal $s(t)$ is then transmitted through a multipath wireless channel characterized by

$$h(t, \tau) \equiv h(\tau) = \sum_{i=0}^{L-1} \alpha_i \cdot c(\tau - \tau_i) \quad (2.17)$$

where we assume that the channel is deterministic and time independent [6]. For a time-independent channel, the received signal $r(t)$ in the time domain is given by

invariant

$$r(t) = s(t) * h(t) + e(t) \quad (2.18)$$

where “*” denotes the convolution and $e(t)$ is an AWGN with iid zero mean, σ_n^2 variance. In addition, $s(t)$ and $r(t)$ respectively represent the transmit data sequence and the received signal in the time domain.

In the case of conventional SC transmission with frequency domain equalization, the transmit signal is composed by a data frame part combined with a GI. The main action of the GI is to keep the cyclic convolution between the multi-path channel and the transmit sequence. To combat IBI and ISI, the GI [11] is added, similar to

the OFDM symbols. In the case of the CP, the last N_g samples of every N symbol are copied and added to the heading part, similar to OFDM scheme.

If we consider the case that GI is inserted every ~~N~~^{it all} elements, the baseband representation of the linear frequency domain representation of the equalizer is then simply described by

$$\hat{\mathbf{s}}_N = \mathbf{W}_N^{-1} \cdot \mathbf{G} \cdot \mathbf{W}_N \cdot \mathbf{r} \quad (2.19)$$

where \mathbf{W}_N is the matrix representation of the Fourier transform of size N .

$$\mathbf{r} = [r_0, r_1, \dots, r_{N-2}, r_{N-1}]^T, \quad (2.20)$$

$$\hat{\mathbf{s}}_N = [\hat{s}_0, \hat{s}_1, \dots, \hat{s}_{N-2}, \hat{s}_{N-1}]^T, \quad (2.21)$$

where $\{r_m\}$ and $\hat{\mathbf{s}}_m$ respectively denote the discrete representation of the received signal and the compensated signal in the time domain. Furthermore, the equalization part is represented by

$$\mathbf{G} = \text{diag}[G_0, G_1, \dots, G_{N-2}, G_{N-1}] \quad (2.22)$$

where G_m is the 1-tap equalizer coefficient on the m -th subcarrier. The linear equalization \mathbf{G} is followed by an IFFT to allow recovery of the original data sequence. However, the addition of a GI every N data symbols directly affects the spectral efficiency of the transmit system. However, it allows relatively low complexity of the equalizer scheme, since only the division of a scalar value on each subcarrier is necessary.

2.3 Heuristic Expression of BER

The one-dimensional Gaussian Q -function, often referred to as the Gaussian probability integral, is defined as the complement (with respect to unity) of the cumulative distribution function (CDF) corresponding to the normalized (zero mean, unit variance) Gaussian random variable. This Gaussian Q -function plays a key role in the performance analysis of digital communication systems with coherent and non-coherent detection [6]. For example, when characterizing the performance of

coherent digital communications, the generic form of the expression for the error probability involves the Gaussian Q -function with an argument proportional to the square root of the instantaneous SNR of the received signal. To evaluate the average error probability in the presence of fading, one must average the Q -function over the fading amplitude distributions. It was the primary motivation for seeking alternative representations that appear in the form of the elementary functions (e.g., an exponential function). One of these alternative representations is the exponential approximation or upper bound for the Q -function.

2.3.1 Approximated BER Expression

In the AWGN channel, considering the performance of QPSK and QAM modulations, the BER is shown to be well approximated by [24]

$$BER \approx 0.2 \cdot \exp \left\{ -1.5 \cdot \frac{\gamma}{M-1} \right\} \quad (2.23)$$

for $0 \leq \gamma < 30$ dB where γ is the SNR and N_m is the number of bits per symbol ($M = 2$ for QPSK, $M = 4$ for 16-QAM and $M = 6$ for 64-QAM).

indent By extension to the Rayleigh fading channel case [25], we can derive the performance of QPSK and QAM modulations. Let $\bar{\gamma}$ and \overline{BER} denote the average SNR and BER respectively. The probability density function of the instantaneous SNR γ is given, for $\gamma > 0$ by

$$p(\gamma) = \frac{1}{\bar{\gamma}} \cdot \exp \left\{ -\frac{\gamma}{\bar{\gamma}} \right\} \quad (2.24)$$

The average BER, denoted \overline{BER} , is evaluated as

$$\overline{BER} \approx \int_0^{\infty} 0.2 \cdot \exp \left\{ -1.5 \cdot \frac{\gamma}{M-1} \right\} \cdot \frac{1}{\bar{\gamma}} \cdot \exp \left\{ -\frac{\gamma}{\bar{\gamma}} \right\} d\gamma \quad (2.25)$$

 and the previous approximation can be bound as [26] and [27]

$$BER \leq a \cdot \exp \left\{ -b \cdot \frac{\gamma}{M-1} \right\}. \quad (2.26)$$

Therefore, we will use this heuristic approximation to evaluate the power allocation scheme and then we adjust the BER approximation based on computer matching.

Table 2.1 summarizes the parameters of a and b for QPSK, 16-QAM and 64-QAM modulations, without channel coding, obtained via computer simulations.

Table 2.1: Transmission modes for coding rate $R = 1$

Modulation	QPSK	16-QAM	64-QAM
a	0.2	0.2	0.15
b	1.66	1.73	1.68

By extension to the MC system, the approximation can be expressed as [28]

$$f(\beta_m, p_m) \approx a \cdot \exp \{ -b \cdot \beta_m \cdot p_m \} \quad (2.27)$$

where β_m is equal to

$$\beta_m = \frac{1}{(M-1) \cdot \sigma_n^2 \cdot |g_m|^2} \quad (2.28)$$

where g_m and σ_n^2 respectively denote the linear equalizer coefficient on the m -th subcarrier and the variance of the AWGN and β_m denotes the received SNR, which depends on the modulation scheme and the equalizer weights on the m -th subcarrier. Furthermore, p_m denotes the transmit power m -th subcarrier. The parameters a and b are to be determined in a heuristic way, namely, via computer simulations.

2.3.2 Convolutional Coded Case

We utilize an approximated BER expression based on convolutional coded [29]-[30] data transmission. The generator polynomial of the mother code is $g = [133, 171]$ of rate $R = 1/2$ and $K = 7$ and the other coding rates ($R = 3/4$ and $R = 2/3$) are obtained from the puncturing pattern described in the WLAN based channel coding. At the receiver, the Viterbi algorithm is performed to recover the original sequence [31]. The coding unit is the transmit frame, which is composed of several OFDM symbols. The total transmit duration is within the coherence time.

Fig. 2.13 shows the validity of the approximation. Extracted curves match well with the exact BER obtained by simulations and the exact BER curves are obtained by software simulations.

Same statement

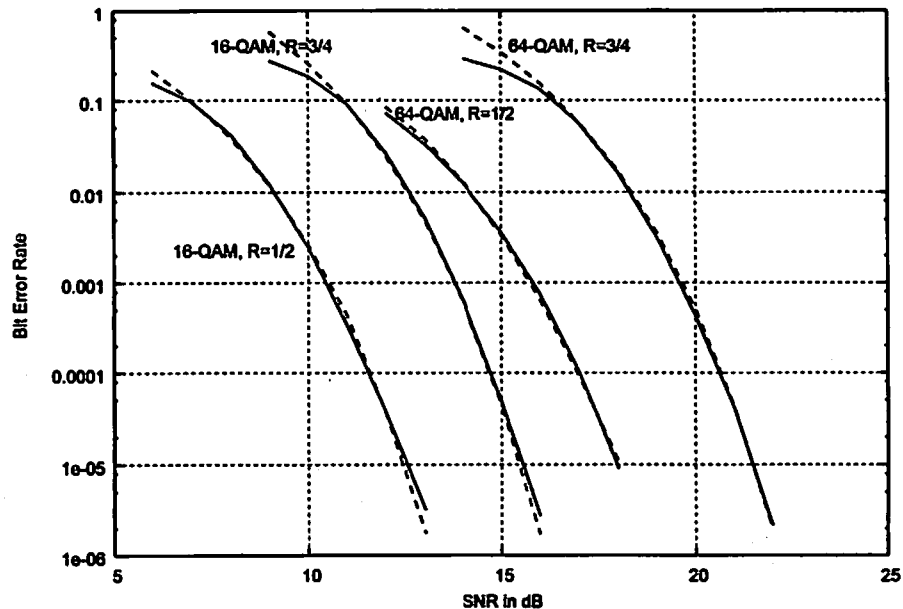


Figure 2.13: BER for different modulations with channel coding $R = 1/2$ and $R = 3/4$ (solid lines denote exact BER and dashed lines are fitting curves to the exact BER)

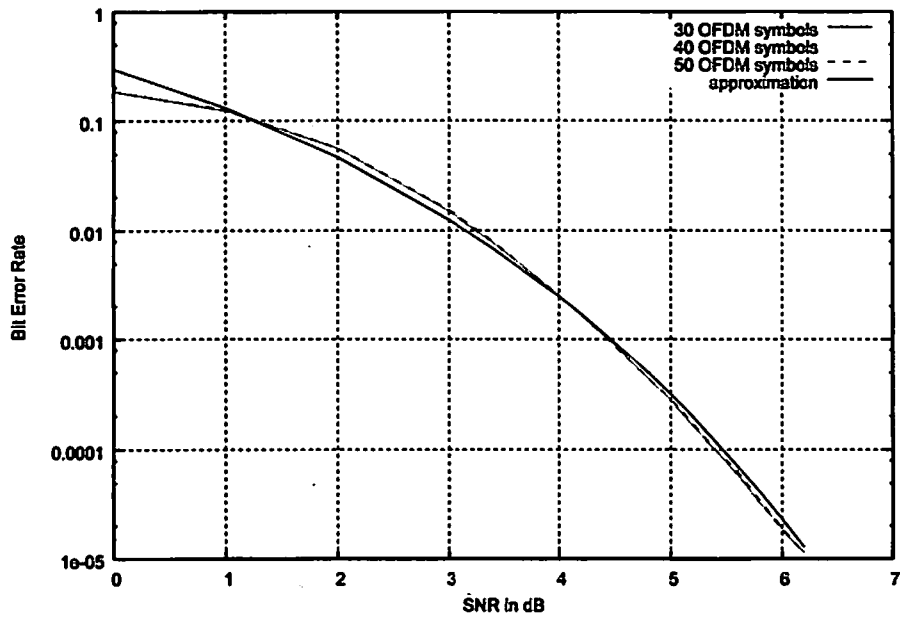


Figure 2.14: BER for different frame size (i.e. number of OFDM symbol per frame) with channel coding $R = 1/2$ and QPSK modulation

Table 2.2: Transmission modes for coding rate $R = 1/2$

Modulation	QPSK	16-QAM	64-QAM
a	7.0	4.0	1.5
b	9.5	11.0	12.0

Table 2.3: Transmission modes for coding rate $R = 3/4$

Modulation	QPSK	16-QAM	64-QAM
a	16.0	14.0	7.0
b	5.4	6.0	6.0

Fig. 2.14 shows the BER versus the SNR in dB for several frame sizes. That corresponds to the number of OFDM symbols per frame in a coded system. In addition, the approximation used for the proposed power allocation scheme is added for reference. For 30, 40 or 50 OFDM symbols, the BER performance is similar and the approximation used in the Chapter is also appropriate for such type of frame configuration.

2.3.3 Turbo Coded Case

With the turbo code in [32], the coding rates are obtained from the puncturing pattern described in [33]. The Max-Log-MAP algorithm with 8 iterations is performed at the decoding part to recover the original data stream [34].

Table 2.4 summarizes the evaluation of the parameter b for turbo coded QPSK and 16-QAM modulations. These values are obtained by computer simulations for different coding rates.

How about a
?

Table 2.4: Parameter of b for several coding rates and modulations

Modulation	Coding Rate (R)	b
QPSK	1/3	9.5
QPSK	1/2	5.4
QPSK	3/4	11
16-QAM	1/3	2.5
16-QAM	1/2	3.4
16-QAM	3/4	5.2

Chapter 3

Proposed Power Allocation Scheme for OFDM Systems

In this **Chapter**, we propose to adapt the transmit power for OFDM transmissions in the frequency domain using a heuristic evaluation of the BER for each subcarrier. The proposed method consists of ordering in terms of fading impact, grouping a certain number of subcarriers and performing local power adaptation in each subcarrier group. The subcarrier grouping is performed in order to equalize the average channel condition of each subcarrier group. Grouping and local power adaptation allow us to take advantage of the channel variations and to reduce the computational complexity of the proposed power distribution scheme, while avoiding the performance degradation due to the suboptimum power adaptation as much as possible. Compared to the conventional power distribution methods, the proposed scheme does not require any iterative process and the power adaptation is directly performed using an analytical formula. Simulations show a gain in terms of BER performance compared to equal power distribution and existing algorithms for power distribution. In addition, due to the subcarrier group specificity, the trade-off between the computational complexity and the performance can be controlled by adjusting the size of the subcarrier groups. Simulation results show significant improvement of BER performance compared to equal power allocation.

3.1 Introduction

OFDM [16] has recently been applied widely in wireless communication systems due to its high data rate transmission capability with high bandwidth efficiency. Since the channel matrix becomes a circulant matrix because a CP is used and the circulant matrix can be diagonalized by a FFT matrix, OFDM transmission can achieve independent parallel flat fading channels. This means that the transmission performance can be improved by adequately (and inequally) distributing the total transmission power among the subcarriers [35]. Assuming that the channel state information (CSI) for all the subcarriers is available at the transmitting part, several power schemes have been proposed, whose optimization criterion is the minimization of the total transmitted power for fixed BER. The Chow's algorithm [36] uses a criterion of minimizing the packet error rate while attaining a certain transmission rate, which also requires a complex iterative process. On the other hand, maximizing the spectral efficiency is another way to optimize the transmission performance [37]-[39]. In [37], the water-filling method is used to allocate power in order to maximize the system capacity. In [38], a multilevel transmit power scheme is proposed for OFDM with adaptive modulation. Finally, in [40], a sub-optimal scheme to improve the BER is proposed and performances in a MC system with diversity are presented. However, the impact of the channel variation (ordering the subcarriers in term of fading impact) and effect of the complexity are not considered.

In this chapter, we propose to first group and order the different subcarriers which compose the OFDM symbol considering their fading impacts and then adapt the transmit power in the frequency domain using a heuristic expression of the BER [10]-[11] for each subcarrier. Simplicity of the BER expression allows us to obtain a closed form expression of the optimum power to be allocated for each subcarrier, which is applicable not only for uncoded OFDM systems but also for coded ones. Although the local power adaptation using a subset of the subcarriers results in poor performance in general, we propose a subcarrier grouping method that minimizes the adverse impact of the local power adaptation by taking the channel gains of all the subcarriers into consideration. The grouping and the power allocation also allow us to control the balance between the transmission performance and the

computational complexity by adjusting the size of the subcarrier group. Simulation results show significant improvements of BER performance both in the uncoded and coded cases compared to the equal power distribution and highlight the performance improvement of the grouping and ordering method.

This chapter is organized as follows. In the next Section, we describe the signal model of the proposed scheme. Then, we firstly introduce the BER approximation and then describe the proposed modulation and power adaptation scheme in the frequency domain. Finally, numerical results over QPSK and QAM modulations with several coding gains are presented and conclusions are drawn.

In the rest of the ~~Chapter~~, we will use the BER expression described in the previous ~~Chapter~~ as an approximated expression to perform power allocation and group selection.

3.2 Proposed Power Allocation Scheme

3.2.1 Subcarrier Ordering and Grouping

Fig. 3.1 illustrates the principle of forming subcarrier groups of size N_s . If transmission performance is to be maximized as the first criterion, power allocation through whole subcarriers is the best. However, the computational complexity of the power allocation increases faster than linearly as the number of subcarriers to consider increases, in general. Hence, the computational complexity can be reduced by performing power distribution for a limited number of subcarriers (N_s) at a time and repeating it N/N_s times. This approach is suboptimal and suffers from performance degradation, while how much the performance degrades depends on how the subcarrier groups are formed.

Let β denotes a vector representation of β_m (with reference to the previous Chapter) as $\beta = [\beta_0 \dots \beta_{N-1}]^T$. We firstly find an $N \times N$ permutation matrix F , which results in the arrangement of the elements of β in descending order as

$$\gamma = F \cdot \beta, \quad (3.1)$$

where $\gamma = [\gamma_0 \dots \gamma_{N-1}]^T$ and $\gamma_0 > \gamma_1 > \dots > \gamma_{N-1}$.

In order to keep the average channel condition of each subcarrier group to be the same for all the subcarrier groups, we rearrange the subcarriers by folding the last half of the element of γ to the first as

$$\alpha = D \cdot \gamma, \quad (3.2)$$

where $\alpha = [\alpha_0 \cdots \alpha_{N-1}]^T$ and D is also an $N \times N$ permutation matrix defined as

$$D = \begin{bmatrix} 1 & 0 & 0 & \cdots & 0 & 0 & 0 \\ 0 & 0 & 0 & \cdots & 0 & 0 & 1 \\ 0 & 1 & 0 & \cdots & 0 & 0 & 0 \\ 0 & 0 & 0 & \cdots & 0 & 1 & 0 \\ \vdots & & & & & & \end{bmatrix}. \quad (3.3)$$

Using α , we finally obtain the subcarrier groups as

$$\alpha^{(t)} = [\alpha_{t \cdot N_s} \cdots \alpha_{t \cdot N_s + N_s - 1}]^T, \quad (3.4)$$

where $\alpha^{(t)}$ is the t -th group of the equivalent SNR, ($t = 0, \dots, N/N_s - 1$). Therefore, defining $p = [p_0 \cdots p_{N-1}]^T$, the transmitted power vector of the t -th subcarrier group $p'^{(t)}$ can therefore be obtained as

$$p' = [p'^{(0)T} \cdots p'^{(N/N_s-1)T}]^T = D \cdot F \cdot p, \quad (3.5)$$

where $p'^{(t)} = [p'_{t \cdot N_s} \cdots p'_{t \cdot N_s + N_s - 1}]^T$.

In the proposed scheme, power allocation is performed for each $p'^{(t)}$ and is repeated N/N_s times. Denoting the optimum vectors of $p'^{(t)}$ and p' as $p_o^{(t)} = [p'_{t \cdot N_s, o} \cdots p'_{t \cdot N_s + N_s - 1, o}]^T$, and p_o' , respectively, we can express the optimum transmitted power vector $p_o = [p_{0,o} \cdots p_{N-1,o}]^T$ as

$$p_o = F^{-1} \cdot D^{-1} \cdot p_o'. \quad (3.6)$$

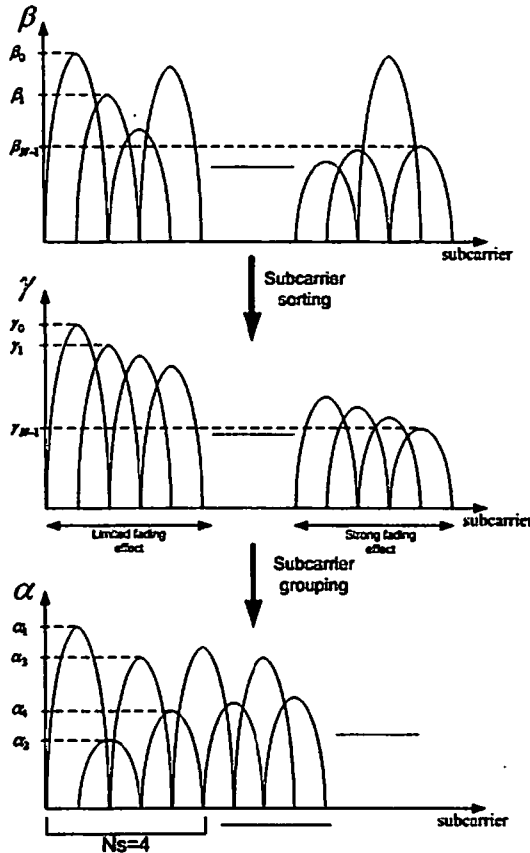


Figure 3.1: Principle of subcarrier group selection

3.2.2 Closed Form Solution of Proposed Power Allocation

In this section, we consider power distribution for the t -th subcarrier group under the condition that the average transmit power and the average modulation level are kept constant to be \bar{P} . The optimization problem can be given by

$$\left\{ \begin{array}{l} \mathbf{p}_o'^{(t)} = \arg \min_{\mathbf{p}'^{(t)}} \sum_{m=0}^{N_s-1} \frac{f(\alpha'_{t,N_s+m}, p'_{t,N_s+m})}{N_s} \\ \text{s.t. } \sum_{m=0}^{N_s-1} p'_{t,N_s+m} = N_s \cdot \bar{P} \end{array} \right. . \quad (3.7)$$

One possibility to solve this optimization problem is to apply the Lagrangian

procedure on each group of subcarrier. The processing can be described as

$$J(p_0, \dots, p_{N_s-1}) = \frac{1}{N_s} \sum_{m=0}^{N_s-1} f(\alpha_m, p_m) + \lambda \cdot \left(\sum_{m=0}^{N_s-1} p_m - N_s \cdot \bar{P} \right) \quad (3.8)$$

Then, optimal solutions are obtained by solving

$$\begin{cases} \frac{1}{N_s} \cdot \frac{\partial}{\partial p_m} \left(\sum_{m=0}^{N_s-1} f(\alpha_m, p_m) \right) + \lambda = 0 \\ \sum_{m=0}^{N_s-1} p_m - N_s \cdot \bar{P} = 0 \end{cases} \quad (3.9)$$

By introducing the explicit estimation of the BER in the set of equations and after calculation and rearrangement, we finally obtain the following general solution

$$p'_{t \cdot N_s + m, o} = \left[\sum_{u=0}^{N_s-1} \frac{\alpha_{t \cdot N_s + m}}{\alpha_{t \cdot N_s + u}} \right]^{-1} \cdot \left[N_s \bar{P} + \sum_{u=0}^{N_s-1} \frac{M}{\alpha_{t \cdot N_s + u} \cdot b} \log \left(\frac{\alpha_{t \cdot N_s + m}}{\alpha_{t \cdot N_s + u}} \right) \right]. \quad (3.10)$$

Since we have ignored the range of $p'_{t \cdot N_s + m}$ for the sake of simplicity, the solution may result in $p'_{t \cdot N_s + m, o} < 0$ for some cases. In this case, we propose to apply equal power distribution for the subcarrier group.

Moreover, contrary to the waterfilling scheme [37], the proposed scheme tends to allocate more power to the subcarriers that are strongly affected by channel fading. The proposed solution tends to flatten the channel variation, so that an uniform coding scheme between the different subcarrier is possible and appropriate.

3.3 Optimal Power Allocation

In the case of uncoded system (i.e. without any channel encoder), it is possible to exactly evaluate the BER performance for both QPSK and QAM modulations. It is well-known that the BER expression is a function of the Q -function [6] defined by $Q(x) \doteq (1/\sqrt{2\pi}) \int_x^\infty \exp(-t^2/2) dt$. However, an optimization problem which consists of minimizing the exact BER expression under a power constraint cannot

be solved analytically. The optimization problem is stated as

$$\left\{ \begin{array}{l} \mathbf{p}_{exact} = \arg \min \sum_{m=0}^{N-1} \frac{Q(\beta_m, p'_{l,m})}{N \cdot N_t} \\ \text{s.t. } \sum_{m=0}^{N-1} p_m = N \cdot \bar{P} \end{array} \right. \quad (3.11)$$

where \mathbf{p}_{exact} , p_m , \bar{P} and β_m respectively denote the optimal power allocation, the power allocation on the m -th subcarrier, the average transmit power per subcarrier and the effect of the channel condition on the m -th subcarrier.

✓ Nevertheless, by using iterative algorithm such as the steepest-descent method [35], the optimization problem can be solved. *✓*

✓ Let us first denote the Lagrangian expression of the optimization problem as

$$J_{exact}(p_0, \dots, p_{N-1}) = \frac{1}{N} \sum_{m=0}^{N-1} Q(\beta_m, p_m) + \lambda \cdot \left(\sum_{m=0}^{N-1} p_m - N \cdot \bar{P} \right) \quad (3.12)$$

The steepest descent algorithm converges to the global optimum in the case of a convex function. The Q -function, which is the exact approximate of the BER functions for QPSK, 16-QAM and 64-QAM modulations, is a convex function.

The adaptive method (i.e. steepest descent algorithm) is applied to find the solution by iterative process. A summary of the iterative algorithm can described as follows

3.4 Computational Complexity

The two main advantages of the proposed scheme are the simplicity compared to the iterative algorithms such as the steepest decent and the low additional complexity [40] compared to the suboptimal solution which does not include any specific group selection based on knowledge of the channel condition in the power allocation process. Complexity of the steepest descent algorithm is basically equal to $O(N_s^3)$. In addition, the iterative process needs to be repeated N/N_s times (for simplicity, we assume that N_s/N is an integer). The complexity of the ordering part of the

N/N_s

Table 3.1: Steepest Descent Algorithm

Step 1:

Set an iteration number $i = 0$,

a step size $\mu(0) = \mu_0$

and equal power distribution as an initial value.

Step 2:

Update the power set among the subcarriers by performing

$$p_m^{(i+1)} = p_m^{(i)} - \mu_0 \frac{\partial}{\partial p_m^{(i)}} J_{exact}(p_0^{(i)}, \dots, p_{N-1}^{(i)})$$

Step 3:

Adjusting the step size of negative power.

If all the components of the calculated power set in Step 2 are non-negative,

then go to Step 4 with $\mu(i + 1) = \mu_0$.

Otherwise, adjust the step size $\mu(i)$

so that the negative components can be non-negative,

and return to Step 2.

Step 4:

Repetition or termination.

If more adaptations are required for convergence,

increase i by one and go to Step 2. Otherwise terminate the procedure.

suboptimum power allocation that we propose, is equal to $O(N \cdot \log(N))$ and is performed only twice for each OFDM frame. The analytical part of the calculation that is performed for the estimation of the power allocation is equal to $O(N_s^2 \cdot \log(N_s))$. Fig. 3.2 shows the computational complexity in term of subcarrier groups. Fig. 3.2 highlights that the complexity of the proposed scheme is less complex than the iterative method. In addition, the obtained complexity is similar to that of the suboptimum proposal.

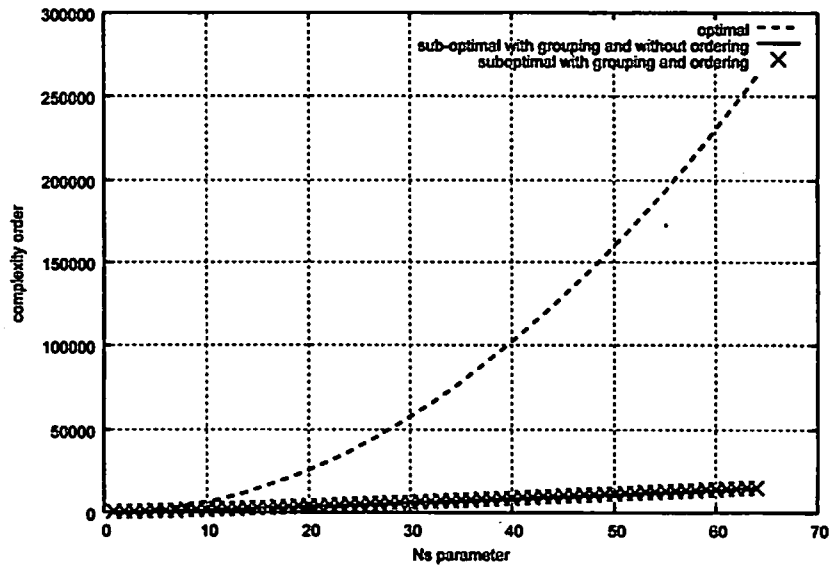


Figure 3.2: Complexity evaluation for $N = 64$ and $0 < N_s < 64$

3.5 Numerical Experimentation

This section gives an evaluation of the performance of the proposed power allocation method for OFDM systems in a multipath fading environment. Simulation parameters are given in Table 4. We assume perfect knowledge of the CSI both at the transmitting and receiving parts. For all simulations, the delay power spectrum is assumed to be an exponential decay model with 1 dB decaying per sampling period. The carrier frequency is equal to 2.4 GHz, the IFFT/FFT size is 64 points and the GI is set to 16 samples. The ZF detection scheme is employed in the receiver.

For comparison, two additional systems have been included in the simulations.

Table 3.2: Simulation Parameters

Carrier frequency	2.4 GHz
Bandwidth	20 MHz
Modulation scheme	QPSK, 16-QAM, 64-QAM
Channel encoder	No code, convolutional codes, turbo codes
Channel estimation	Perfect CSI
Number of data subcarriers	64
GI length	16
Channel model	10-path, Rayleigh Fading
Sample period	0.05 μ s
Number of data packets	40
Group size (N_s)	2, 4, 8, 16, 32, 64

For uncoded and fixed modulation, the optimal power allocation based on the exact function of the BER for QPSK and QAM modulations, combined with a steepest descent algorithm, optimal power allocation is estimated and adapted. The second system is the sub-optimal case described in [40]. This suboptimum case consists of performing power allocation without any consideration for the channel variation in the subcarrier groups. In the rest of the Chapter, the optimum system will be represented by the plot denoted "optimal" *which* expresses the power allocation scheme based on the exact BER expression with grouping and ordering. The sub-optimal system with grouping and without ordering will be denoted "sub-optimal with grouping and without ordering". Finally, the proposed scheme will be *indifferently* denoted "sub-optimal with grouping and ordering" or "proposed power distribution".

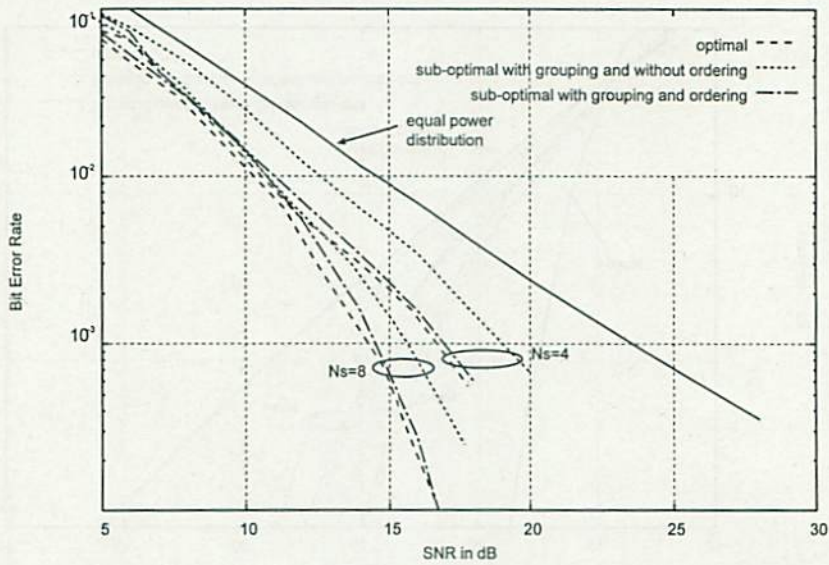


Figure 3.3: BER performance for uncoded OFDM with QPSK modulation

3.5.1 Uncoded OFDM

Fig. 3.3 shows the BER versus the average total received SNR (dB) of the proposed scheme (i.e. suboptimal with grouping and ordering) with QPSK modulation schemes and various ^{two}~~various~~ subcarrier group sizes N_s . The BER performances of the equal power distribution, the optimal scheme and the BER based sub-optimal solution with grouping and without ordering both described in [40] are also plotted in the same figure. According to simulations, at average $\text{BER}=10^{-3}$, 7 and 9 dB gains are respectively obtained for $N_s = 4$ and 8 compared to the equal power distribution scheme. For any group size, the proposed allocation scheme outperforms the sub-optimal solutions. At $\text{BER}=10^{-3}$, 2 to 3 dB gains are obtained simply by performing the proposed subcarrier selection and ordering followed by the power allocation scheme. In addition, compared to the optimal case, the proposed solution is less than 0.5 dB degraded. Figs. 3.4 and 3.5 show the BER performance with 16-QAM and 64-QAM, respectively, for several subcarrier group sizes. From these figures, we can see that the proposed scheme can achieve significant performance gain also for uncoded 16-QAM and 64-QAM schemes. Moreover, comparing the performance between the proposed scheme with and without ordering at $\text{BER}=10^{-3}$, 1.5dB gains

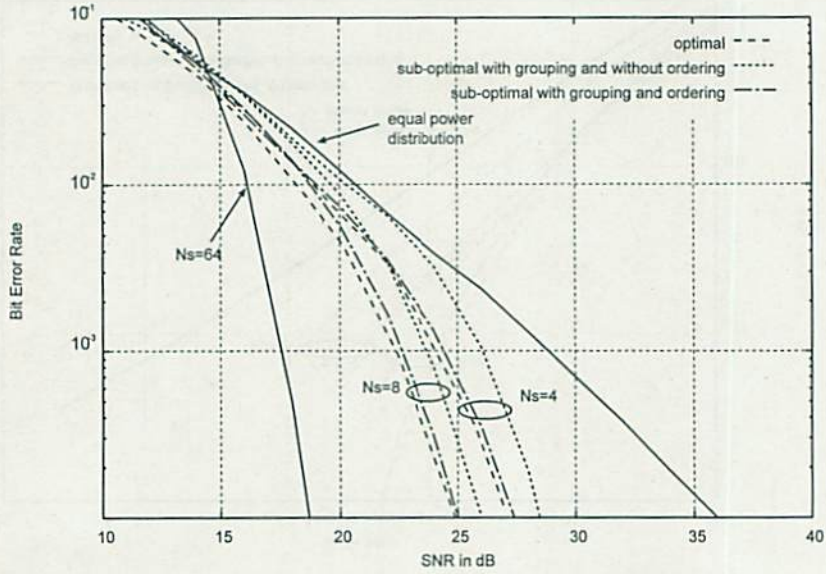


Figure 3.4: BER performance for uncoded OFDM with 16-QAM

are obtained on average, for any size of subcarrier grouping (i.e., value of N_s) simply by performing the proposed subcarrier ordering compared to the subcarrier selection proposed in [40]. In addition, due to the structure of the proposed power distribution scheme, the ordering part does not affect the performance of the specific case $N_s = N$. However, due to the structure of the proposed power distribution scheme, there is a trade-off between the subcarrier grouping size and the computational complexity.

3.5.2 Convolutional Coded OFDM

In Fig. 3.6, the benefit of performing the proposed scheme (i.e. suboptimal with grouping and ordering) is highlighted for the specific case of $R = 1/2$, ZF detection scheme, and QPSK and 64-QAM modulations. The simulation results show that at average $\text{BER} = 10^{-4}$, between 4dB and 8dB gains are obtained depending on the subcarrier ordering size ($N_s = 2, 4, 8, 16$, and 64) for QPSK modulation compared to the equal power distribution. In the case of 64-QAM modulation, the proposed power allocation with ordering allows to obtain 3 to 5 dB gains, depending on the size of the subcarrier groups, N_s . The benefit in term of gain for QAM modulation is

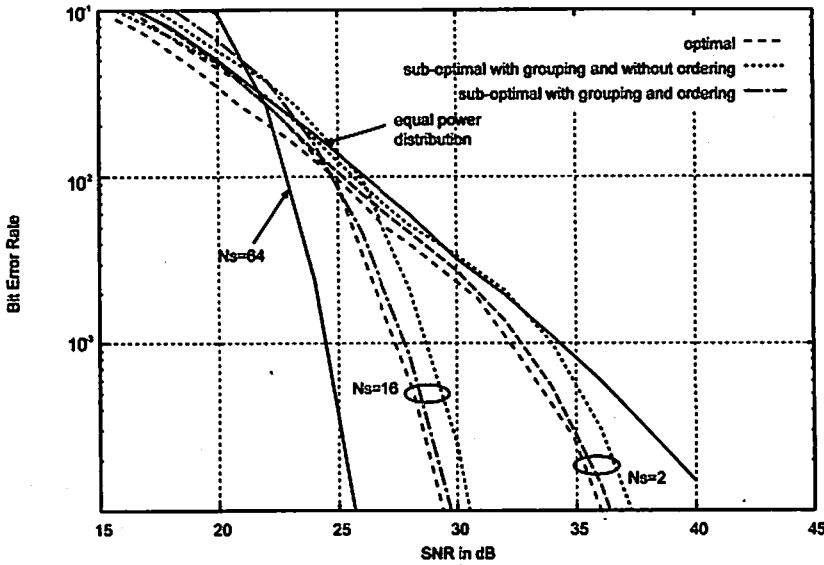


Figure 3.5: BER performance for uncoded OFDM with 64-QAM

comparable to that for QPSK modulation. In Fig. 3.7, the impact of the subcarrier grouping size on the results is presented for the QPSK and 64-QAM modulations with $R = 3/4$.

In Figs. 3.8 and 3.9 illustrate the benefit of performing the proposed power allocation scheme on coded OFDM system with QAM modulation. Results are presented for a wide range of subcarrier group size, (i.e., N_s) between 2 to 64. The simulation results show that for an average $\text{BER} = 10^{-4}$, significant gain are obtained simply by performing the proposed power distribution scheme. In addition, the influence of the subcarrier ordering and subcarrier group size are also highlighted. In the proposed scheme, the impact of the subcarrier group size strongly affects the BER performance. The proposed scheme outperforms the sub-optimal solution presented in [40] also for the coded systems. As a summary, this series of results, presented with computer simulations, highlight the fact that the trade-off between the value of the group size and performance should be taken into account to define the most appropriate selection of the parameter N_s .

The BER performance of coded OFDM depends on the correlation among the frequency responses, while, for the uncoded case, the BER of each subcarrier is solely determined by the SNR of each subcarrier. This means that the parameters

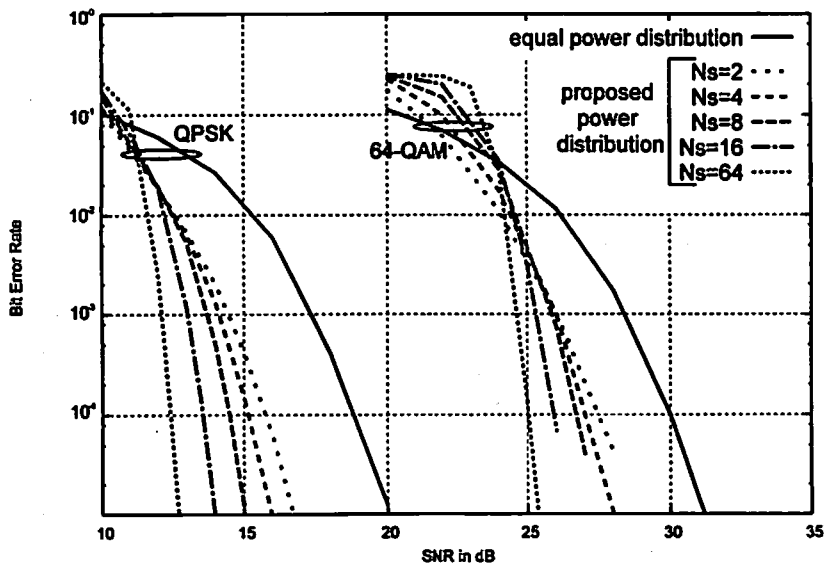


Figure 3.6: BER performance of coded OFDM with $R=1/2$ for QPSK and 64-QAM modulations

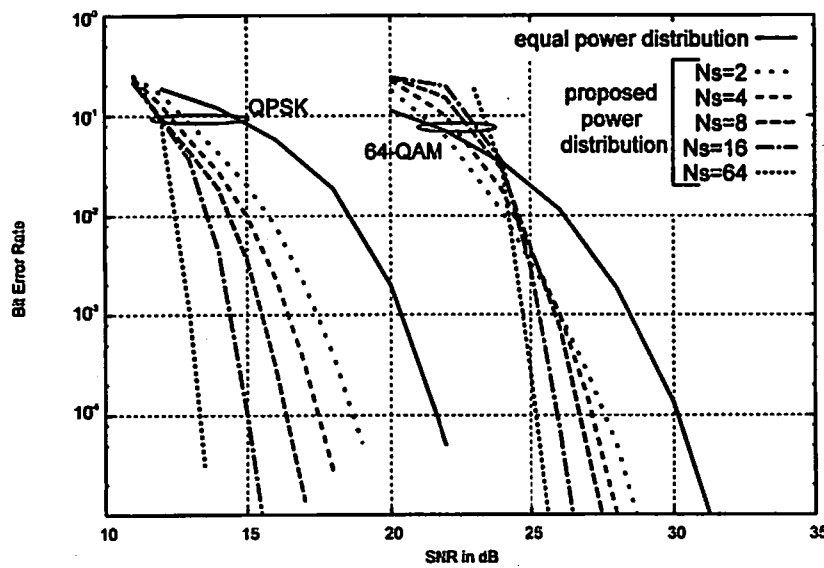


Figure 3.7: BER performance of coded OFDM with $R=3/4$ for QPSK and 64-QAM modulations

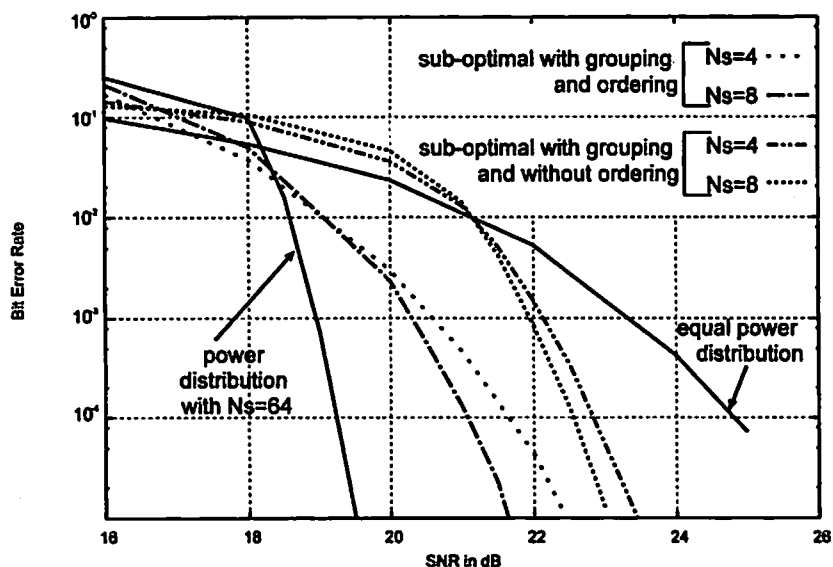
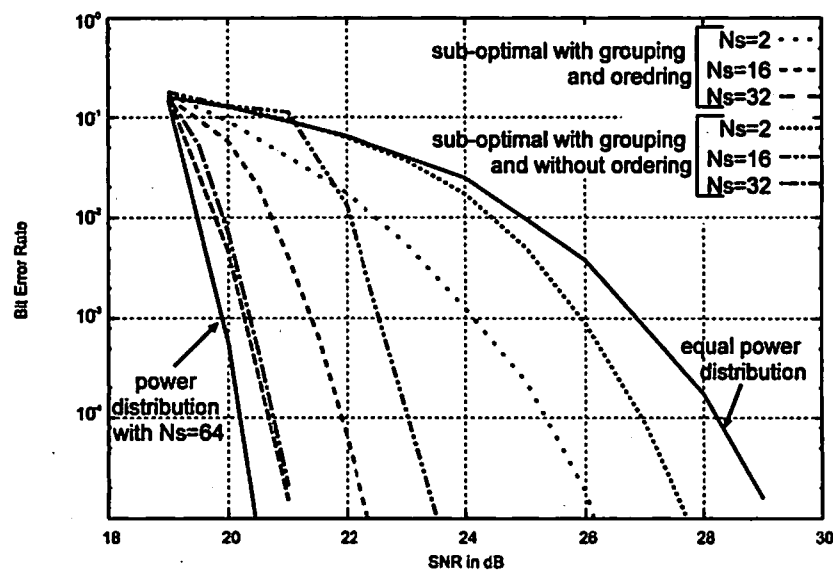
Figure 3.8: BER performance for coded OFDM with 16-QAM and $R = 1/2$ Figure 3.9: BER performance for coded OFDM with 16-QAM and $R = 3/4$

Table 3.3: Parameters of a_m and b_m : QPSK modulation (Coding Rate: 1/2)

Decaying factor	0.5	1.0	1.5
a_m	5.6	7	7.8
b_m	10.5	9.5	8.9

of a_m and b_m for the BER approximation have to be changed depending on the delay spread in practical scenarios in order to obtain the best performance by the proposed method. Table 3.3 shows the parameters obtained by computer simulations for QPSK convolutionally coded ($R = 1/2$) OFDM in 10-path Rayleigh fading exponential decay model with 0.5, 1, and 1.5 dB decaying per sampling period. From the table, we can see that the optimum values of a_m and b_m actually depend on the decaying factor of the channel. Changing the parameters depending on the channel condition, however, may not be practical due to the complexity. Fig. 3.10 shows the BER performance against the total SNR in dB with optimized and non-optimized coefficients, a_m and b_m . The 10-path Rayleigh fading exponential decay model with 1 dB decaying per sampling period is considered for evaluation. The performance of equal power distribution and the proposed scheme for two group sizes are plotted. Optimized coefficients correspond to $a_m = 7$ and $b_m = 9.5$, whereas the non optimized coefficients correspond to the specific channel of 0.5dB decay model (i.e. $a_m = 5.6$ and $b_m = 10.5$). From the figure, we can recognize a certain performance degradation due to the inappropriate parameters for the two different group sizes. However, at $\text{BER}=10^{-4}$, the degradation for non-optimized coefficients is less than 0.8dB for both $N_s = 2$ and $N_s = 8$. Compared to the equal power distribution, at average $\text{BER}=10^{-4}$, respectively 2.5dB and 4dB gains are still obtained simply by performing the proposed scheme even in the case of inappropriate coefficients selection.

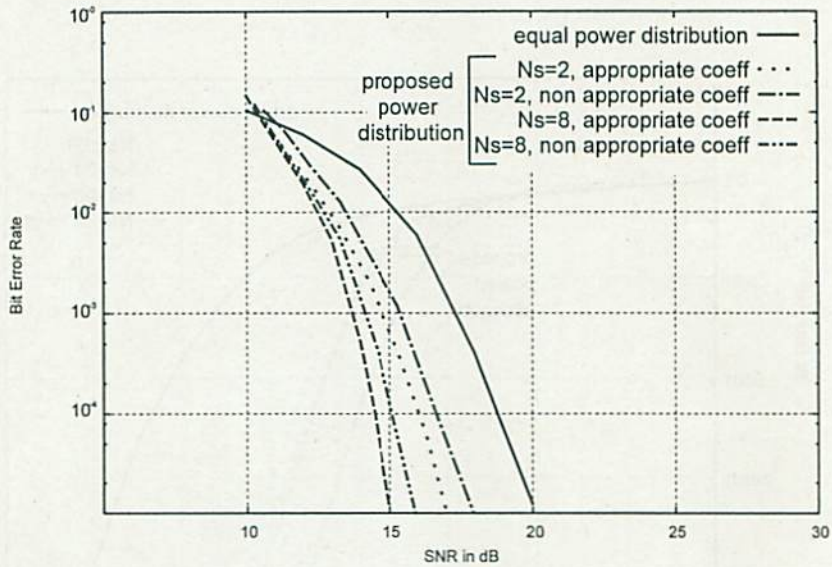


Figure 3.10: BER performance for coded OFDM with QPSK modulation using optimized and non-optimized a_m and b_m

3.5.3 Turbo Coded OFDM

Fig. 3.11, 3.12 and 3.13 show the Bit Error Rate (BER) versus the average total received SNR (dB) for turbo coded QPSK modulation and several subcarrier grouping sizes. Both conventional (i.e. equal power distribution) and proposed schemes are plotted in these figures and results are presented for ZF detection scheme.

In Fig. 3.11, the benefit of performing the proposed scheme is highlighted for the case of $R = 1/3$. Simulation results show that at average $\text{BER} = 10^{-4}$, respectively 1.5dB, 1.7dB and 2dB gains are obtained for the proposed power distribution scheme with ordering and $N_s = 2$, $N_s = 4$ and $N_s = 8$. In addition, the specific case of the proposed power allocation scheme with $N_s = 32$ is plotted and the performance gain is about 2.5dB compare to the equal power distribution scheme.

Fig. 3.12 shows the results in the case of QPSK modulation and $R = 1/2$. The performance gain obtained by performing the proposed power allocation scheme with ordering becomes equal to 2dB for $N_s = 2$ and 2.5dB for $N_s = 16$ at average $\text{BER} = 10^{-4}$.

Moreover, comparing the performance between the proposed scheme with and

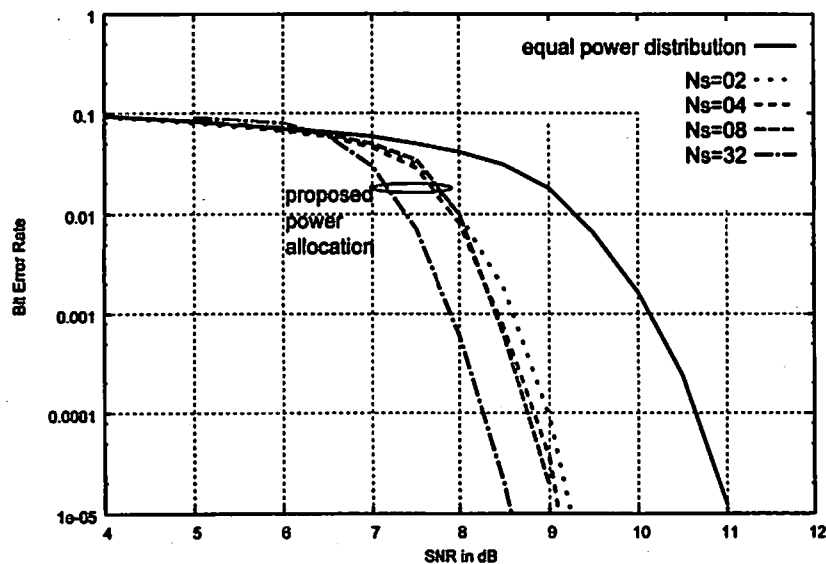


Figure 3.11: BER performance for $R = 1/3$ and QPSK modulation

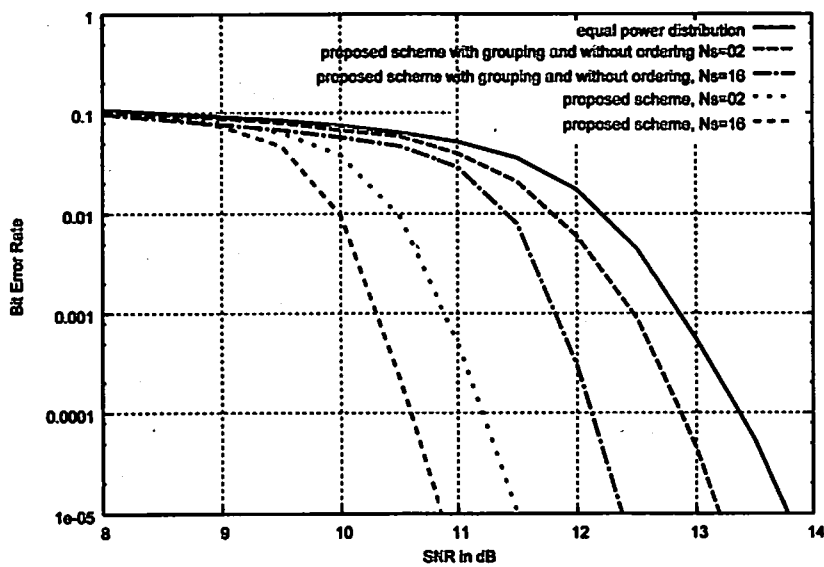


Figure 3.12: BER performance for $R = 1/2$ and QPSK modulation

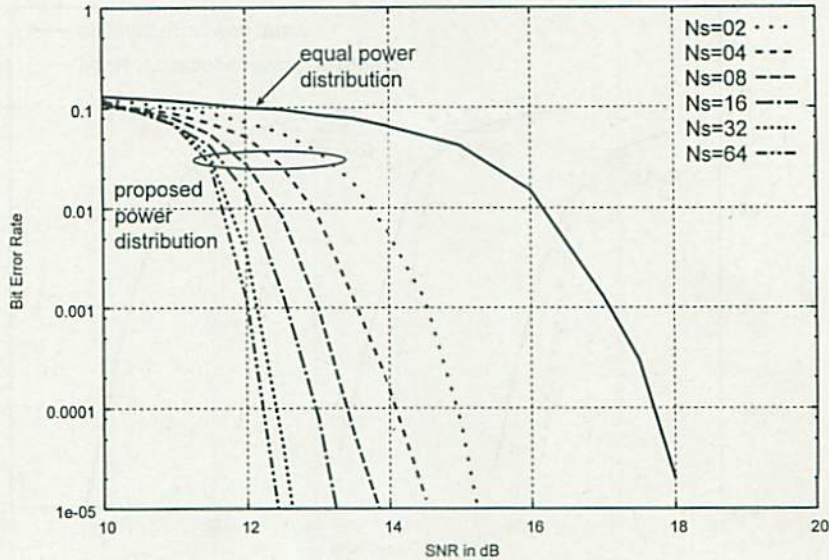


Figure 3.13: BER performance for $R = 3/4$ and QPSK modulation

without ordering, we can see that an average of 1.25dB improvement is obtained for any size of subcarrier grouping (i.e. N_s) simply by performing the proposed subcarrier ordering.

Fig. 3.13 shows the BER versus the average total received SNR (dB) of the proposed scheme with QPSK modulation, $R = 3/4$ and various subcarrier group sizes N_s . The BER performance of the conventional scheme (equal power distribution) is also plotted in the same figure. The simulation results show that, at average $\text{BER}=10^{-4}$, 2.5, 3.1, 3.5, 3.9, 4.2 and 4.5dB gains are obtained for $N_s=2, 4, 8, 16, 32$, and 64, with ordering respectively.

Finally, Fig. 3.14 shows the performance gains of the proposed power distribution scheme with ordering and $N_s=4$ for 16-QAM modulation and three different turbo coding rates, $R=1/3, 1/2$ and $3/4$. Between 1 and 2dB performance gains are obtained by simply comparing the proposed power distribution scheme and the equal power allocation.

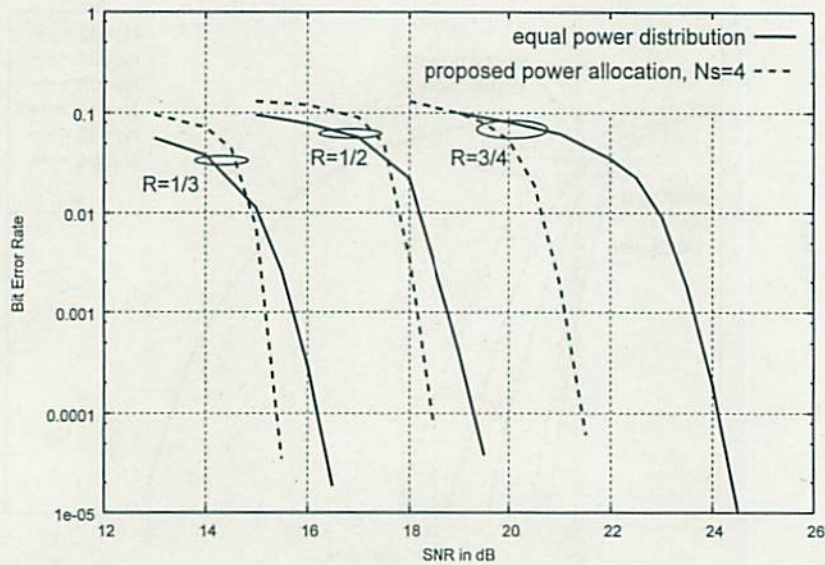


Figure 3.14: BER performance for 16-QAM modulation

3.6 Conclusion

This Chapter proposes a novel scheme for OFDM that adapts the transmit power in the frequency domain using a heuristic expression of the BER for each subcarrier. A closed form expression of the optimum power to be allocated for each subcarrier is presented for uncoded OFDM transmission as well as coded scheme. The proposed scheme allows to reduce the computational complexity, by including a subcarrier grouping method with local power adaptation for each subcarrier group. Our subcarrier grouping method minimizes the adverse impact of the local power adaptation by taking into consideration the channel gains of all the subcarriers. The characteristics allow us to control the trade-off between the transmission performance and the computational complexity by adjusting the sizes of subcarrier groups. The simulation results show significant improvement of BER performance both in the uncoded and coded cases for QPSK and QAM modulations compared to the equal power allocation scheme. In this Chapter, we have limited the channel coding scheme to the convolutional code and turbo code. However, other powerful coding schemes such as the low density parity check (LDPC) [41]-[42], with appropriate consideration on the impact of the number of information bits per frame due to the interleaver depth on

3.6 Conclusion

the BER performance, can also be included in the modulated transmission. Finally, future orientation for this work would include the introduction of the error in the channel estimation [43].

Chapter 4

Extension of Proposed Power Allocation to Various MC Systems

This Chapter examines the benefits of extending the power allocation scheme to different MC systems. First, We begin this Chapter with the extension of the proposed power allocation for OFDM systems combined with adaptive modulation. Specifically, we examine the performance enhancement made possible by using the proposed power allocation scheme for OFDM described in the previous Chapter in conjunction with adaptive modulation. Then, we propose several power allocation schemes for MIMO-OFDM transmission based on the minimization of an approximated BER expression. The schemes, illustrated in this extension, serve to allocate power among the different transmit antennas and the different subcarriers which compose the MIMO-OFDM transmitted signal. Several solutions are available to perform power allocation. Frequency domain power allocation, spatial domain power allocation and combined spatial and frequency power allocation are evaluated. Finally, we propose to extend the proposed power allocation scheme for coded MC-CDMA systems with two dimensional spreading and multiple antennas. For each extension, we begin with basic fundamentals of the specific MC system, followed by a detailed description of the proposed scheme, simulations, and our conclusions from them. By the end of this work, we should have a better understanding of the different proposed schemes.

4.1 Introduction

Mobile communications is increasingly required to provide a variety of multimedia applications for mobile users. The current 3rd generation mobile system (based on CDMA technology and time domain equalization) is not promising enough to provide such broadband multimedia services with its one carrier transmission system. So the challenge to provide high data rate over a hostile mobile environment with limited spectrum and ISI caused by multipath fading, has led to the introduction of MC transmission systems. This type of transmission system has been identified as a potential candidate for the 4G broadband mobile communication system. This is because it is able to deliver high rate data by splitting them into a number of lower rate streams that are transmitted simultaneously over a number of subcarriers. An approach called link adaptation techniques has emerged as a tool to increase data rate and spectral efficiency. In this technique, modulation and/or other signal transmission parameters, such as power allocation, are dynamically adapted to the channel condition to increase the system performance in terms of BER and throughput in various conditions such as multi-path channel environment, Doppler spreads and fading.² Another trend is the interest in the field of multi-antenna processing technique. In rich multipath environment, space division multiplexing (SDM) [17] with MIMO systems [44] can increase the transmission rate and has enormous communication capacity because of its spectral efficiency. Therefore, combining OFDM and SDM techniques [45] is a highly promising approach to realizing high data-rate wireless communications [46]. In the previous Chapter, a computationally efficient power allocation method for OFDM transmission has been proposed. It consist of allocating power for single-input single-output (SISO) OFDM based on an approximated expression of the BER, where the proposed subcarrier grouping method enables us to decrease the computational complexity with limited performance degradation. In the previous Chapter, we have considered the case for single transmit antenna OFDM systems. Furthermore, OFDM based transmission, CDMA concepts [8], [47] and their hybrid solutions such as MC-CDMA with two dimensional spreading combined with multiple antennas [48] are regarded as a possible candidate for Beyond 3G (B3G) mobile communications [49], especially for synchronous DL

[50]-[51]. This is mainly due to the robustness of OFDM against the radio channel time-dispersion, but also to the flexibility and adaptability in the assignment of the frequency resources [52]-[63].

The focus of this Chapter is to provide a review of these link adaptation techniques based on power allocation and also to develop an evolutive solution to adapt power allocation for different MC systems in a simple and efficient way.

The rest of the chapter is organized as follows. In the next Section, we summarize the principle of adaptive modulation and describe the proposed scheme that combines adaptive modulation and power allocation scheme for OFDM system. Then, we describe in detail the extension of the proposed power allocation scheme to MIMO-OFDM. This description includes three different power allocation schemes such as the frequency domain power allocation, the spatial domain power allocation and the combined spatial and frequency domains power allocation. Finally, we propose the extension of the power allocation scheme to MIMO MC-CDMA transmission with two-dimensional spreading. To verify the validity of the different extensions, performance results are presented for different channel environments and several channel coding scheme. For the specific extension of MIMO MC-CDMA, results including ~~channel limited feedback~~ are also introduced. Finally, conclusions are drawn.

4.2 Proposed Power Allocation Scheme for Adaptive Modulation OFDM Systems

4.2.1 Subcarrier Adaptive Modulation

Adaptive transmission techniques enable a spectrally efficient transmission over frequency selective channels. The basic premise is to estimate the channel at the receiver and feed this estimate back to the transmitter, so that the transmission scheme can be adapted relative to the channel characteristics. In the case of not adapting to the fading conditions, the error probability is dominated by the subcarriers in deep fade. Thus, a fixed link margin is required to maintain an acceptable performance under worse-case channel conditions. This results in a suboptimal use of the channel. Adapting to the channel fading can increase the average through-

put or reduce average BER by taking advantage of channel conditions. Subcarrier Adaptive Modulation is a form of adaptive transmission technique that assigns to each subcarrier the most efficient modulation under the system constraints.

4.2.2 State-of-Art of Subcarrier Adaptive Modulation

The principle of adapting transmission parameters to the channel conditions in narrowband fading channels was first proposed by Hayes [53] in 1968, and by Cavers [54] in 1972. In 1989, Kalet [55] proposed, for the first time, adaptive modulation over OFDM, and later Czylwik ^{et} al. [56], Chow and al. [36] further developed this idea. These pioneer works on subcarrier adaptive modulation emphasize the benefits of the adaptive modulation scheme in frequency-selective channels. Furthermore, when the channel conditions are available to both the transmitter and the receiver, the channel capacity is achieved if the modulation of individual subcarriers as well as power are optimally adapted to the sub-channel fading conditions, where the optimal power allocation is the "water-filling" [37]. However, while "water-filling" yields the optimal solution, it is computationally expensive and assumes infinite granularity in constellation size, which is not realizable. There are several theoretical works that propose sub-optimal but practical adaptive loading (modulation and/or power) algorithms. In [57], Z. Song et al. proposed a statistical adaptive modulation for quadrature amplitude modulation (QAM)-OFDM systems. The modulation selection is performed by an iterative process so as to minimize the BER, which implies high computational and system complexity. [58] proposes two different block adaptive modulation techniques, which allocate the same modulation level for adjacent subcarriers following an iterative Greedy process [59]. However, joint power allocation is not included in [58] and the adjacent criteria to allocate similar modulation is affected both by the channel variations and also the system parameters. In [39], a method to improve the modulation selection including the long-term power prediction scheme is proposed. The data rate and the transmit power are both adapted to maximize the spectral efficiency. However, in the methods presented in [37]-[39], the adaptative modulation and/or the power allocation are performed among all the subcarriers by an iterative process. In addition, some of the current wireless OFDM standards, such as the Wireless LAN IEEE 802.11a [29] and 802.11g [30]

Indent

standards, use the same modulation and coding type across all subcarriers, and adapt the modulation and coding scheme to the temporal variations in the channel rather than its frequency variations. On the other hand, some other standards use a form of adaptive modulation and coding (AMC) similar to the subcarrier AMC. The closest standard is the IEEE 802.16e with OFDMA that has been selected by the WiMAX Forum as the basic technology for portable and mobile applications. In this standard, to keep the signalling overhead low, the subcarriers are grouped into a small number of blocks (e.g. 10) and different modulation and coding modes are used across different blocks, while a single mode is used across all subcarriers within a block. In WiMAX, the FFT-size can vary from 128 to 2,048 depending on the available bandwidth, but the subcarrier spacing is fixed at 10.94 kHz [5]. Similar approach has been recently validated at the 3GPP level for the 3G LTE [4].
 Wired cable modem standards, such as digital subscriber line (DSL) [60], use subcarrier adaptive modulation technique, but as these systems have very stable channel characteristics, they are quite different from the wireless case. In particular, during the initialization phase of each session, they can spend a long time to acquire accurate SNR estimations. However, the overhead from such protocol cannot be afforded by the changing wireless channel.

4.2.3 Proposed Power Allocation Combined with Adaptive Modulation

In this section, we consider power distribution combined with adaptive modulation for the t -th subcarrier group under the condition that the average transmit power and the average modulation level are kept constant to be \bar{P} and \bar{B} , respectively.

Similarly, the power distribution described in Chapter 3, we define a modulation level vector and a modulation level vector for the t -th subcarrier as $\mathbf{B} = [B_0 \dots B_{N-1}]^T$ and $\mathbf{B}'^{(t)} = [B'_{t,N_s} \dots B'_{t,N_s+N_s-1}]^T$, respectively. Also, we denote optimum vectors of \mathbf{B} and $\mathbf{B}'^{(t)}$ as $\mathbf{B}_o = [B_{0,o} \dots B_{N-1,o}]^T$ and $\mathbf{B}'_o^{(t)} = [B'_{t,N_s,o} \dots B'_{t,N_s+N_s-1,o}]^T$, respectively. \mathbf{B}_o is expressed as

$$\mathbf{B}_o = \mathbf{F}^{-1} \cdot \mathbf{D}^{-1} \cdot \mathbf{B}'_o. \quad (4.1)$$

where $\mathbf{B}'_o = [\mathbf{B}'_o^{(0)T} \dots \mathbf{B}'_o^{(N/N_s-1)T}]^T$.

The optimization problem can be given by

$$\left\{ \begin{array}{l} (\mathbf{p}_o'^{(t)}, \mathbf{B}_o'^{(t)}) = \arg \min_{\mathbf{p}'^{(t)}, \mathbf{B}'^{(t)}} \sum_{k=0}^{N_s-1} \frac{f(M'_{t \cdot N_s + k}, p'_{t \cdot N_s + k})}{N_s} \\ \text{s.t. } \sum_{m=0}^{N_s-1} B'_{t \cdot N_s + m} = N_s \cdot \bar{B} \\ \text{s.t. } \sum_{m=0}^{N_s-1} p'_{t \cdot N_s + m} = N_s \cdot \bar{P} \end{array} \right. \quad (4.2)$$

where $M'_{t \cdot N_s + k} = 2^{B'_{t \cdot N_s + k}} - 1$. To solve the problem, we have firstly to obtain a closed form solution for the power distribution in terms of modulation levels by solving

$$\left\{ \begin{array}{l} \mathbf{p}_o'^{(t)} = \arg \min_{\mathbf{p}'^{(t)}} \sum_{m=0}^{N_s-1} \frac{f(M'_{t \cdot N_s + m}, p'_{t \cdot N_s + m})}{N_s} \\ \text{s.t. } \sum_{m=0}^{N_s-1} p'_{t \cdot N_s + m} = N_s \cdot \bar{P} \end{array} \right. \quad (4.3)$$

Since this is a common minimization problem with a linear constraint, we can solve it by using the Lagrange multiplier method. The closed form optimum solution is expressed as

$$\begin{aligned} p'_{t \cdot N_s + m, o} &= \left[\sum_{u=0}^{N_s-1} \frac{M'_{t \cdot N_s + u} \cdot \alpha_{t \cdot N_s + m} \cdot b_m}{M'_{t \cdot N_s + m} \cdot \alpha_{t \cdot N_s + u} \cdot b_u} \right]^{-1} \cdot \left[N_s \bar{P} \right. \\ &\quad \left. + \sum_{u=0}^{N_s-1} \frac{M'_{t \cdot N_s + m}}{\alpha_{t \cdot N_s + u} \cdot b_u} \log \left(\frac{M'_{t \cdot N_s + u} \cdot \alpha_{t \cdot N_s + m} \cdot a_m \cdot b_m}{M'_{t \cdot N_s + m} \cdot \alpha_{t \cdot N_s + u} \cdot a_u \cdot b_u} \right) \right]. \end{aligned} \quad (4.4)$$

Since we have ignored the range of $p'_{t \cdot N_s + m}$ for the sake of simplicity, the solution may result in $p'_{t \cdot N_s + m, o} < 0$ for some cases. In this case, we propose to apply equal power distribution for the subcarrier group.

By substituting (4.3) into (4.2), we obtain an optimization problem for the adap-

tive modulation as

$$\left\{ \begin{array}{l} \mathbf{B}_o^{(t)} = \arg \min_{\mathbf{B}'^{(t)}} \sum_{m=0}^{N_s-1} \frac{f(M'_{t \cdot N_s+m}, p'_{t \cdot N_s+m, o})}{N_s} \\ \text{s.t. } \sum_{m=0}^{N_s-1} B'_{t \cdot N_s+m} = N_s \cdot \bar{B} \end{array} \right. . \quad (4.5)$$

Unlike (4.3), it is difficult to obtain a closed form solution of (4.5). However, thanks to a lower number of subcarriers due to the proposed subcarrier group selection and the limited number of choices of modulation level in general, we can search modulation schemes exhaustively in order to obtain the solution of (4.5). More precisely, we firstly select all the possible modulation level vectors which satisfy the constraint on the average modulation level. For each modulation level vector, the optimum transmission power of each subcarrier is obtained by (4.4). Then, we compute the cost function in (4.5) for this modulation level vector, and finally, we select a vector which minimizes the average BER.

4.3 Power Allocation Scheme for MIMO OFDM Systems

In this section, we will use this heuristic BER approximation to evaluate the power allocation scheme and then we adjust the BER approximation based on computer matching. The approximation can be expressed as

$$f(\beta_{l,m}, p_{l,m}) \approx a \cdot \exp \{ -b \cdot \beta_{l,m} \cdot p_{l,m} \} \quad (4.6)$$

where $\beta_{l,m}$ is equal to

$$\beta_{l,m} = \frac{1}{(2^{N_m} - 1) \cdot \sigma_n^2 \cdot \sum_{n=0}^{N_r-1} |g_m^{(l,n)}|^2} \quad (4.7)$$

where σ_n^2 denotes the variance of the AWGN and $\beta_{l,m}$ denotes the received SNR, which depends on the modulation scheme and the equalizer weights on the m -th subcarrier and l -th transmit antenna. $p_{l,m}$ denotes the transmit power m -th sub-

and

carrier and l -th transmit antenna. The parameters a and b are to be determined in a heuristic way, namely, via computer simulations.

The proposed scheme is based on a procedure which consists of optimizing the transmit power in terms of an expression for the approximated BER under power constraint and considering the subcarrier grouping scheme for frequency domain based power allocation. We next review the possible strategies to allocate power for both optimal and suboptimal solutions.

Let us first define the matrix representation of transmit power as

$$\mathbf{p}'_o = \begin{bmatrix} p'_{0,0,o} & \cdots & p'_{0,N-1,o} \\ \vdots & & \vdots \\ p'_{N_t-1,0,o} & \cdots & p'_{N_t-1,N-1,o} \end{bmatrix} \quad (4.8)$$

In this Chapter, we consider power distribution with the condition that the average transmit power per symbol is kept constant to be \bar{P} .

4.3.1 Combined Spatial and Frequency Domains Power Allocation

The basic principle of the combined spatial and frequency domains power allocation for MIMO-OFDM signal is to combine spatial and frequency domains optimization [62] of the transmit power as a function of the heuristic BER expression [63] defined previously. The Lagrangian optimization method will be used to obtain an analytical value of the power allocation for each load subcarrier. Furthermore, a constraint is added in order to keep the global transmit power at the transmitter constant. The optimal case is to consider the power allocation scheme through one MIMO-OFDM symbol which is represented by $(N \cdot N_t)$ elements. However, due to the computation complexity to perform this power allocation scheme, we propose to perform it through a limited number of N_s subcarriers and then repeat the allocation scheme N/N_s times.

Let us first define the proposed transmit power matrix of the t -th subcarrier group
indent

as

$$\mathbf{p}_o'^{(t)} = \begin{bmatrix} p_{0,t \cdot N_s, o}' & \cdots & p_{0,(t+1) \cdot N_s - 1, o}' \\ \vdots & & \vdots \\ p_{N_t - 1, t \cdot N_s, o}' & \cdots & p_{N_t - 1, (t+1) \cdot N_s - 1, o}' \end{bmatrix} \quad (4.9)$$

with

$$\boldsymbol{\beta}'^{(t)} = [\beta'_{t \cdot N_s} \cdots \beta'_{t \cdot N_s + N_s - 1}]^T, \quad (4.10)$$

where $\boldsymbol{\beta}'^{(t)}$ denotes the t -th group of elements, $(t = 0, \dots, N/N_s - 1)$.

Then, the optimization problem can be stated as

$$\left\{ \begin{array}{l} \mathbf{p}_o'^{(t)} = \arg \min \sum_{l=0}^{N_t-1} \sum_{m=0}^{N_s-1} \frac{f(\beta'_{l,t \cdot N_s + m}, p'_{l,t \cdot N_s + m})}{N_s \cdot N_t} \\ \text{s.t. } \sum_{l=0}^{N_t-1} \sum_{m=0}^{N_s-1} p'_{l,t \cdot N_s + m} = N_s \cdot N_t \cdot \bar{P} \end{array} \right. \quad (4.11)$$

After calculation and rearrangement for $0 \leq l < N_t$ and $0 \leq m < N_s$, we obtain

$$\begin{aligned} p_{l,t \cdot N_s + m, o} &= \left[\sum_{u=0}^{N_t-1} \sum_{v=0}^{N_s-1} \frac{\beta_{l,t \cdot N_s + m}}{\beta_{u,t \cdot N_s + v}} \right]^{-1} \cdot \left[N_t \cdot N_s \cdot \bar{P} \right. \\ &\quad \left. + \frac{1}{b} \cdot \sum_{u=0}^{N_t-1} \sum_{v=0}^{N_s-1} \frac{1}{\beta_{u,t \cdot N_s + v}} \cdot \log \left(\frac{\beta_{l,t \cdot N_s + m}}{\beta_{u,t \cdot N_s + v}} \right) \right] \end{aligned} \quad (4.12)$$

We repeat the power allocation process for each subset of subcarriers and transmit antennas which compose the MIMO-OFDM symbol and each transmit antenna.

4.3.2 Spatial Domain Power Allocation Scheme

For the specific case of spatial domain power allocation, the optimization problem described in (4.11) can be simplified and described for $0 \leq m < N$ as

$$\left\{ \begin{array}{l} \mathbf{p}_o'^{(t)} = \arg \min \sum_{l=0}^{N_t-1} \frac{f(\beta'_{l,m}, p'_{l,m})}{N_t} \\ \text{s.t. } \sum_{l=0}^{N_t-1} p'_{l,m} = N_t \cdot \bar{P} \end{array} \right. \quad (4.13)$$

Then, after some calculations and similar rearrangements presented in the previous Section, we obtain the following solution for $0 \leq m < N$

$$p_{l,m} = \left[1 + \sum_{\substack{u=0 \\ u \neq l}}^{N_t-1} \frac{\beta_{l,m}}{\beta_{u,m}} \right]^{-1} \cdot \left[N_t \bar{P}_m + \frac{1}{b} \times \sum_{\substack{u=0 \\ u \neq l}}^{N_t-1} \frac{1}{\beta_{u,m}} \times \log \left(\frac{\beta_{l,m}}{\beta_{u,m}} \right) \right] \quad (4.14)$$

4.3.3 Frequency Domain Power Allocation Scheme

Without considering the spatial freedom axis, the optimization problem, described in (4.11), can be restricted to the frequency domain. Then, the problem description is, for $0 \leq l < N_t$, equal to

$$\begin{cases} p_o'(t) = \arg \min \sum_{m=0}^{N_s-1} \frac{f(\beta'_{l,t \cdot N_s+m}, p'_{l,t \cdot N_s+m})}{N_s} \\ \text{s.t. } \sum_{m=0}^{N_s-1} p'_{l,t \cdot N_s+m} = N_s \cdot \bar{P} \end{cases} \quad (4.15)$$

We solve the optimization problem by performing the Lagrange multiplier using similar rearrangements as previously presented. The closed form optimal solution is obtained, for $0 \leq l < N_t$, as

$$p'_{l,t \cdot N_s+m, so} = \left[\sum_{u=0}^{N_s-1} \frac{\beta'_{l,t \cdot N_s+m}}{\beta'_{l,t \cdot N_s+u}} \right]^{-1} \cdot \left[N_s \bar{P} + \sum_{u=0}^{N_s-1} \frac{1}{\beta'_{l,t \cdot N_s+u} \cdot b} \log \left(\frac{\beta'_{l,t \cdot N_s+m}}{\beta'_{l,t \cdot N_s+u}} \right) \right]. \quad (4.16)$$

4.4 Power Allocation Scheme for MIMO MC-CDMA Systems

4.4.1 State-of-Art of MIMO MC-CDMA Systems

OFDM based transmission, CDMA concepts [8], [47] and their hybrid solutions such as MC-CDMA with two dimensional spreading combined with multiple antennas [48] are regarded as a possible candidate for the B3G mobile communications [49], especially for synchronous DL [50]-[51]. This is mainly due to the robustness of OFDM against the radio channel time-dispersion, but also to the flexibility and adaptability in the assignment of the frequency resources [52]-[63].

One major advantage of MC-CDMA compared to multi-user OFDM transmission is that a higher order of frequency diversity is achieved because each user utilizes all the subcarriers, and code diversity can be also obtained by the users. A conventional MC-CDMA transmitter uniformly distributes available power among the users and spreads the signal into all the subcarriers, however, adaptive power allocation depending on the channel condition can improve the performance. In [64], an on-off control scheme is proposed to adapt power distribution and spreading code allocation to the different active users. In [65], the authors have considered the problem of allocating power among the subcarriers of each user. In [40], the authors have proposed a simple and analytical method to allocate power in the frequency domain for OFDM signals, but no extension to MC-CDMA or MIMO system has been proposed. More recently, we have proposed a simple power allocation scheme for MIMO OFDM systems [66] based on an analytical minimization of average BER.

4.4.2 Proposed Power Allocation Scheme for MIMO MC-CDMA Systems

In this section, we will use this heuristic BER approximation to evaluate the power allocation scheme based on the expression

$$f(\beta_{k,m}^l, p_{k,m}^l) \approx a \cdot \exp \{ - b \cdot \beta_{k,m}^l \cdot p_{k,m}^l \}, \quad (4.17)$$

$$\beta_{k,m}^l = \frac{1}{(2^\zeta - 1) \cdot \sigma_n^2 \cdot F_{k,m}^l}, \quad (4.18)$$

with

$$F_{k,m}^l = \frac{1}{SF_f} \cdot \sum_{n=0}^{N_r-1} \sum_{q=0}^{SF_f-1} |G_{q+SF_f, m}^{(k,l,n)}|^2, \quad (4.19)$$

where a and b are heuristic parameters to be evaluated and ζ is the number of bits per modulated symbol.

The proposed method is a joint optimization procedure of the power distribution for the code and the spatial domains, in other words, the active users and the transmit antennas, therefore, we can obtain a global solution of the power allocation. The goal of the proposed power allocation for a two-dimensional spreading MC-CDMA signal with multiple antennas is to obtain the transmit power distribution that minimizes the average BER of all the active users by utilizing the approximated

BER expression. Furthermore, a constraint on the maximum total transmit power is imposed [63].

The global power resource assigned by the proposed algorithm satisfies a constraint that the total transmit power is kept constant among the transmit antenna and the active users, namely, for the m -th modulated element ($m = 0, \dots, N/SF_f$)

$$\sum_{l=0}^{N_t-1} \sum_{k=0}^{N_u-1} p_{k,m}^l = N_t \cdot N_u \cdot \bar{P}. \quad (4.20)$$

Based on the optimization method described in [40], the average BER becomes minimal when the BER is minimized for each given channel state. The optimization problem for the m -th modulated element is described by

$$\left\{ \begin{array}{l} p_{k,m,o}^l = \arg \min \sum_{l=0}^{N_t-1} \sum_{k=0}^{N_u-1} \frac{f(\beta_{k,m}^l p_{k,m}^l)}{N_t \cdot N_u} \\ \text{s.t. } \sum_{l=0}^{N_t-1} \sum_{k=0}^{N_u-1} p_{k,m}^l = N_t \cdot N_u \cdot \bar{P} \end{array} \right. \quad (4.21)$$

where $p_{k,m,o}^l$ represents the optimum solution of the proposed problem. Since this is a common minimization problem with a linear constraint, we can solve it by using Lagrange multiplier method and the closed form optimum solution is obtained as

$$p_{k,m,o}^l = \left[\sum_{\alpha=0}^{N_t-1} \sum_{\gamma=0}^{N_u-1} \frac{F_{\gamma,m}^\alpha}{F_{k,m}^l} \right]^{-1} \cdot \left[N_t \cdot N_u \cdot \bar{P} + \sum_{\alpha=0}^{N_t-1} \sum_{\gamma=0}^{N_u-1} \frac{1}{b \cdot \beta_{\gamma,m}^\alpha} \cdot \log \left(\frac{F_{\gamma,m}^\alpha}{F_{k,m}^l} \right) \right]. \quad (4.22)$$

Since we have ignored the range of $p_{k,m}$ so far for simplicity, the Lagrangian procedure sometimes results in negative values. In this case we propose to use the equal power distribution scheme.

4.5 Numerical Experimentation

4.5.1 Power Allocation with Adaptive Modulation

This section gives an evaluation of the performance of the proposed power allocation method for OFDM systems in a multipath fading environment. Simulation parameters are given in Table 4. We assume perfect knowledge of the CSI both at the transmitting and receiving parts. For all simulations, the delay power spectrum is

Table 4.1: Simulation Parameters

Carrier frequency	2.4 GHz
Bandwidth	20 MHz
Modulation scheme	QPSK, 16-QAM, 64-QAM
Channel encoder	No code and convolutional codes
Channel estimation	Perfect CSI
Number of data subcarriers	64
GI length	16
Channel model	10-path, Rayleigh Fading
Sample period	0.05 μ s
Number of data packets	40
Group size (N_s)	2, 4, 8, 16, 32, 64

assumed to be an exponential decay model with 1 dB decaying per sampling period. The carrier frequency is equal to 2.4 GHz, the IFFT/FFT size is 64 points and the GI is set to 16 samples. The ZF detection scheme is employed in the receiver.

Figs. 4.1 and 4.2 show the BER performances against the total SNR in dB for the adaptive modulation combined with power distribution case, for three different coding gains, $R=1/2$, $3/4$, and 1. For reference, the BER performance of the adaptive modulation scheme without power adaptation is plotted. It consists of selecting the sequence of modulation levels that minimizes the heuristic expression of the BER in the specific configuration with equal distribution of the power through an exhaustive search of the OFDM symbol. The minimization is performed through all the subcarriers ($N_s = 64$). For the proposed adaptive modulation and power distribution, the results are presented for two sizes of subcarrier grouping, $N_s = 4$

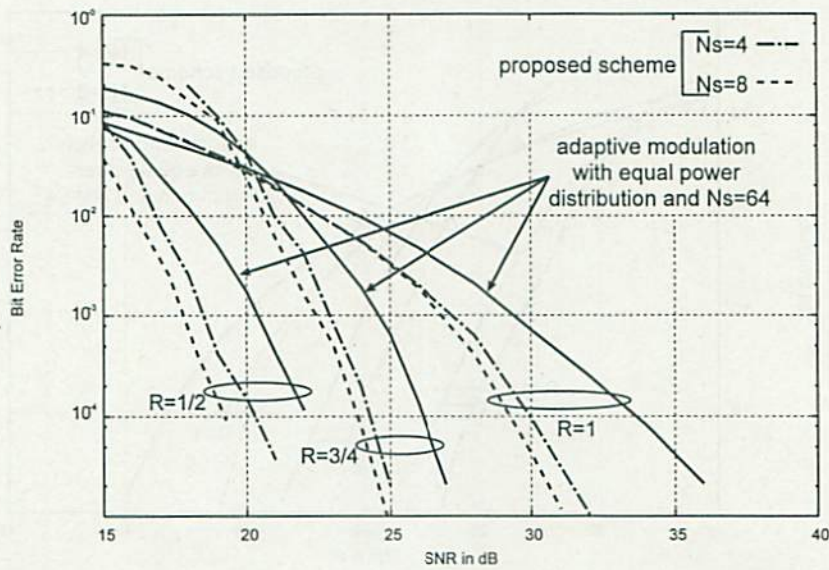


Figure 4.1: BER performance for uncoded and coded OFDM with $\bar{B} = 3$

and 8. Fig. 4.1 shows significant performance gain by simply performing the proposed power allocation scheme combined with adaptive modulation for an average bits per symbol of 3. At $BER=10^{-4}$ and $R = 1$, an average performance gain of 3dB is obtained for the case of $N_s = 4$. The performance gain increases to 4dB for the case $N_s = 8$. In addition, coding gain does not affect the performance gain of the proposed scheme. A similar gain is obtained for the two sizes of subcarrier grouping for $R=1/2$ and $3/4$. Fig. 4.2 shows the BER performance for the case that the average number of bits per symbol is equal to 5. A significant performance gain is also obtained by performing the proposed adaptive modulation and power allocation scheme. *The gain of 2.5dB gain* is obtained, on average, for the different coding gains and $N_s = 4$. However, these results highlight the limited gain performed by large sizes of subcarrier groups. The difference of the gain is only 1dB between $N_s = 4$ and $N_s = 8$ for the case of $R = 1$ and only 0.5dB gain is obtained which is low, compared to the coding gains for $R = 1/2$ and $3/4$.

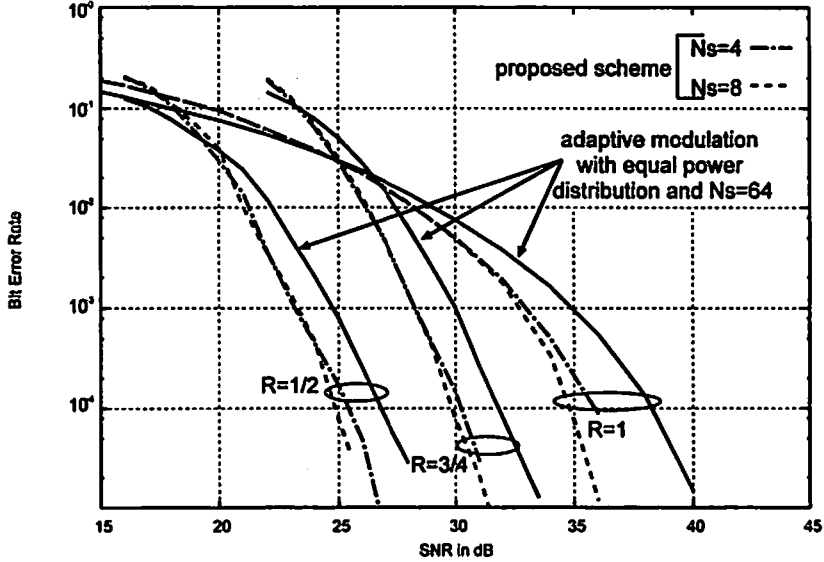


Figure 4.2: BER performance for uncoded and coded OFDM with $\bar{B} = 5$

4.5.2 Power Allocation Scheme for MIMO OFDM Systems

Software Simulation

We now evaluate the performance of the proposed power allocation method for MIMO-OFDM scheme in a multi-path fading environment with ZF detection. We assume, as described in Table 4.2 perfect knowledge of the channel variations both at the transmitting and receiving parts. An exponentially decaying (1-dB decay) multi-path model is assumed and the carrier frequency is equal to 2.4 GHz. The IFFT/FFT size is 64 points and the GI is set to be 16 samples [30].

The effect of the combined frequency and spatial domains power allocation scheme for several subset sizes is highlighted for the specific antenna configuration $N_t = N_r = 4$, without channel encoder $R=1$ for QPSK and QAM modulations.

Figs. 4.3, 4.4, and 4.5 show the BER versus the total received SNR (dB) of the proposed scheme with various subcarrier group sizes N_s . The BER performance of the conventional scheme (equal power distribution) is also plotted in the same figure.

The simulation results in Fig. 4.3 show that, for QPSK modulation at average $\text{BER}=10^{-4}$, 2.8, 4.5, 5.2, 6.1, and 8.7 dB gains are obtained respectively for $N_s=2, 4, 8, 16$ and 64. For reference, we have plotted the performance of the exact

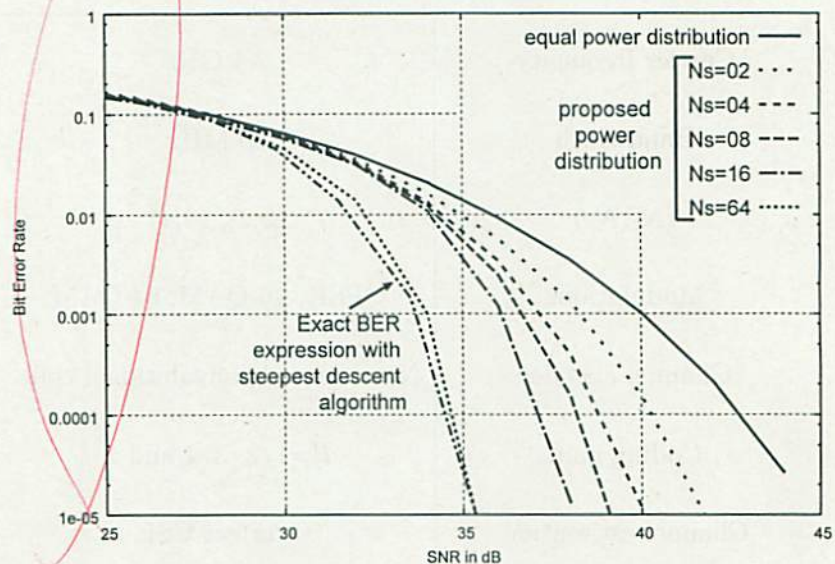


Figure 4.3: BER performance for QPSK modulation and coding rate $R=1$

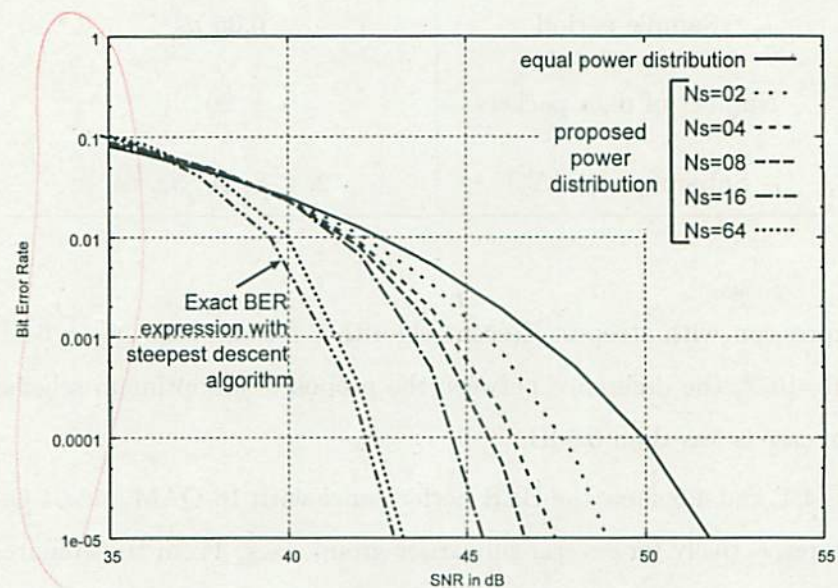


Figure 4.4: BER performance for 16-QAM modulation and coding rate $R=1$

Table 4.2: Simulation Parameters

Carrier frequency	2.4 GHz
Bandwidth	20 MHz
(N_t, N_r)	(2,2), (4,4)
Modulations	QPSK, 16-QAM, 64-QAM
Channel encoder	No code and convolutional code
Coding gain	$R=1/2, 3/4$ and 1
Channel estimation	Perfect CSI
Number of data subcarriers	64
GI length	16
Channel model	5-path, Rayleigh Fading
Sample period	$0.05 \mu s$
Number of data packets	20
Subgroup size (N_s)	2, 4, 8, 16, 32, 64

BER expression with steepest descent algorithm for the case $N_s = 64$. At average BER= 10^{-4} , the difference between the proposed suboptimum scheme and the optimum case is less than 0.6dB.

Figs. 4.4, and 4.5 show the BER performance with 16-QAM and 64-QAM modulations, respectively for several subcarrier group sizes. From these figures, we can see that the proposed scheme can achieve significant performance gain also for QAM modulations.

It is shown that the subcarrier grouping size strongly affects the performance of the proposed scheme for both QPSK and QAM modulations. However, due to the

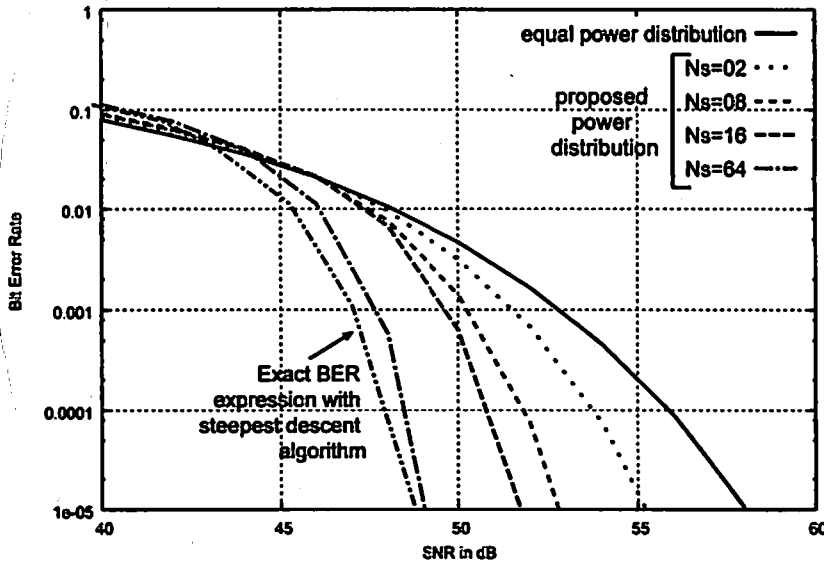


Figure 4.5: BER performance for 64-QAM modulation and coding rate $R=1$

structure of the proposed power distribution scheme, there is a trade-off between the subcarrier grouping size and the computational complexity.

Field Experimentation

We now evaluate the performance of the different power allocation methods for the MIMO-OFDM system in a real environment. The main system parameters are based on the IEEE 802.11a standard with time division multiplexing for pilot structure. In addition, a Viterbi algorithm is included to decode the received signal. Experimentation was carried out in an indoor environment and the channel was considered quasi-static during one frame transmission [67]. Channel 3 in the 5 GHz frequency band ($F_c = 5210\text{MHz}$) was used to transmit data and to evaluate the channel response. Furthermore, off-line processing was performed to extract the channel gains and delay for each significant path. The transmitter comprised two IEEE 802.11a WLAN cards and the separation between the antenna elements was equal to 6λ , where λ represents the carrier wavelength. The receiving part was composed of a two-element antenna and the adjacent spacing was equal to $3\lambda/2$. Such spacing was employed since the mutual coupling influence is low with this distance [68]. In addition, the ZF detection scheme was employed in the receiver

and the baseband processing was performed off-line for all the experimentations.

Fig. 4.6 shows the layout of the room where experimentation was done and the different positions of the different antenna elements. Typically, NLOS scenario is highlighted in this experimentation. The environment simulates a typical modern open office where several desks are set up in the same room.

Experimental Results for Position 1

Table 4.3 shows the average transmit SNR in dB for an average $\text{BER}=10^{-5}$ in the case of channel coding $R = 1/2$ and several modulation schemes (i.e. QPSK, 16-QAM and 64-QAM). For reference in the table, S domain, F domain and S+F domain respectively denote the spatial power allocation scheme, the frequency domain power allocation, and the combined spatial and frequency domain power distribution. In addition, equal power denotes the conventional transmission without any specific power allocation. As described in Table 4.3, a gain of about 4dB is obtained by performing simply the combined spatial and frequency domains power allocation scheme with $N_s = 16$, compared to the equal power distribution method for the QPSK modulation. In the case of 16-QAM and 64-QAM modulations, a gain of about 3dB is obtained for the conditions described above. In the case of the power allocation scheme in the spatial domain, 0.7, 0.4 and 0.3dB gains are obtained for QPSK, 16-QAM and 64-QAM modulations respectively. In addition, on average, 0.4dB gain is obtained for the three different modulations (QPSK, 16-QAM, 64-QAM) by extending the power allocation to both the spatial and frequency domains compared to the frequency domain only.

Experimental Results for Position 2

Table 4.4 the average transmit SNR in dB for an average $\text{BER}=10^{-5}$ in the case of channel coding $R = 1/2$ and several modulation schemes (i.e. QPSK, 16-QAM and 64-QAM). In this table, the effect of the different power allocation schemes for several subset sizes is highlighted for the antenna configuration $N_t = N_r = 2$ at the position denoted 2 in Fig. 4.6 for QPSK and QAM modulations.

For QPSK modulation scheme, channel coding rate $R = 1/2$, the specific MIMO configuration $N_t = N_r = 2$ and various subcarrier group sizes N_s , the BER performances of the conventional scheme (equal power distribution) is also plotted in the same figure. According to the experimentations, at average $\text{BER}=10^{-5}$, 0.3dB gains

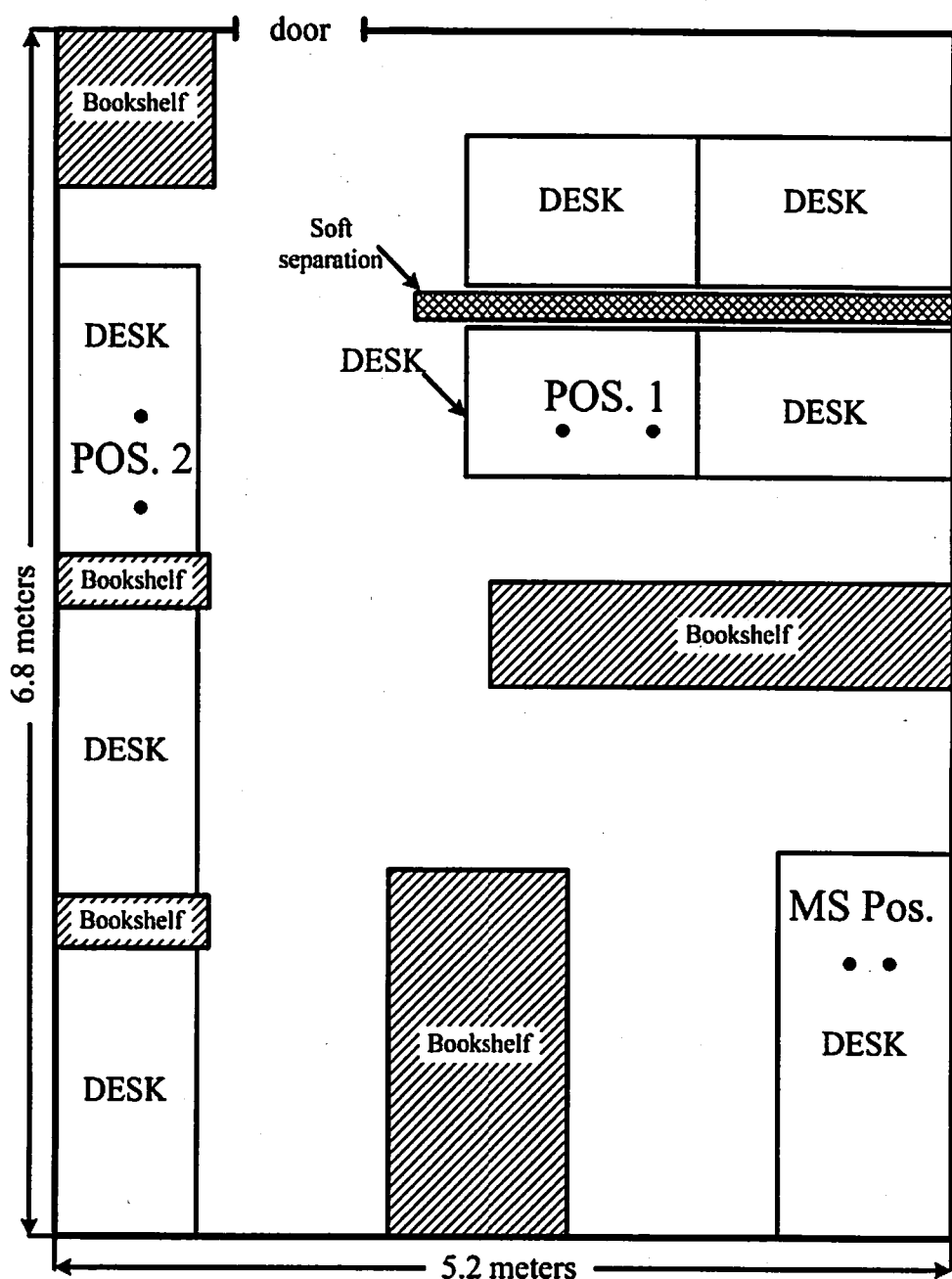


Figure 4.6: Layout of the room

Table 4.3: Average SNR (dB) for $BER=10^{-5}$ at the position 1

Modulation	QPSK	16-QAM	64-QAM
equal power	30.5	35.4	37.5
S domain	29.8	35.0	37.2
F domain, $N_s = 2$	29.6	34.4	36.9
F domain, $N_s = 4$	28.9	34.1	36.5
F domain, $N_s = 8$	28.1	33.9	35.8
F domain, $N_s = 16$	27.1	33.0	35.0
S+F domains, $N_s = 2$	29.3	34.0	36.6
S+F domains, $N_s = 4$	28.4	33.75	36.3
S+F domains, $N_s = 8$	27.8	33.5	35.6
S+F domains, $N_s = 16$	26.6	32.6	34.7

is obtained for the spatial domain power allocation scheme compared to the conventional scheme. In the case of the frequency domain power allocation, respectively 0.5, 1.3, 2.1 and 3.1dB gains are obtained for $N_s = 2$, $N_s = 4$, $N_s = 8$ and $N_s = 16$, compared to the equal power distribution. For frequency and spatial domains power distribution, gains of 0.7, 1.6, 2.3 and 3.4dB are obtained for $N_s = 2$, $N_s = 4$, $N_s = 8$ and $N_s = 16$, respectively, compared to the equal power distribution. So, for QPSK modulation and $N_t = N_r = 2$, the main gain is obtained by the frequency domain power allocation for MIMO-OFDM transmission. Extension to the spatial domain allows an additional 0.3dB gain compare to the equal power distribution.

Table 4.4 presents the average transmit SNR in dB for an average $BER=10^{-5}$ of the different power allocation schemes with QAM modulations and various subcar-

Table 4.4: Average SNR (dB) for $BER=10^{-5}$ at the position 2

Modulation	QPSK	16-QAM	64-QAM
equal power	30.3	33.4	36.9
S domain	30.0	33.1	36.6
F domain, $N_s = 2$	29.8	32.8	36.2
F domain, $N_s = 4$	29.0	33.2	35.6
F domains, $N_s = 8$	28.1	31.1	34.2
F domains, $N_s = 16$	27.0	29.9	32.9
S+F domain, $N_s = 2$	29.4	32.5	35.9
S+F domain, $N_s = 4$	28.8	31.8	35.2
S+F domains, $N_s = 8$	27.9	30.8	34.0
S+F domains, $N_s = 16$	26.7	29.6	32.4

rier group sizes N_s too. Similarly to the QPSK modulation, limited gain is obtained, compared to the equal power distribution, for the spatial domain based power allocation. The main additional gain is highlighted for the frequency domain power allocation and large number for N_s .

4.5.3 Power Allocation Scheme for MIMO MC-CDMA Systems

We now evaluate the performance of the proposed power allocation for the two dimensional spreading MC-CDMA scheme with multiple antennas in multi-path fading environments. The simulation parameters are shown in Table 4.5. In all the simulation results, we assume uncorrelated spatial channel model between the different transmit and receive antennas. In addition, the active users are assumed

Table 4.5: Simulation Parameters

Carrier Frequency	2 GHz
Bandwidth	20 MHz
Modulations	QPSK, 16-QAM, 64-QAM
Channel Coding	$R = 1/3, 1/2, 3/4$
Coding Scheme	Convolutional Code (CC), Turbo Code (TC)
Spreading Factor	$SF = 16$
Channel estimation	Perfect CSI
Number of data subcarriers	128
GI length	32
Channel model	Multipath environment
(N_t, N_r)	(2,2), (4,4) and (8,8)
Number of data packets	30

to be randomly spread in the cell and the channel fading is independent between the active users. Simulation environment is similar to [19]. Finally, we assume perfect knowledge of the CSI both at the transmitting and receiving parts. In all the simulation results, conventional scheme means equal power distribution among the different transmit antennas and active users. The proposed scheme denotes the power distribution among the transmit antennas and the active users that we have developed in the previous section.



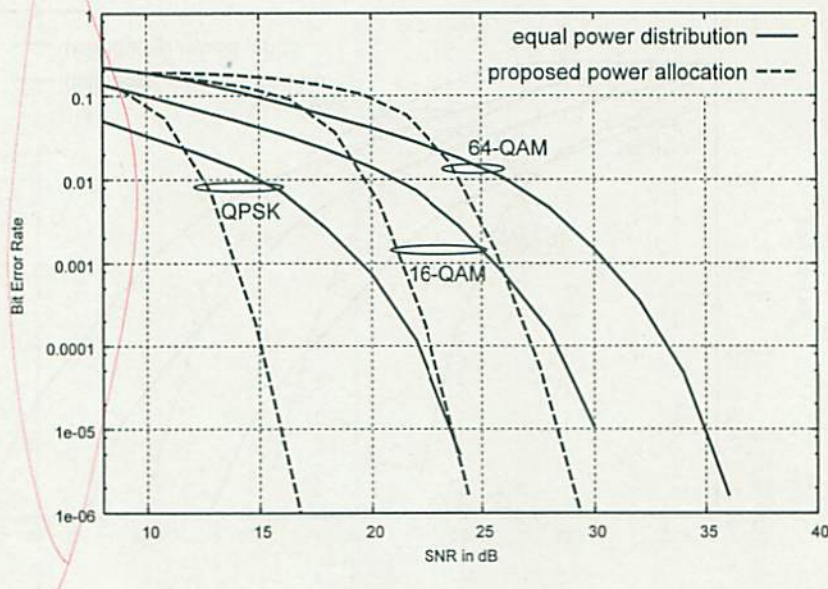


Figure 4.7: BER performance for $N_t = N_r = 2$, $SF_f = SF_t = 4$ and $R = 1/2$

Two Dimensional Spreading with Convolutional Code

Fig. 4.7 shows the BER performance for the two-dimensional spreading and the antenna configuration ($N_t = N_r = 2$) and 12 active users. It is shown that proposed scheme outperforms the equal power distribution for BER value lower than 10^{-2} . Since the parameter b in Eq. (10) has been determined so that the approximated BER fits the simulated BER in the region from 10^{-3} to 10^{-5} , the mismatch between the true and approximated BER could degrade the performance of the proposed scheme outside this region. However, due to practical wireless transmissions requirements for low BER, we especially focus on the average BER lower than 10^{-3} .

It is shown that for the configuration ($N_t = N_r = 2$), respectively 7, 6 and 5dB gains are obtained the QPSK, 16-QAM and 64-QAM modulations. Figs. 4.8 and 4.9 show the computer simulation results for channel coding rate $R = 1/2$, and two spatial configurations. The spreading configuration ($SF_f = SF_t = 4$), 12 active users and different spatial configurations. For $N_t = N_r = 4$, the performance gains obtained by the proposed power allocation schemes are equal to 5dB for QPSK modulation, 6dB for QPSK modulation, 5.5dB for 16-QAM modulation and 4.6dB for 64-QAM modulation at average BER= 10^{-4} . For the spatial configuration $N_t =$

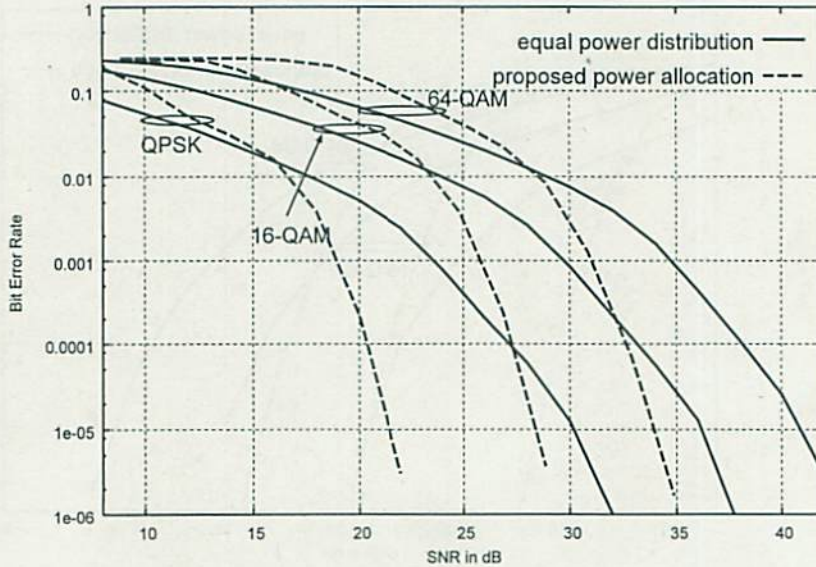


Figure 4.8: BER performance for $N_t = N_r = 4$, $SF_f = SF_t = 4$ and $R = 1/2$

$N_r = 8$, the performance gains are about 7dB for QPSK modulation, 6dB for 16-QAM modulation and 4.9dB for 64-QAM modulation at average $\text{BER}=10^{-4}$.

Fig. 4.10 shows the required SNR for $\text{BER}=10^{-4}$ for the proposed and equal power distribution schemes versus the total number of active users for QPSK, 16-QAM and 64-QAM modulations and $N_t = N_r = 4$. The convolutional code with coding rate of $R = 3/4$ is also employed. The results are presented in the case of two-dimensional spreading ($SF_f = SF_t = 4$) with ZF detection scheme. The performance gains obtained by the proposed power allocation are respectively equal to 5dB, 4dB and 3.8dB for QPSK, 16-QAM and 64-QAM modulations for 12 active users for instance.

Two Dimensional Spreading with Turbo Code

Figs. 4.11 and 4.12 show the BER performance versus the total SNR with 14 active users, frequency domain spreading sequence (i.e. $SF_f = SF_t = 4$), QPSK modulation and different spatial configurations, $N_t = N_r = 2$ and $N_t = N_r = 4$. With the appropriate adaption of the parameter b shown in the table 3, significant

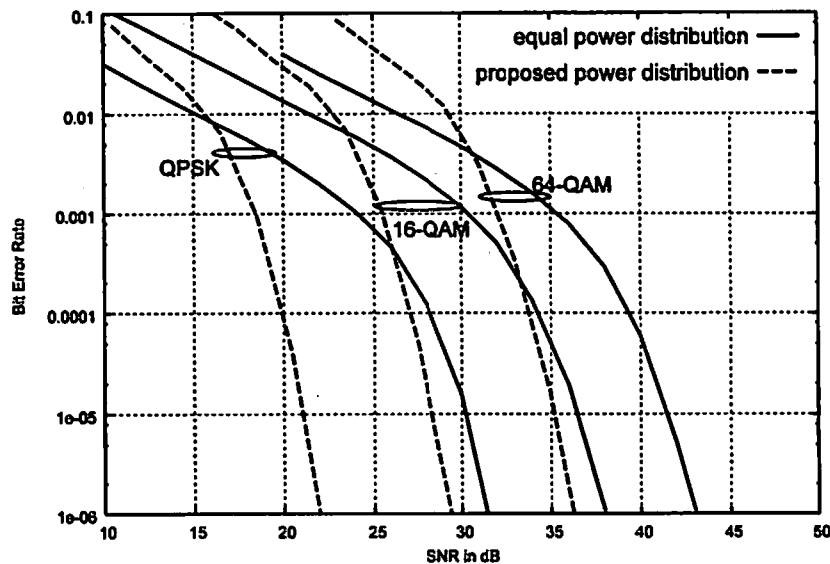


Figure 4.9: BER performance for $N_t = N_r = 8$, $SF_f = SF_t = 4$ and $R = 1/2$

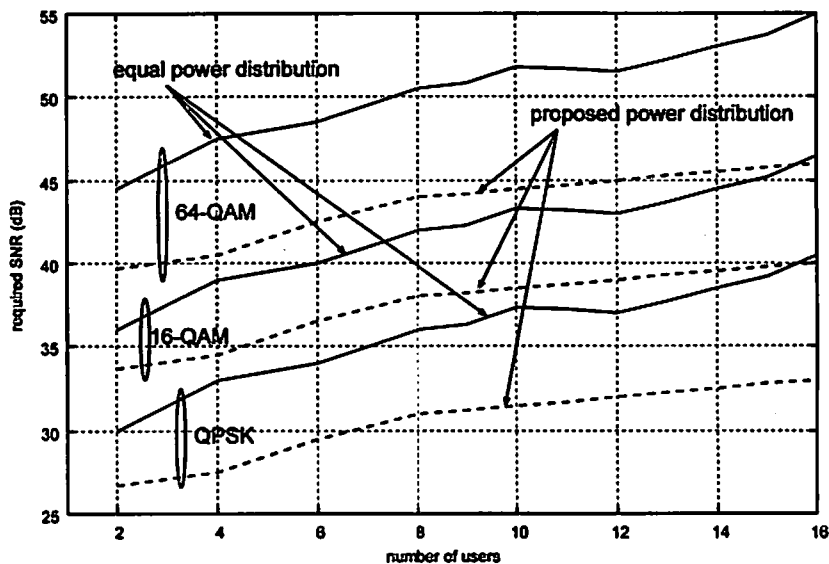


Figure 4.10: Required SNR at $\text{BER}=10^{-4}$ for $N_t = N_r = 4$, $SF_t = SF_f = 4$ and $R = 3/4$

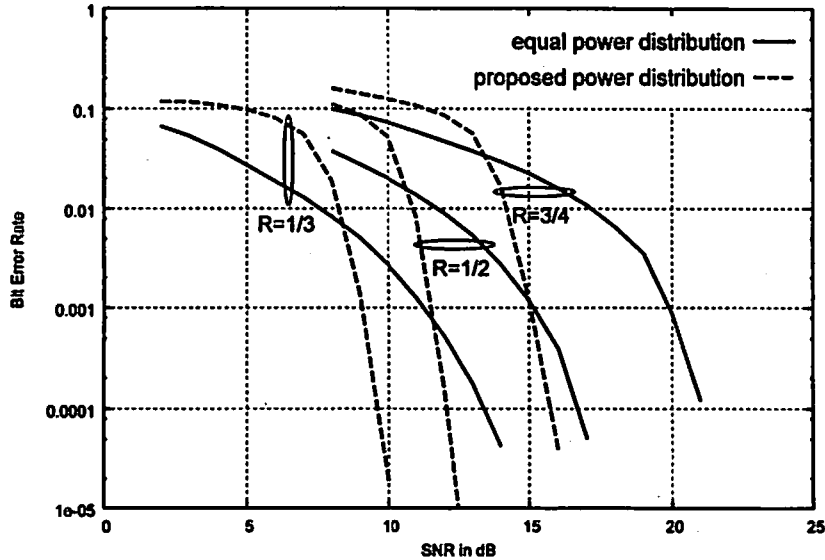


Figure 4.11: BER performance for $N_t = N_r = 2$, $SF_f = SF_t = 4$ and QPSK modulation

gains are obtained for any spatial and channel coding configurations. For example, at $\text{BER}=10^{-4}$ and $N_t = N_r = 4$, respectively 3.5, 4, and 5.5dB gains are obtained by comparing simply the proposed power distribution with the equal equal distribution scheme for $R = 1/3, 1/2$ and $3/4$.

Finally, Figs. 4.13 and 4.14 show the effect of the QAM modulations on the proposed power distribution scheme. The performance gain is highlighted between the proposed distribution and the equal power distribution.

4.5.4 Impact of the Limited Feedback

In a realistic system, quantization errors affect the channel feedback transmission [43]. In [69], detailed description are included for practical scenarios. Since the feedback channel is capacity-limited, the channel response needs to be quantized and the main effect is the inclusion of errors for CSI feedback. In this section, we evaluate the impact of the quantization due to the limited feedback on the proposed power allocation scheme. Let $Q_B(z)$ denote the B bits representation of the real

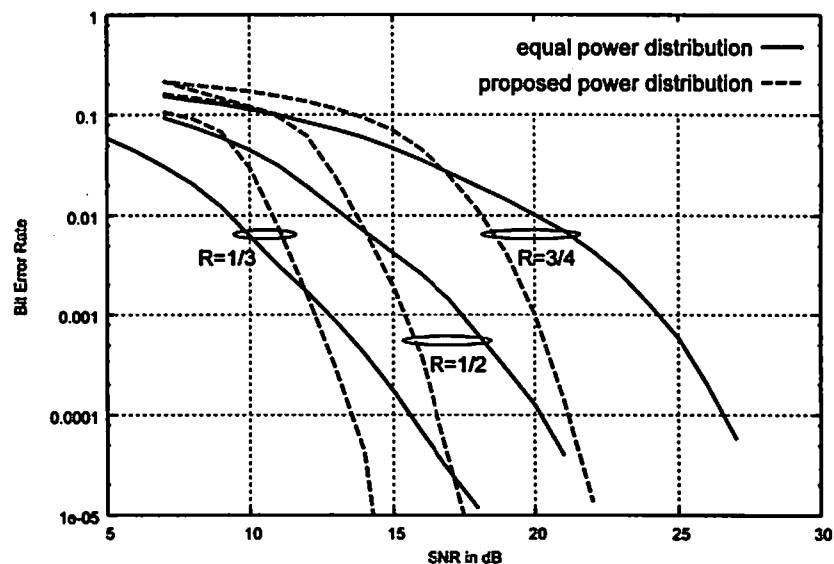


Figure 4.12: BER performance for $N_t = N_r = 4$, $SF_f = SF_t = 4$ and QPSK modulation

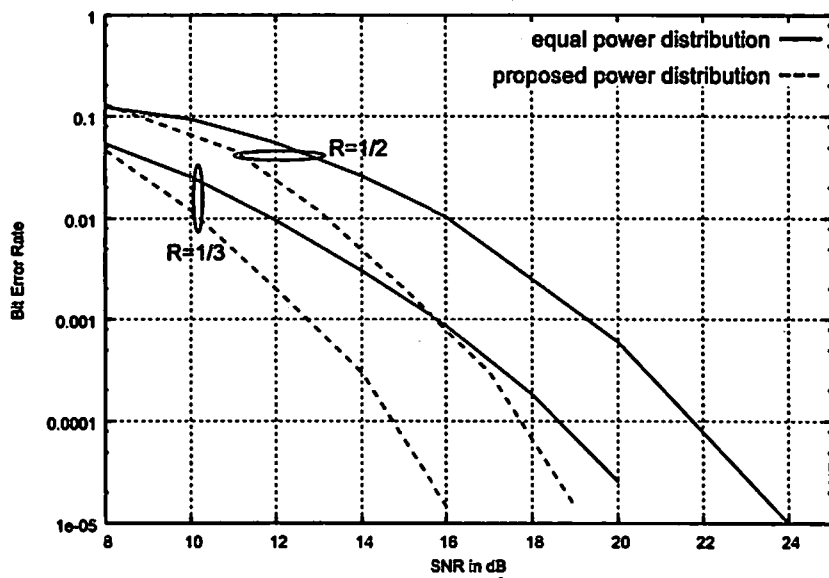


Figure 4.13: BER performance for $N_t = N_r = 4$, 14 active users, and 16-QAM modulation

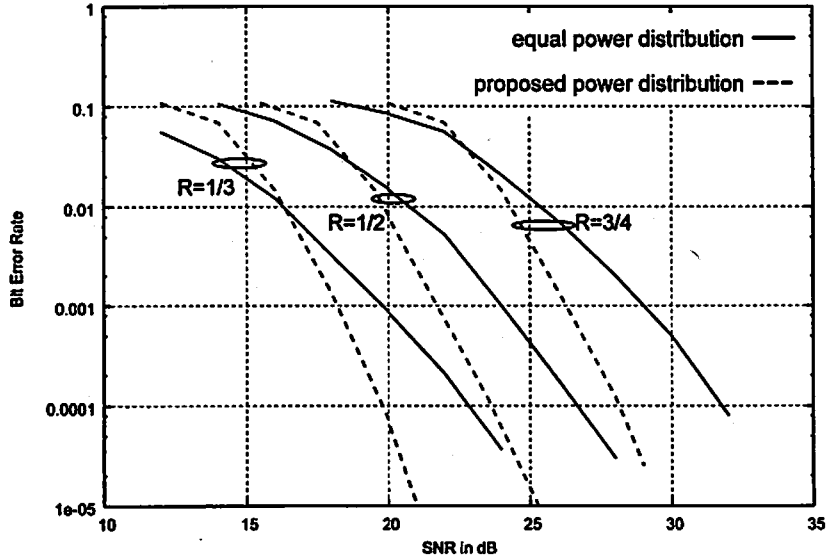


Figure 4.14: BER performance for $N_t = N_r = 4$, 14 active users, and 64-QAM modulation

value z described in [70]. The closed form optimum solution becomes equal to:

$$p_{k,m,o}^l = \left[\sum_{\alpha=0}^{N_t-1} \sum_{\gamma=0}^{N_u-1} \frac{\tilde{F}_{\gamma,m}^\alpha}{\tilde{F}_{k,m}^l} \right]^{-1} \cdot \left[N_t \cdot N_u \cdot \bar{P} + \sum_{\alpha=0}^{N_t-1} \sum_{\gamma=0}^{N_u-1} c \cdot \tilde{F}_{\gamma,m}^\alpha \cdot \log \left(\frac{\tilde{F}_{\gamma,m}^\alpha}{\tilde{F}_{k,m}^l} \right) \right], \quad (4.23)$$

where

$$\tilde{F}_{k,m}^l = \frac{1}{SF_f} \cdot \sum_{n=0}^{Nr-1} \sum_{q=0}^{SF_f-1} \frac{1}{|Q_B(\xi_{k,q+SF_f \cdot m}^{(n,l)})|^2}, \quad (4.24)$$

and

$$c = \frac{(2^B - 1) \cdot \sigma_n^2}{b}. \quad (4.25)$$

In Fig. 4.15, we evaluate the effects of the limited feedback on the proposed power allocation for the case of QPSK modulation, the spatial configuration of $N_t = N_r = 2$, the channel coding $R = 1/3$ and the spreading configuration of $SF_f = SF_t = 4$. For reference, the performances of equal power allocation and proposed power distribution without quantization are shown in the same figure. The effect of the quantization is limited if the number of bits for quantization, B , is greater than 10.

Fig. 4.16 shows the effect of the limited feedback on the BER performance for the specific case of 64-QAM, $N_t = N_r = 4$, $R=1/2$, and $SF_f = SF_t = 4$. The 14-bit

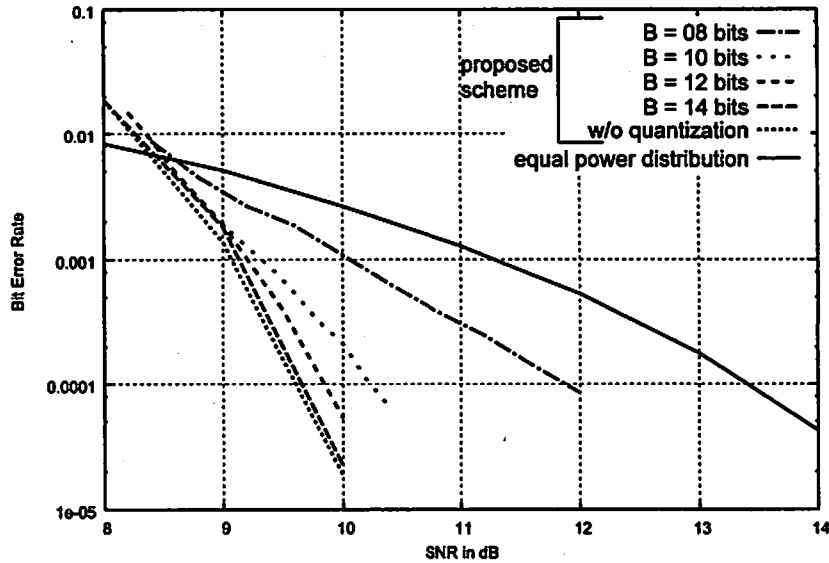


Figure 4.15: BER performance for $N_t = N_r = 2$, 12 active users QPSK modulation and $R=1/3$

quantization does not affect the performance of the proposed scheme. However, due to the sensitivity of the 64-QAM modulation, 12-bit and 10-bit quantization schemes affect the BER performance by about 1dB and 2dB respectively.

4.6 Conclusion

This Chapter proposes an extension of the proposed power allocation scheme to different MC systems. First, we adapt the power allocation scheme to OFDM transmission with adaptive modulation. The proposed extension allows to reduce the computational complexity, by including a subcarrier grouping method with local power allocation in conjunction with adaptive modulation for each subcarrier group. Then, we propose a field trial evaluation of power distribution for MIMO-OFDM transmission in a quasi-static multipath environment. It consists of adapting the transmit power in the spatial and/or frequency domain using a heuristic expression of the BER for each subcarrier. A review of the different power allocation strategies based on a closed form expression of the optimum power to be allocated for each subcarrier is presented. Finally, we evaluate the proposed power allocation scheme

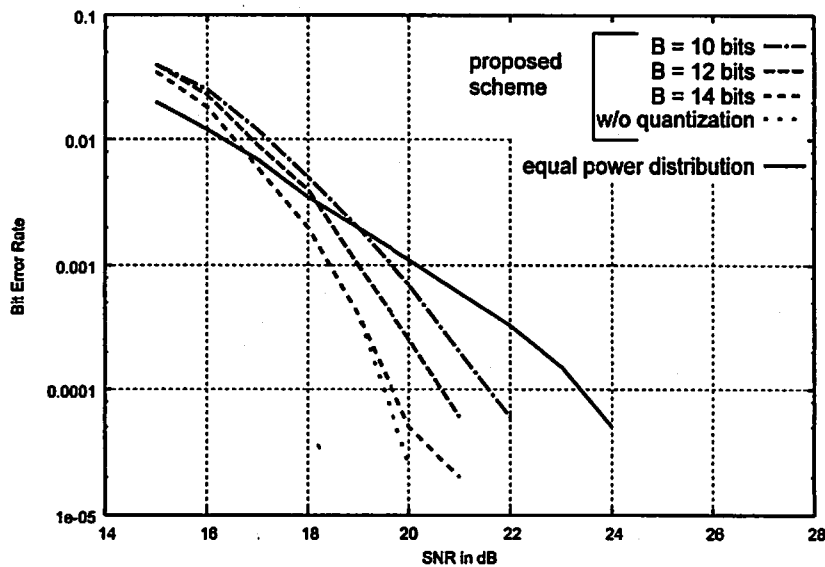


Figure 4.16: BER performance for $N_t = N_r = 2$, 12 active users 64-QAM modulation and $R=1/2$

for MIMO MC-CDMA based transmission. In addition, the simulation results show significant improvement of BER performance both in the uncoded and coded cases for QPSK and QAM modulations and several antenna configurations.

Chapter 5

Systematic Design of Overlap FDE Systems

This chapter proposes a systematic design method of overlap FDE for SC transmission without GI. Based on analysis of the SINR of the equalizer output for each symbol, we adaptively determine the block of the overlap FDE, where the block is defined as a set of symbols at the equalizer output with sufficiently low error rate, for a certain fixed sliding window size, which corresponds to a ~~an~~ FFT window size. The proposed method takes advantage of the fact that the utility part of the equalized signal is localized around the center of the FFT window. In addition, we also propose to adjust the block size in order to control the computational complexity of the equalization per processed sample according to the average BER of the system. Simulation results show that the proposed scheme can achieve comparable BER performance to the conventional SC-FDE scheme with sufficient GI insertion for both the coded and uncoded cases with various modulation levels, while requiring lower computational complexity compared to SC overlap FDE transmission with fixed block.

5.1 Introduction

Since the 90's, SC-FDE has been thoroughly studied and has been drawing much attention due to the effectiveness and simplicity of the transceiver [71]. When the

SC-FDE is used with CP as a GI, the SC-FDE not only outperforms the OFDM system in the absence of channel coding, but also loosens the requirement on the power amplifiers due to the low peak to average power ratio (PAPR) of the transmitted signals. Recently, both OFDM and SC-FDE have been seen as complementary solutions to each other since they can coexist in a dual-mode multiple access system [72] allowing some parts of the signal processing to shift from the mobile to the BS in the UL transmission. However, the GI is considered as a main limiting factor to achieve highly efficient signal transmission. For example, for IEEE 802.11a/g [29], [30] based transmission, the GI represents 25% of the bandwidth occupation. In order to reduce the length of the GI, transmission with an insufficient GI insertion has been studied [73]-[75]. Moreover, some authors have even proposed a "no GI" transmission method, which can reduce the impact of the interference caused by the absence of the GI at the cost of increased computational complexity [76]-[78]. Their solution is called overlap frequency domain equalization (overlap FDE). The basic idea of the SC overlap FDE is that, instead of adding redundancy to the transmitted signal, the head and tail parts of the FDE output, which are empirically known to be deteriorated by interference, are wasted. While the number of the FDE operations is increased, since only some portion of the FDE output is extracted as a reliable part (we call it "block" in this Chapter), the SC overlap FDE can achieve comparable performance to the conventional SC-FDE if the block size is small enough. In the overlap FDE, how to set the block or the block size is the key issue, because both the computational complexity and the performance largely depend on the way of setting the block, however, to the best of our knowledge, no systematic method for the determination of the block has been proposed.

In this Chapter, we propose a systematic design method of overlap FDE for SC transmission without GI. Based on a mathematical description of the IBI and the ISI for virtual vector transmission, we evaluate the SINR of each symbol at the FDE output and determine the block of the overlap FDE, so that all the symbols in the block satisfy a certain required SINR. The proposed method takes advantage of the fact that the utility part of the equalized signal is localized around the center of the FFT window. In addition, the adjustment of the block size can also be realized based on the computational complexity of the equalization per processed

sample according to the average BER. Note that the proposed design method is based on instantaneous SINR calculated by using each channel realization, therefore, the method could be worthwhile even when the statistical nature of the channel is known a priori. Simulation results show that the proposed systematic overlap FDE design scheme achieves comparable BER performance to the conventional SC-FDE scheme with sufficient GI insertion for both the coded and uncoded cases with various modulation levels. Furthermore, we highlight the complexity decrease due to the adaptive block sizing, compared to the SC overlap FDE transmission with the fixed block.

The rest of this Chapter is organized as follows. First, we show the system description of the SC overlap FDE and the SINR of each FDE output is evaluated. The next section describes in detail the proposed method to determine the temporal position and the size of the block based on the SINR. Then, we present numerical results to demonstrate the performance of the proposed method for coded and uncoded QPSK and QAM in multipath channel environment. Finally, conclusions are drawn.

5.2 System Description

5.2.1 Signal Modeling and Channel Representation

The SC transmission is a traditional digital transmission scheme, in which data are transmitted as a serial stream of amplitude and/or phase modulated symbols. Let $\{x_n\}$ denote the stream of the transmitted symbols, and α_i , $i = 0, \dots, L - 1$ time-invariant channel impulse response including pulse shaping filters. The received signal sequence $\{r_n\}$ can be written as

$$r_n = \sum_{i=0}^{L-1} \alpha_i x_{n-i} + e_n, \quad (5.1)$$

where $\{e_n\}$ is AWGN, assumed to be zero mean and i.i.d. with variance σ_n^2 [6].

Although the transmitted and the received signals are both serial streams in the SC overlap FDE system, we rewrite the relation between the signals using matrix and vector notation because the received signal $\{r_n\}$ is processed in a block

by block manner. Defining the i -th virtual transmitted signal vector of size N as $\mathbf{x}^{(i)} = [x_0^{(i)}, \dots, x_{N-1}^{(i)}]^T$, the corresponding received signal vector of size N , $\mathbf{r}^{(i)} = [r_0^{(i)}, \dots, r_{N-1}^{(i)}]^T$, can be expressed as

$$\mathbf{r}^{(i)} = \mathbf{H}_0 \mathbf{x}^{(i)} + \mathbf{H}_1 \mathbf{x}^{(i-1)} + \mathbf{e}^{(i)}, \quad (5.2)$$

where $\mathbf{e}^{(i)} = [e_0^{(i)}, \dots, e_{N-1}^{(i)}]^T$ denotes a corresponding AWGN vector, \mathbf{H}_0 and \mathbf{H}_1 denote the $N \times N$ channel matrices defined as

$$\mathbf{H}_0 = \begin{bmatrix} \alpha_0 & 0 & \dots & \dots & \dots & 0 \\ \vdots & \ddots & \ddots & & & \vdots \\ \alpha_{P-1} & & \ddots & \ddots & & \vdots \\ 0 & \ddots & & \ddots & \ddots & \vdots \\ \vdots & \ddots & \ddots & & \ddots & 0 \\ 0 & \dots & 0 & \alpha_{P-1} & \dots & \alpha_0 \end{bmatrix}, \quad (5.3)$$

and

$$\mathbf{H}_1 = \begin{bmatrix} 0 & \dots & 0 & \alpha_{P-1} & \dots & \alpha_1 \\ \vdots & & & \ddots & \ddots & \vdots \\ & & & & \ddots & \alpha_{P-1} \\ \vdots & & & & & 0 \\ \vdots & & & & & \vdots \\ 0 & \dots & \dots & \dots & \dots & 0 \end{bmatrix}. \quad (5.4)$$

Here we define a circulant channel matrix as

$$\mathbf{H}_c = \mathbf{H}_0 + \mathbf{H}_1. \quad (5.5)$$

Due to the property of circulant matrices, the circulant channel matrix can be re-written as

$$\mathbf{H}_c = \mathbf{W}^H \boldsymbol{\Lambda} \mathbf{W}, \quad (5.6)$$

where \mathbf{W} is a unitary DFT matrix of size $N \times N$, whose (p, q) element is $(1/\sqrt{N}) \exp(-j\frac{2\pi pq}{N})$ and Λ is the diagonal matrix representing the channel frequency response, whose diagonal elements are obtained by the DFT of the first column of \mathbf{H}_c . Note that, if the CP is added as the GI before the transmission, namely for the case of conventional SC-FDE, the received signal vector is given by

$$\mathbf{r}_{cp}^{(i)} = \mathbf{H}_c \mathbf{x}^{(i)} + \mathbf{e}^{(i)}. \quad (5.7)$$

5.2.2 SC Overlap FDE Receiver and Equalization

In the SC overlap FDE receiver, the same one-tap FDE as the conventional SC-FDE is firstly performed to the received signal $\mathbf{r}^{(i)}$. Since the received signal model of the conventional SC-FDE is given by (5.7), the FDE based on both the ZF and MMSE linear equalizers can be written in the form $\mathbf{W}^H \Gamma \mathbf{W}$, where Γ is a diagonal matrix defined as

$$\Gamma = \begin{cases} (\Lambda^H \Lambda)^{-1} \Lambda^H & \text{for ZF} \\ & \Lambda^{-1} \\ (\Lambda^H \Lambda + \sigma_n^2 \mathbf{I}_N)^{-1} \Lambda^H & \text{for MMSE}, \end{cases} \quad (5.8)$$

and \mathbf{I}_N is the identity matrix of size $N \times N$.

While for the case of conventional SC-FDE all of the FDE output $\mathbf{W}^H \Gamma \mathbf{W} \mathbf{r}_{cp}^{(i)}$ is used for the detection, only M ($\leq N$) symbols of the FDE output are picked up in the SC overlap FDE receiver[78]-[81]. Denoting the extraction operation of M symbols, which corresponds to the size of block to be optimized, out of N symbols, which is the size of FFT window, by a matrix $\mathbf{V}^{N \rightarrow M}$, the FDE output after extraction, in other words, the output of the overlap FDE, can be obtained as

$$\mathbf{y}^{(i)} = \mathbf{V}^{N \rightarrow M} \mathbf{W}^H \Gamma \mathbf{W} \mathbf{r}^{(i)}. \quad (5.9)$$

The basic procedure of the SC overlap FDE is summarized in Fig. 5.1.

The received signal vector $\mathbf{r}^{(i)}$ is composed by windowing the received signal stream of $\{r_n\}$ with a window of width N . Then, M symbols of the FDE output are extracted to obtain the overlap FDE output $\mathbf{y}^{(i)}$. The following received signal

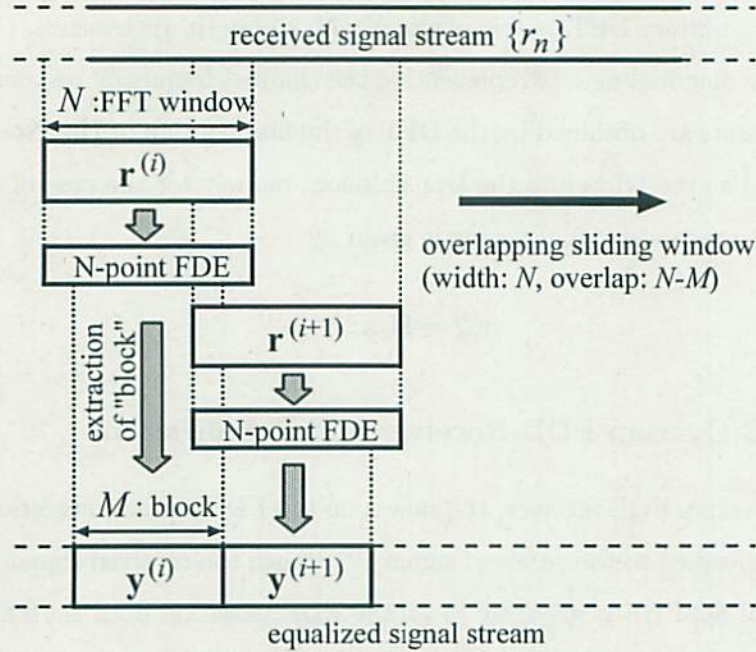


Figure 5.1: Basic procedure of overlap FDE

vectors are composed by sliding the window in an overlapping manner so that the series of the extracted blocks covers the whole signal sequence.

How to determine the extraction matrix $\mathbf{V}^{N \rightarrow M}$ is the main scope of this Chapter and the proposed scheme will be discussed in detail in the following section. In conventional SC overlap FDE with a fixed block [77]-[78], the selection is based on the central part of the processed sequence, therefore, for this case the extraction matrix is given by [79]

$$\mathbf{V}_{\text{fix}}^{N \rightarrow M} = \text{diag}_N(\underbrace{0, \dots, 0}_{(N-M)/2}, \underbrace{1, \dots, 1}_M, \underbrace{0, \dots, 0}_{(N-M)/2}), \quad (5.10)$$

where $\text{diag}_N(\cdot)$ is the diagonal matrix of size $N \times N$.

5.2.3 SINR Analysis of FDE Output

The output of the FDE before the extraction can be expressed as

$$\mathbf{z}^{(i)} = \mathbf{W}^H \boldsymbol{\Gamma} \mathbf{W} \mathbf{r}^{(i)} \quad (5.11)$$

Substituting Eq. (5.2) into Eq. (5.11), we obtain

$$\mathbf{z}^{(i)} = (\mathbf{W}^H \boldsymbol{\Gamma} \boldsymbol{\Lambda} \mathbf{W} - \mathbf{W}^H \boldsymbol{\Gamma} \mathbf{W} \mathbf{H}_1) \mathbf{x}^{(i)} + \mathbf{W}^H \boldsymbol{\Gamma} \mathbf{W} \mathbf{H}_1 \mathbf{x}^{(i-1)} + \mathbf{W}^H \boldsymbol{\Gamma} \mathbf{W} \mathbf{e}^{(i)}. \quad (5.12)$$

By defining

$$\boldsymbol{\Theta} = \mathbf{W}^H \boldsymbol{\Gamma} \boldsymbol{\Lambda} \mathbf{W} - \mathbf{W}^H \boldsymbol{\Gamma} \mathbf{W} \mathbf{H}_1, \quad (5.13)$$

$$\boldsymbol{\Psi} = \mathbf{W}^H \boldsymbol{\Gamma} \mathbf{W} \mathbf{H}_1, \quad (5.14)$$

$$\boldsymbol{\Omega} = \mathbf{W}^H \boldsymbol{\Gamma} \mathbf{W}, \quad (5.15)$$

The equation
Eq.(5.12) can be re-written as

$$\mathbf{z}^{(i)} = \boldsymbol{\Theta} \mathbf{x}^{(i)} + \boldsymbol{\Psi} \mathbf{x}^{(i-1)} + \boldsymbol{\Omega} \mathbf{e}^{(i)}. \quad (5.16)$$

Based on the signal representation above, the SINR of the v -th element at the output of the FDE is defined by

$$\beta_v = \frac{E\left[|\boldsymbol{\Theta} \mathbf{x}^{(i)}|_v^2 \right]}{E\left[|\boldsymbol{\Psi} \mathbf{x}^{(i-1)} + \boldsymbol{\Omega} \mathbf{e}^{(i)}|_v^2 \right]}, \quad (5.17)$$

where $[.]_v$ and $E[.]$ respectively denote the v -th element of the vector and expectation operation with respect to the transmitted symbols and the additive noise. Assuming that the symbols and the noise are uncorrelated, the SINR can be expressed as

$$\beta_v = \frac{P_s \sum_{u=0}^{N-1} |\boldsymbol{\Theta}_{v,u}|^2}{P_s \sum_{u=0}^{N-1} |\boldsymbol{\Psi}_{v,u}|^2 + \sigma_n^2 \sum_{u=0}^{N-1} |\boldsymbol{\Omega}_{v,u}|^2} \quad (5.18)$$

where P_s is the transmit power per data symbol and $\boldsymbol{\Theta}_{v,u}$, $\boldsymbol{\Psi}_{v,u}$ and $\boldsymbol{\Omega}_{v,u}$ are respectively the (v, u) element of $\boldsymbol{\Theta}$, $\boldsymbol{\Psi}$ and $\boldsymbol{\Omega}$.

For the specific case of ZF equalization, the SINR can be further simplified as

$$\beta_v = \frac{\sum_{k=0}^{N-1} \left| \frac{a_k - b_{v,k}}{a_v} \right|^2}{\sum_{k=0}^{N-1} \left| \frac{b_{v,k}}{a_v} \right|^2 + \frac{\sigma_n^2}{P_s} \sum_{u=0}^{N-1} |\boldsymbol{\Omega}_{v,u}|^2}, \quad (5.19)$$

with

$$a_k = \sqrt{N} \sum_{i=0}^{P-1} \alpha_i \exp\left(-j \frac{2\pi k i}{N}\right), \quad (5.20)$$

and

$$b_{v,k} = \sum_{c=N-P+1}^{N-1} \sum_{k'=0}^{c-N+P-1} \alpha_{N-b+k} \cdot \exp\left(-j \frac{2\pi((v+k')_N k)}{N}\right), \quad (5.21)$$

where $((\cdot))_N$ denotes mod N operation. Therefore, the variation of the SINR among different symbols depends only on the value of $b_{v,k}$. When $b_{v,k}$ is close to zero, the SINR of all the symbols tend to $\frac{P_s}{\sigma_n^2}$, which means all the FDE outputs have the same reliability. When $b_{v,k}$ tends to the value of a_k , then the SINR value tends to zero. In addition, the SINR can be evaluated by knowledge of the channel response and the ratio of the variance of the noise and the transmitted signal power.

5.3 Proposed Systematic Design of the SC Overlap FDE

We assume the availability of the channel response, the transmitted signal power and the variance of the additive noise for the evaluation of the SINR of the FDE output. Such an assumption will be valid if a pilot signal with CP as the GI is used. Practically, we can suppose the integration of the GI only during the pilot transmission. Let β denote a vector representation of the SINR as $\beta = [\beta_0, \dots, \beta_{N-1}]^T$. Firstly, the element of β with the highest SINR is identified and is denoted as β_{\max} . ~~And~~ Then, β_{\max} is used as a criterion to determine the block to be optimized. To be more precise, defining ξ ($0 \leq \xi \leq 1$) to be the acceptable SINR degradation, we set the minimum required SINR to be $\xi \cdot \beta_{\max}$. Here, ξ close to 1 means that the requirement on the performance is strict, while ξ close to 0 results in low computational complexity operation. From a viewpoint of computational complexity, the block size should be as large as possible, while a small block size is desirable from the performance point of view. Therefore, the proposed method finds the longest consecutive sequence of elements that satisfies the minimum required SINR $\xi \cdot \beta_{\max}$ and determines the sequence to be the block of the overlap FDE. To be more precise, given the window size of N , the number of complex multiplications of the FDE is equal to $2N \log N + N$, since N -point FFT and IFFT operations and a multiplication of a diagonal matrix is involved. Therefore, given the block size of the overlap FDE M , the number of complex operations of the SC-FDE and the SC overlap FDE per symbol are given by $2 \log N + 1$ and $(2 \log N + 1)N/M$, respectively. In the

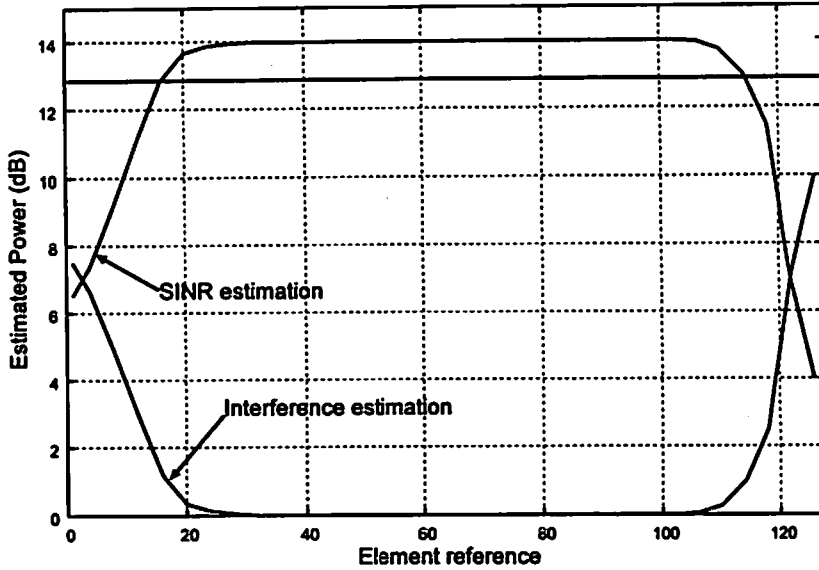


Figure 5.2: Examples of SINR and interference power for the window size $N = 128$

SC overlap FDE, the factor of N/M can be considered as the penalty on the computational complexity compared with the conventional SC-FDE, while the overlap FDE does not require the GI. We can see that by increasing the size of the block M the computational complexity per symbol can be reduced. Note that the proposed approach can be easily applied to the case when the minimum required SINR is designated in different manner, such as the required QoS defined in an upper layer.

In practice, we propose to use a simple iterative process through the selected block of symbols that allows to define the longest sequence validating the constraint on the acceptable range of the SINR. It has been demonstrated in [81] via computer simulations that the effects of the ISI and ICI due to the loss of the cyclic convolution property are mainly visible at the two extreme parts of the FDE output, namely the head and tail parts of the N symbols. Fig. 5.2 shows typical examples of the interference power and the associated SINR based on Eq. (5.19) at the FDE output with the window size of $N = 128$ symbols. We can also see from the figure that the interferences affect the two extreme parts and that the central part of the FFT window is not degraded by the interferences. Based on the observation above, we propose a simple procedure to determine the block of the overlap FDE as shown in Table 5.1 and Fig. 5.3. We define M_{\max} to be the index corresponding to β_{\max} .

Table 5.1: Proposed algorithm for utility part selection

Initialization:

Index corresponding to maximum SINR:

$$M_{\max} = \arg_m \max(\beta_m)$$

Maximum SINR:

$$\beta_{\max} = \beta_{M_{\max}}$$

Initialization of upper and lower indexes of block:

$$M_{\sup} = M_{\max}$$

$$M_{\inf} = M_{\max}$$

Iterative process to determine upper index of block:

While ($\beta_{M_{\sup}+1} \geq \xi \cdot \beta_{\max}$) {

$M_{\sup} = M_{\sup} + 1$ (increment of upper index of block)

}

Iterative process to determine lower index of block:

While ($\beta_{M_{\inf}-1} \geq \xi \cdot \beta_{\max}$) {

$M_{\inf} = M_{\inf} - 1$ (decrement of lower index of block)

}

Final step:

Block size: $M_{\text{opt}} = M_{\sup} - M_{\inf}$

Extraction matrix:

$$\mathbf{V}^{N \rightarrow M} = \text{diag}_N(\underbrace{0, \dots, 0}_{M_{\inf}}, \underbrace{1, \dots, 1}_{M_{\text{opt}}}, \underbrace{0, \dots, 0}_{N-M_{\sup}})$$

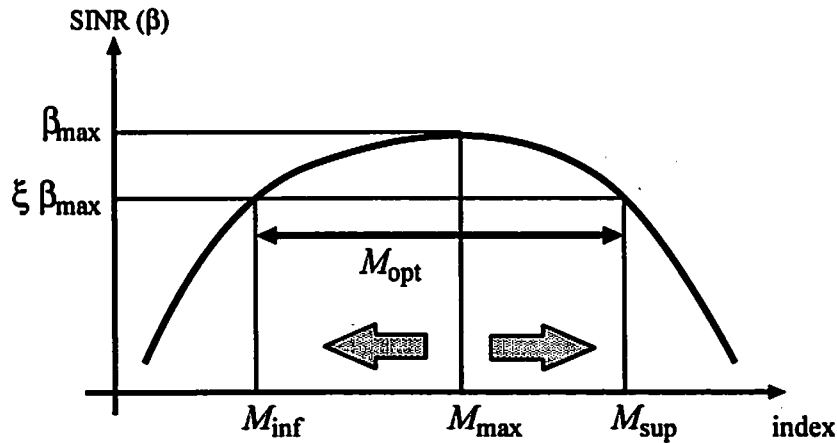


Figure 5.3: M_{inf} and M_{sup} at the end of iterative process

Assuming that M_{\max} is somewhere around the center of the window, we extend the block by moving both of its upper and lower indexes, which are respectively denoted as M_{sup} and M_{inf} , 1-by-1 from M_{\max} , as far as the SINR of the extended index is greater than $\xi \cdot \beta_{\max}$. Finally, the block of the overlap FDE is determined by the upper and the lower indexes.

5.4 Numerical Simulation

We now evaluate the performance of the proposed method to adaptively determine the block of the overlap FDE in multi-path fading environments via computer simulations. The main simulation parameters are summarized in Table 5.2. For the conventional SC-FDE, the equalization scheme described in [71]-[72] with (or without) appropriate GI insertion is employed. To verify the behavior of the equalization and selection method based on the SINR of each symbol at the output of the FDE, we evaluate the performance using 10-path frequency selective Rayleigh fading environment with maximum delay spread of $0.45 \mu\text{s}$ for uncoded and convolutionally coded cases. Since the system model in Table 5.2 is based on IEEE 802.11g standard [30], we have set the channel model from the system parameters of IEEE 802.11g. Throughout the simulations, we use $\zeta\%$, rather than ξ , to denote the SINR degradation from β_{\max} , which is defined as the percentage degradation of the SINR in dB,

Table 5.2: Simulation parameters

Carrier frequency	2.4 GHz
Bandwidth	20 MHz
Modulation scheme	QPSK, 16-QAM, 64-QAM
Channel encoder	uncoded or convolutionally coded
Channel estimation	Perfect CSI
Sample period	$0.05 \mu\text{s}$
Number of data packets	30
Number of paths	10
Resolution of paths	$0.05\mu\text{s}$ (i.e. one sample period)
Maximum delay spread	$0.45\mu\text{s}$

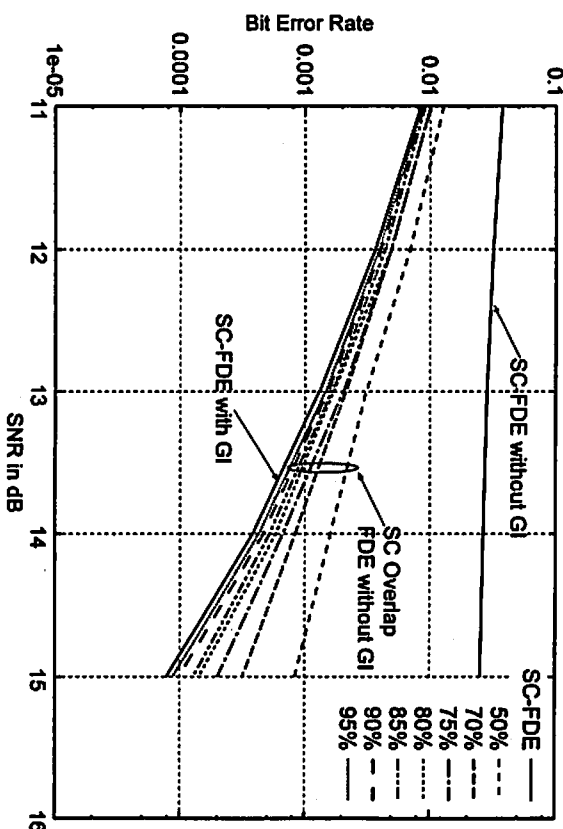


Figure 5.4: BER performance for QPSK modulation, $R = 1$ and $N = 64$ namely the degradation of $\zeta\%$ corresponds to the SINR in dB of $(\zeta\%/100) \cdot 10 \log \beta_{\max}$.

5.4.1 Uncoded System

Figs. 5.4, 5.5 and 5.6 show the BER versus the SINR for three different modulations, namely QPSK, 16-QAM and 64-QAM, without any channel encoding scheme. The window size is set to $N = 64$ and the results are presented for several values of $\zeta\%$. In addition, the impact of the $\zeta\%$ on the block size is also presented in Fig. 5.7. From all the figures, we can see that the SC overlap FDE can achieve almost the same BER performance as that of conventional SC-FDE with GI when the value of $\zeta\%$ is large. Specifically, for the QPSK modulation, Figs. 5.4 and 5.7 show that a relatively large number of the block size M is allowed for small degradation of the BER performance.

For instance, for a value of $\zeta\%$ equal to 80% and the window size of 64 symbols, we obtain an average block size of 40 symbols. For the case of 16-QAM or 64-QAM in Figs. 5.5, 5.6 and 5.7, we can see that the acceptable block size is relatively smaller than that of QPSK. This is because of the high sensitivity to interference due to the short constellation distance for the higher modulation levels.

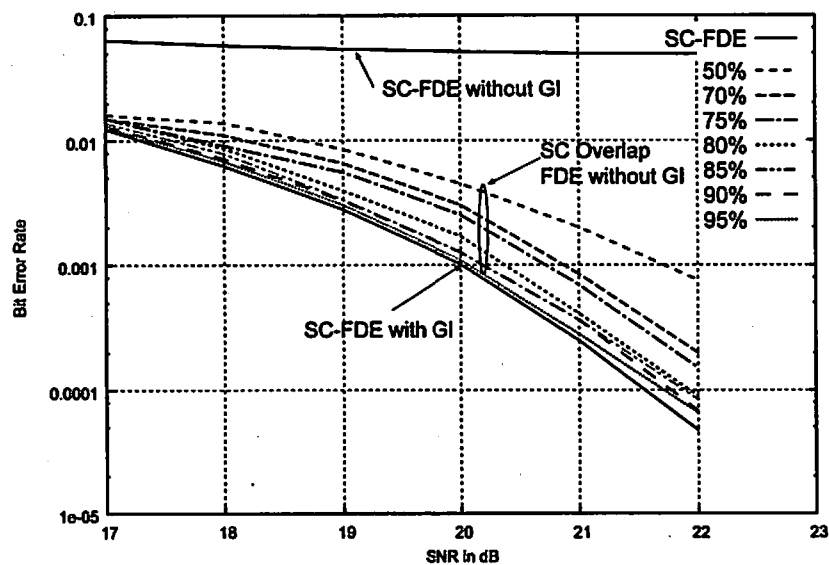


Figure 5.5: BER performance for 16-QAM modulation, $R = 1$ and $N = 64$

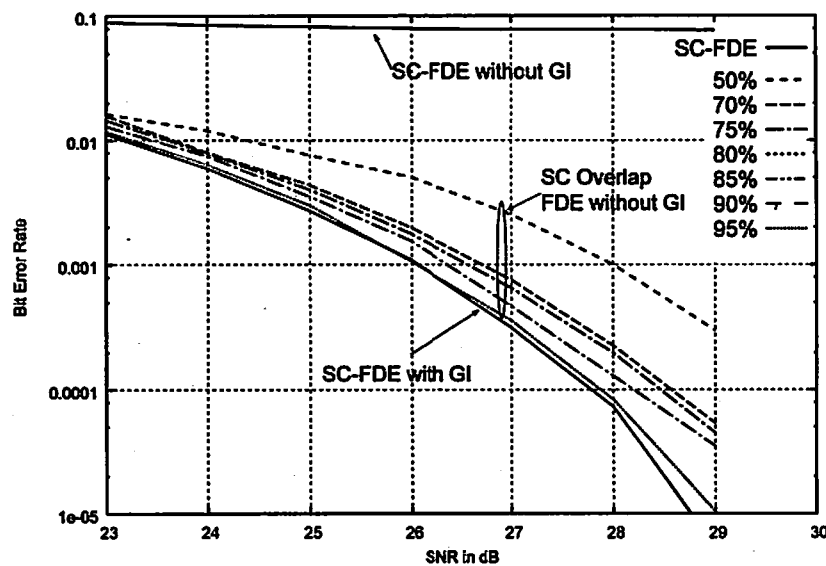


Figure 5.6: BER performance for 64-QAM modulation, $R = 1$ and $N = 64$

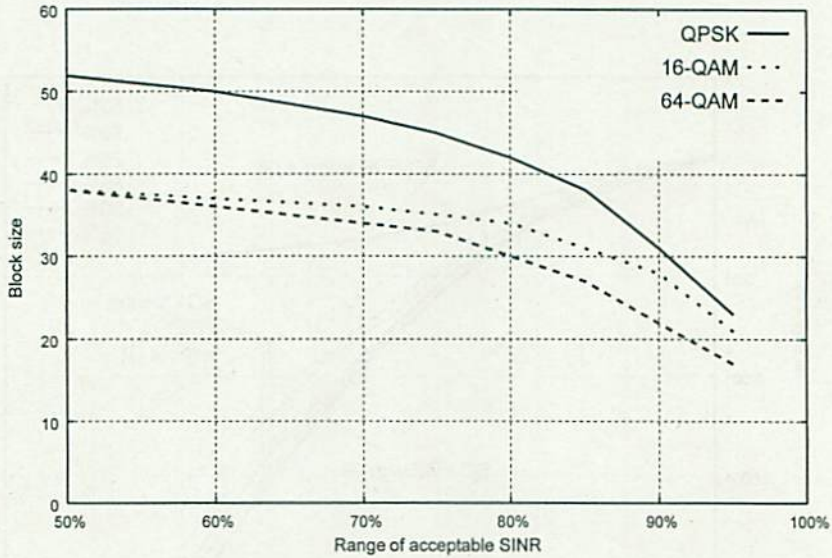


Figure 5.7: Impact of SINR range on block size, $R = 1$ and $N = 64$

5.4.2 Coded System

Figs. 5.8, 5.9 and 5.10 illustrate the BER performances of the proposed scheme with convolutionally coded case for QPSK 16-QAM and 64-QAM, and Fig. 5.11 shows the corresponding block size obtained by the proposed algorithm for the coded case.

Again, we can see that the SC overlap FDE can achieve almost the same BER performance as that of the conventional SC-FDE with sufficient GI for small block sizes. Also, the trade-off relationship between the BER performance and the computational complexity, in other words, the block size, can be observed in the coded case as well. It can be concluded that the proposed method can be utilized to balance between them for both the uncoded and coded cases. In addition, similar to the results presented in [82] and [83], impact of channel encoder on the interference is limited. Compared to the uncoded case, improvement can be obtained in term of BER. However, this improvement is limited due to the non-accurate equalization.

5.5 Conclusion

This chapter proposed a systematic design of the overlap FDE for SC transmission. Based on analysis of the SINR of each symbol at the FDE output, an adaptive ad-

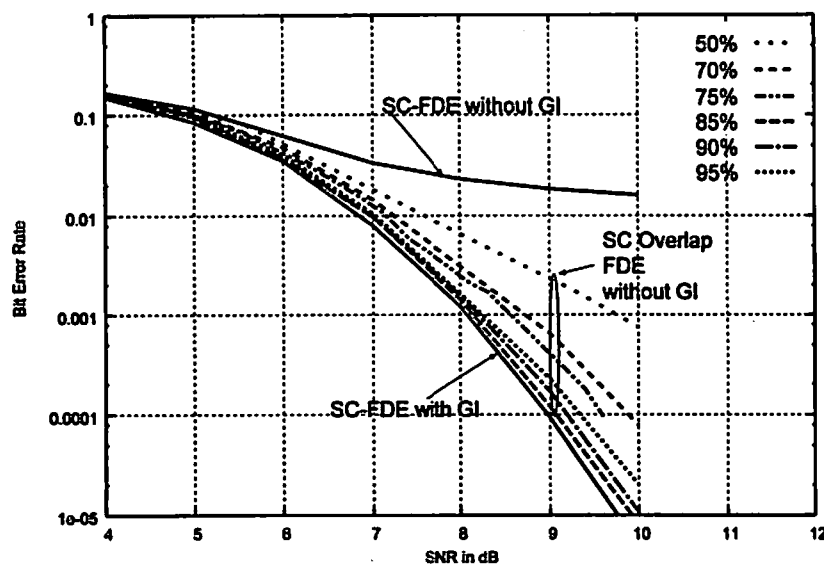


Figure 5.8: BER performance for QPSK modulation, $R = 1/2$ and $N = 64$

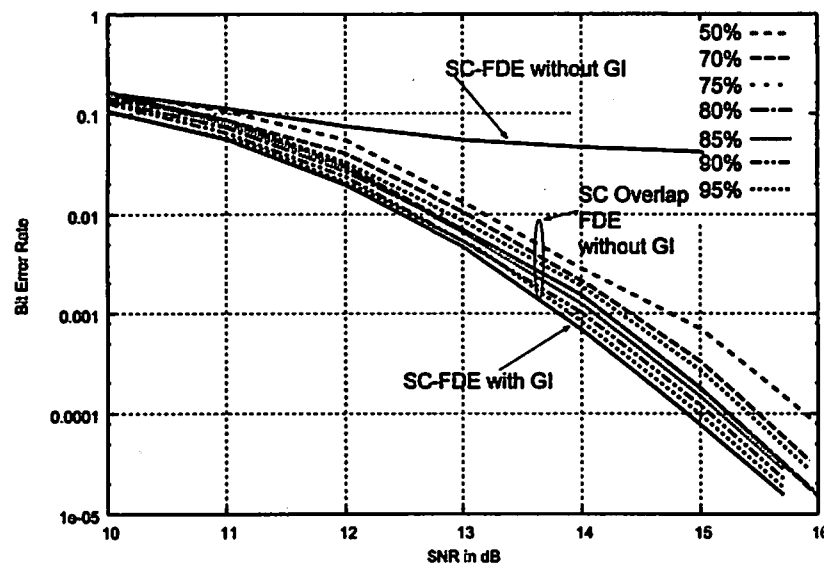


Figure 5.9: BER performance for 16-QAM modulation, $R = 1/2$ and $N = 64$

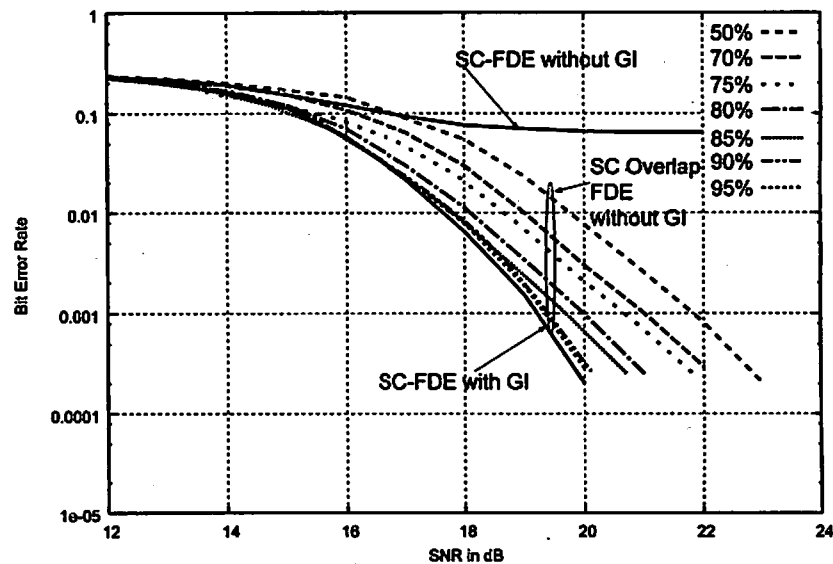


Figure 5.10: BER performance for 64-QAM modulation, $R = 1/2$ and $N = 64$

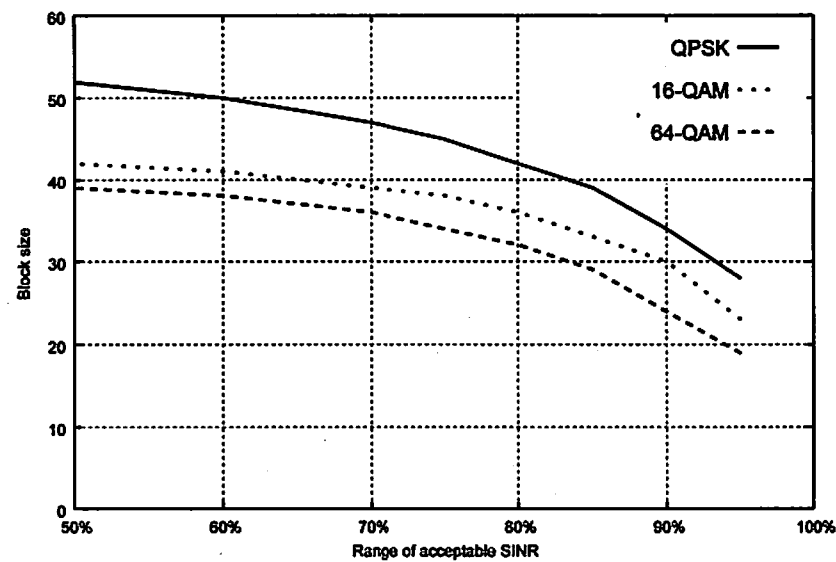


Figure 5.11: Impact of SINR range on block size, $R = 1/2$ and $N = 64$

justment of the block of the overlap FDE, which is defined as a utility part of the FDE output, is proposed. The proposed method consists of evaluating the SINR and adjusting the upper and the lower index bounds of the block so as to maximize the block size for computational complexity reduction while keeping the required performance. In addition, we propose to adjust the block size in order to control the computational complexity of the equalization per processed sample according to the average BER of the system. The simulation results have validated the proposed method in terms of BER performance with QPSK and QAM modulations for uncoded and convolutionally coded cases.

In this Chapter, we have only used SINR for the performance measure in the determination of the block, however, we can directly employ the BER as the performance metric by using *Q*-function representation [6] for the uncoded case or an approximated BER expression [26] for the coded case. Results show that this modulation scheme, so-called SC overlap FDE, could be identified as a candidate for next generation mobile communication system due to the performance and the simplicity of the scheme, especially when it is combined with systematic block design. Moreover, the proposed method could be extended to any other advanced equalization or multi-input multi output (MIMO) signal processing for SC overlap FDE transmission and any powerful channel encoder such as the turbo codes [32] or the low density parity check codes [41]-[42].

Chapter 6

Conclusions and Further Research

In this chapter, we summarize the main conclusions of this thesis and provide some suggestions for further research.

Chapter 2 has provided some background materials, including OFDM, MIMO, MC-CDMA and SC-FDE description. The objective of the Chapter is to review basic signal models that are used in the thesis. Then, we set up the basic framework of the power allocation scheme based on the In addition, we have also highlighted a heuristic expression of BER and confirmed the validity of the expression for both uncoded and coded cases.

In Chapter 3, we have proposed a novel scheme for OFDM that adapts the transmit power in the frequency domain using a heuristic expression of the BER for each subcarrier. A closed form expression of the optimum power to be allocated for each subcarrier is presented for uncoded OFDM transmission as well as coded scheme. The proposed scheme allows reducing the computational complexity, by including a subcarrier grouping method with local power adaptation for each subcarrier group. Our subcarrier grouping method minimizes the adverse impact of the local power adaptation by taking into consideration the channel gains of all the subcarriers. The characteristics allow us to control the trade-off between the transmission performance and the computational complexity by adjusting the sizes of subcarrier groups. The simulation results show significant improvement of BER

performance both in the uncoded and coded cases for QPSK and QAM modulations.

In Chapter 4, we have extended the proposed power scheme to several MC extensions. First, we have extended it to adaptive modulation OFDM scheme. Results show significant performance improvement in term of BER by including the proposed power allocation scheme in the case of adaptive OFDM modulation. Then, we have proposed power distribution schemes for MIMO-OFDM transmission and evaluated the performance in a quasi-static multipath environment via field trial evaluations. The proposed methods consist of adapting the transmit power in the spatial and/or frequency domain using the heuristic expression of the BER for each subcarrier. Finally, we have applied the power allocation scheme to MIMO MC-CDMA based transmissions. The proposed method includes the use of a heuristic expression of the BER to transmit in a multi-user scheme with linear detection. Basic process consists of allocating power at the transmit side as a function of the channel conditions, so that the heuristic value of the BER is minimized. The simulation results show promising performance in terms of BER for QPSK and QAM modulations and different spatial configurations.

In Chapter 5, we have proposed a systematic design of the overlap FDE for SC transmission. Based on the analysis of the SINR of each symbol at the FDE output, an adaptive adjustment of the block of the overlap FDE, which is defined as the utility part of the FDE output, is proposed. The proposed method consists of evaluating the SINR and adjusting the upper and the lower index bounds of the block so as to maximize the block size for computational complexity reduction while keeping required performance. The simulation results have validated the proposed method in terms of BER performance with QPSK and QAM modulations for uncoded and convolutional coded cases.

For future work, we also plan to include the error of the channel estimation in the evaluation of the power adaptation. In addition, in the case of OFDM and MIMO-OFDM, we have limited the access to one single user per frame. Extension of the multi-user OFDM, so called OFDMA, should also be explored. Combining the multi-user scheduler with the proposed power allocation could also be an interesting direction.

Bibliography

- [1] Recommendation ITU-R M.1645, "Framework and overall objectives of the future development of IMT- 2000 and systems beyond IMT-2000," *International Telecommunication Union*, <http://www.itu.int/rec/R-REC-M.1645/e>, June. 2003.
- [2] Report ITU-R M.2078, "Estimated spectrum bandwidth requirements for the future development of IMT-2000 and IMT-Advanced, ITU-R," *International Telecommunication Union*, <http://www.itu.int/publ/R-REP-M.2078/en>, 2006.
- [3] Resolution ITU-R 57, "Principles for the process of development of IMT-Advanced, ITU-R," *International Telecommunication Union*, <http://www.itu.int/publ/R-RES-R.57/en>, 2007.
- [4] P. Lescuyer and Th. Lucidarme, *Evolved Packet System (EPS): The LTE and SAE Evolution of 3G UMTS*, Wiley, 2008.
- [5] J. G. Andrews, A. Ghosh, and R. Muhamed, *Fundamentals of WiMAX: Understanding Broadband Wireless Networking*, Upper Saddle River, NJ: Prentice Hall, 2007.
- [6] J. Proakis, *Digital Communications, 3rd Edition*, Singapore, McGraw-Hill, 1995.
- [7] R. Van Nee and R. Prasad, *OFDM for Wireless Multimedia Communications*, Artech House, 2000.

- [8] N. Yee, J.-P. Linnartz1 and G. Fettweis, "Multi-carrier CDMA in indoor wireless radio networks," in *Proc. IEEE International Symposium on Personal, Indoor, and Mobile Radio Communications* (PIMRC'93), pp. 109–113, Sept. 1993.
- [9] A. Chouly, A. Brijal and S. Jourdan, "Orthogonal multicarrier techniques applied to direct sequence spread spectrum CDMA systems," in *Proc. IEEE Global Telecommunications Conference* (Globecom'93), vol. 3, pp. 1723-1728, Nov. 1993.
- [10] Q. Chen, E. S. Sousa and S. Pasupathy, "Performance of a coded multi-carrier DS-CDMA system in multipath fading channels," *Wireless Personal Communications*, vol. 2, nos. 1–2, pp. 167–187, Mar. 1995.
- [11] B. Muquet, M. de Courville, G. B. Giannakis, Z. Wang and P. Duhamel, "Reduced complexity equalizers for zero-padded OFDM transmissions," in *Proc. IEEE International Conference on Acoustics, Speech, and Signal Processing* (ICASSP 2000), vol. 5, pp. 2973–2976, June 2000.
- [12] A. Van Zelst and T. C. W. Schenk, "Implementation of a MIMO-OFDM-based wireless LAN system," *IEEE Trans. Signal Processing*, vol. 52, no. 2, pp. 483–494, Feb. 2004.
- [13] E. Biglieri, G. Caire, and G. Taricco, "Limiting performance of block-fading channels with multiple antennas," *IEEE Trans. Inform. Theory*, vol. 47, no. 4, pp. 1273–1289, May 2001.
- [14] N. Maeda, H. Atarashi, S. Abeta, and M. Sawahashi, "Throughput comparison between VSF-OFCDM and OFDM considering effect of sectorization in forward link broadband packet wireless access," in *Proc. IEEE Vehicular Technology Conference Fall* (VTC-Fall 2002), vol. 1, pp. 47–51, Sept. 2002.
- [15] M. Maeda, H. Atarashi, and M. Sawahashi, "Performance comparison of channel interleaving  methods in frequency domain for VSF-OFCDM broadband wireless access in forward link," *IEICE Trans. Commun.*, vol. E86-B, no. 1, pp. 300–313, Jan. 2003.

- [16] L. J. Cimini, "Analysis and simulation of a digital mobile channel using orthogonal frequency division multiplexing," *IEEE Trans. Commun.*, vol. 33, no. 7, pp. 665–675, July 1985.
- [17] A. Van Zelt, R. van Nee, and G. A. Awate, "Space division multiplexing (SDM) for OFDM systems," in *Proc. IEEE Vehicular Technology Conference Spring* (VTC-Spring 2000), vol. 2, pp. 1070–1074, May. 2000.
- [18] H. Sampath, S. Talwar, J. Tellado, V. Erceg, and A. Paulraj, "A fourth-generation MIMO-OFDM broadband wireless system: Design, performance, and field trial results," *IEEE Commun. Mag.*, vol. 40, no. 9, pp. 143–149, Sep. 2002.
- [19] H. Atarashi, S. Abeta, and M. Sawahashi, "Variable spreading factor orthogonal frequency and code division multiplexing (VSF-OFCDM) for broadband packet wireless access," *IEICE Trans. Commun.*, vol. E86-B, no. 1, pp. 291–299, Jan. 2003.
- [20] H. Sari, G. Karam, and I. Jeanclaude, "An analysis of orthogonal frequency-division multiplexing for mobile radio applications," in *Proc. IEEE Vehicular Technology Conference* (VTC'94), vol. 3, pp. 1635–1639, June. 1994.
- [21] A. Gusmao, R. Dinis, J. Conceicao and N. Esteves, "Comparison of two modulation choices for broadband wireless communications," in *Proc. IEEE Vehicular Technology Conference Spring* (VTC-Spring 2000), vol. 2, pp. 1300–1305, May, 2000.
- [22] P. Montezuma and A. Gusmao, "A pragmatic coded modulation choice for future broadband wireless communications," in *Proc. IEEE Vehicular Technology Conference Spring* (VTC-Spring 2001), vol. 2, pp. 1324–1328, May 2001.
- [23] A. Gusmao, R. Dinis and N. Esteves, "On frequency-domain equalization and diversity combining for broadband wireless communications," *IEEE Trans. Commun.*, vol. 51, no. 7, pp. 1029–1033, July 2003.

- [24] M. -S. Alouini and A. Goldsmith, "Adaptive modulation over Nakagami fading channels," *Kluwer Journal on Wireless Communications*, vol. 13, no. 1-2, pp. 119–143, May 2000.
- [25] G. J. Foschini and J. Salz, "Digital communications over fading radio channels," *Bell Systems Technical Journal*, vol. 62, pp. 429–456, Feb. 1983.
- [26] X. Qiu and K. Chawla, "On the performance of adaptive modulation in cellular system," *IEEE Trans. Commun.*, vol. 47, no. 6, pp. 884–895, June 1999.
- [27] Q. Liu, S. Zhou, and G. Giannakis, "Cross-layer combining of adaptive modulation and coding with truncated ARQ over wireless links," *IEEE Trans. Wireless Commun.*, vol. 3, no. 5, pp. 1746–1755, May 2004.
- [28] L. Hanzo, M. Munster, B. J. Choi, and T. Keller, *OFDM and MC-CDMA for Broadband Multi-User Communications, WLANs and Broadcasting*, Wiley-IEEE Press, 2003.
- [29] IEEE Std. 802.11a, "ISO/IEC 8802-11", IEEE, 1999.
- [30] Draft IEEE Std. 802.11g, "Further higher speed physical layer extension in the 2.4GHz band," IEEE, 2001.
- [31] F. J. MacWilliams and N. J. A. Sloane, *The Theory of Error-Correcting Codes*, North-Holland: New York, NY, 1977.
- [32] C. Berrou, A. Glavieux, and P. Thitimajshima, "Near Shannon limit error-correcting coding and decoding: Turbo-codes," in *Proc. IEEE International Conference on Communications (ICC'93)*, vol. 2, pp. 1064–1070, May 1993.
- [33] 3GPP Technical Specification Group, "Universal mobile telecommunication system (UMTS); multiplexing and channel coding (FDD)," TS 25.212 v3.4.0. Sept. 2000.
- [34] P. Robertson, E. Villebrun, and P. Hoeher, "A comparison of optimal and sub-optimal MAP decoding algorithms operating in the log domain," in *Proc. IEEE International Conference on Communications (ICC'95)*, vol. 2, pp. 1009–1013, June 1995.

- [35] B. Widrow and S. D. Stearns, *Adaptive Signal Processing*, Englewood Cliffs, NJ: Prentice-Hall, 1985.
- [36] P. Chow, J. Cioffi, and J. Bingham, "A practical discrete multitone transceiver loading algorithm for data transmission over spectrally shaped channels," *IEEE Trans. Commun.*, vol. 43, no. 2–4, pp. 773–775, Feb.–Mar.–Apr. 1995.
- [37] W. Yun and J. Cioffi, "On constant power water-filling," in *Proc. IEEE International Conference on Communications* (ICC 2001), vol. 6, pp. 1665–1669, June 2001.
- [38] T. Yoshiki, S. Sampei, and N. Morinaga, "High bit rate transmission scheme with a multilevel transmit power control for OFDM based adaptive modulation systems," in *Proc. IEEE Vehicular Technology Conference Spring* (VTC-Spring 2001), vol. 1, pp. 727–731, May 2001.
- [39] S. Falahati, A. Svensson, M. Sternad, and T. Ekman, "Adaptive modulation systems for predicted wireless channels," *IEEE Trans. Commun.*, vol. 52, no. 2, pp. 307–316, Feb. 2004.
- [40] C. S. Park and K. B. Lee, "Transmit power allocation for BER performance improvement in multicarrier systems," *IEEE Trans. Commun.*, vol. 52, no. 10, pp. 1658–1663, Oct. 2004.
- [41] R. Gallager, *Low Density Parity Check codes*, Cambridge, MIT press, 1963
- [42] J. Chen and M. P. C. Fossorier, "Near optimum universal belief propagation based decoding of low-density parity check codes," *IEEE Trans. Commun.*, vol. 50, no. 3, pp. 406–414, Mar. 2002.
- [43] G. E. Oien, H. Holm, and K. J. Hole, "Adaptive coded modulation with imperfect channel state information: system design and performance analysis aspects," in *Proc. IEEE Int. Symp. Advances in Wireless Commun.* (ISWC 2002), pp. 19–20, Sept. 2002.
- [44] G. J. Foschini, G. D. Golden, R. A. Valenzuela, and P. W. Wolniansky, "Simplified processing for high spectral efficiency wireless communication employing

- multi-element arrays," *IEEE J. Sel. Areas Commun.*, vol. 17, no. 11, pp. 1841–1852, Nov. 1999.
- [45] H. Sampath, S. Talwar, J. Tellado, V. Erceg, and A. Paulraj, "A fourth-generation MIMO-OFDM broadband wireless system: design, performance and field trial results," *IEEE Commun. Mag.*, vol. 40, no. 9, pp. 143–149, Sept. 2002.
- [46] Y. G. Li, J. H. Winters, and N. R. Sollenberger, "MIMO-OFDM for wireless communications: signal detection with enhanced channel estimation," *IEEE Trans. Commun.*, vol. 50, no. 9, pp. 1471–1477, Sept. 2002.
- [47] S. Hara and R. Prasad, "Overview of multicarrier CDMA," *IEEE Commun. Mag.*, vol. 35, no. 12, pp. 126–133, Dec. 1997.
- [48] H. Rohling, T. May, K. Bruninghaus, and R. Grunheid, "Broad-band OFDM radio transmission for multimedia applications," *Proceedings of the IEEE*, vol. 87, no. 10, pp. 1778–1789, Oct. 1999.
- [49] S. Hara and R. Prasad, "Design and performance of multi-carrier CDMA system in frequency-selective Rayleigh fading channels," *IEEE Trans. Veh. Technol.*, vol. 48, no. 5, pp. 1584–1595, May 1999.
- [50] K. Fazel and S. Kaiser, *Multi-Carrier Spread-Spectrum and Related Topics*, Kluwer Academic Publishers, Boston, 2002.
- [51] A. Sumasu, T. Nihei, K. Kitagawa, M. Uesugi, and O. Kato, "An OFDM-CDMA system using combination of time and frequency domain spreading," in *Proc. IEICE Technical Report*, vol. 100, no. 21, RCS2000-3, pp. 13–18, Apr. 2000.
- [52] A. Persson, T. Ottosson, and E. Strom, "Time frequency localized CDMA for downlink multi-carrier systems," in *Proc. IEEE International Symposium on Spread Spectrum Techniques and Applications (ISSSTA 2002)*, vol. 1, pp. 118–122, Sept. 2002.
- [53] J. F. Hayes, "Adaptive feedback communications," *IEEE Trans. Commun.*, vol. 16, no. 1, pp. 29–34, Feb. 1968.

- [54] J. K. Cavers, "Variable-rate transmission for Rayleigh fading channels," *IEEE Trans. Commun.*, vol. 20, no. 1, pp. 15–22, Feb. 1972.
- [55] I. Kalet, "The multitone channel," *IEEE Trans. Commun.*, vol. 37, no. 2, pp. 119–124, Feb. 1989.
- [56] A. Cyzlik, "Adaptive OFDM for wideband radio channels," in *Proc. IEEE Global Telecommunications Conference (Globecom'96)*, vol. 1, pp. 713–718, Nov. 1996.
- [57] Z. Song, K. Zhang, and Y. L. Guan, "Statistical adaptive modulation for QAM-OFDM systems," in *Proc. IEEE Global Telecommunications Conference (Globecom 2002)*, vol. 1, pp. 706–710, Nov. 2002.
- [58] A. Kannu, T. Sivanadyan, and S. Subramaniam, "Performance of block adaptive modulation schemes for OFDM based WLAN systems," in *Proc. IEEE International Conference on Personal Wireless Communications*, pp. 6–10, Dec. 2002.
- [59] T. H. Cormen, C. E. Leiserson, R. L. Rivest, and C. Stein, *Introduction to Algorithms*, MIT Press and McGraw-Hill, 2000.
- [60] T. Starr, J. M. Cioffi, and P. J. Silverman, *Understanding Digital Subscriber Line Technology*, Prentice Hall, 1999.
- [61] W. Bocquet, K. Hayashi, and H. Sakai, "Frequency domain power adaptation scheme for coded OFDM transmissions," in *Proc. European Wireless Conference (EW 2007)*, Apr. 2007.
- [62] W. Bocquet, K. Hayashi, and H. Sakai, "Combined frequency and spatial domains power distribution for MIMO-OFDM transmission," in *Proc. IEEE International Symposium on Personal, Indoor and Mobile Radio Communications (PIMRC 2007)*, pp. 1–5, Sept. 2007.
- [63] Z. Jiang, Y. Ge, and Y. Li, "Max-Utility wireless resource management for best-effort traffic," *IEEE Trans. Wireless Commun.*, vol. 4, no. 1, pp. 100–111, Jan. 2005.

- [64] Y. Zhu and E. Gunawan, "Performance of MC-CDMA system using control MRC with power control in Rayleigh fading channel," *IEEE Electronics Letters*, vol. 36, no. 8, pp. 752–753, Apr. 2000.
- [65] J. Zhu and Y. Bar-Ness, "Power allocation algorithm in MC-CDMA," in *Proc. IEEE International Conference on Communications (ICC 2001)*, vol. 2, pp. 931–935, May 2002.
- [66] W. Bocquet, K. Hayashi, and H. Sakai, "A power allocation scheme for coded MIMO multi-carrier systems," in *Proc. OFDM Workshop 2006*, pp. 96–100, Aug. 2006.
- [67] Q. T. Tran, "A study on phased array antenna with RF-MEMS phase shifters," *Master Thesis, Osaka University*, Feb. 2005.
- [68] J. P. Kermoal, L. Schumacher, P. E. Mogensen, Pedersen, K.I.; "Experimental investigation of correlation properties of MIMO radio channels for indoor pico-cell scenarios," in *Proc. IEEE Vehicular Technology Conference Fall (VTC-Fall 2000)*, vol. 1, pp. 14–21, Sept. 2000.
- [69] A. Pascual Iserte, D. P. Palomar, A. I. Perez-Neira, and M. A. Lagunas, "A robust maximum approach for MIMO communications with imperfect channel state information based convex optimization," *IEEE Trans. Signal Processing*, vol. 54, no. 1, pp. 346–360, Jan. 2006.
- [70] B. Murray and I. Collings, "AGC and quantization effects in a zero-forcing MIMO wireless system," in *Proc. IEEE Vehicular Technology Conference Fall (VTC-Spring 2006)*, vol. 4, pp. 1802–1806, Sept. 2006.
- [71] H. Sari, G. Karam, and I. Jeanclaude, "Transmission techniques for digital terrestrial TV broadcasting," *IEEE Commun. Mag.*, vol. 33, no. 2, pp. 100–109, Feb. 1995.
- [72] D. Falconer, S. L. Ariyavisitakul, A. Benyamin-Seeyar, and B. Eidson, "Frequency domain equalization for single-carrier broadband wireless systems," *IEEE Commun. Mag.*, vol. 40, no. 4, pp. 58–66, Apr. 2002.

- [73] K. Hayashi and H. Sakai, "Interference cancellation schemes for single carrier block transmission with insufficient cyclic prefix," *EURASIP Journal on Wireless Communications and Networking*, vol. 2008, Article ID 130747, 2008. doi:10.1155/2008/130747.
- [74] K. Hayashi and H. Sakai, "Per-tone equalization for single carrier block transmission with insufficient cyclic prefix," *IEICE Trans. Information and Systems*, vol. E88-D, no. 7, pp. 1323–1330, July 2005.
- [75] D. Kim and G. L. Stuber, "Residual ISI cancellation for OFDM with applications to HDTV broadcasting," *IEEE J. Sel. Areas Commun.*, vol. 16, no. 8, pp. 1590–1599, Oct. 1998.
- [76] L. Martoyo, T. Weiss, F. Capar, and F. K. Jondral, "Low complexity CDMA downlink receiver based on frequency domain equalization," in *Proc. IEEE Vehicular Technology Conference Fall (VTC-Fall 2003)*, vol. 2, pp. 987–991, Oct. 2003.
- [77] W. Bocquet and M. Nakamura, "Novel frame structure and equalization processing for ZP-OFDM transmission," in *Proc. International Symposium on Wireless Personal Multimedia Communications (WPMC 2004)*, vol. 2, pp. 1–5, Sept. 2004.
- [78] K. Takeda, H. Tomeba, and F. Adachi, "Iterative overlap FDE for DS-CDMA without GI," in *Proc. IEEE Vehicular Technology Conference Fall (VTC-Fall 2006)*, pp. 1–5, Sept. 2006.
- [79] H. Tomeba, K. Takeda, and F. Adachi, "Overlap MMSE-frequency-domain equalization for multi-carrier signal transmissions," in *Proc. International Symposium on Wireless Personal Multimedia Communications (WPMC 2006)*, pp. 751–755, Sept. 2006.
- [80] H. Gacanin, S. Takaoka, and F. Adachi, "Bit error rate analysis of OFDM/TDM with frequency-domain equalization," *IEICE Trans. Commun.*, vol. E89-B, no. 2, pp. 509–517, Feb. 2006.

- [81] K. Ishihara, Y. Takatori and S. Kubota, "Multiuser detection using an array antenna for asynchronous single carrier systems," in *Proc. IEICE Technical Report*, vol. 106, no. 555, RCS2006-237, pp. 5-8, Feb. 2007.
- [82] W. Bocquet and M. Nakamura, "Low complexity equalizer for multi-carrier CDMA signal without guard interval," in *Proc. International Symposium on Image and Video Communications over Fixed and Mobile Networks (ISIVC'04)*, pp. 125-129, July 2004.
- [83] W. Bocquet and Y. Tanaka, "Frequency domain channel equalization for Wireless OFDM system," in *Proc. IEICE Technical Report*, vol. 103, no. 254, RCS2003-125, pp. 47-51, Aug. 2003.

Publications

Journal papers

- [1] W. Bocquet, K. Hayashi, and H. Sakai, "Systemtic design of single carrier overlap frequency domain equalization," *Journal of Systems Science and Complexity*, (In press).
- [2] W. Bocquet, K. Hayashi, and H. Sakai, "On the power distribution for MIMO coded MC-CDMA systems with two dimensional spreading and its application to turbo code scheme," *Wireless Communications and Mobile Computing, Interscience Wiley Publications*, (Conditional acceptance).
- [3] W. Bocquet, K. Hayashi, and H. Sakai, "Power distribution methods for MIMO-OFDM systems and field experimentations," *Wireless Communications and Mobile Computing, Interscience Wiley Publications*, (Conditional acceptance). In press
- [4] W. Bocquet, K. Hayashi, and H. Sakai, "A novel power distribution scheme with channel ordering and adaptive modulation for wireless multi-carrier systems," *IEICE Trans. Commun.*, (In press).

International conference papers

- [5] A. Nakano and W. Bocquet, "Dynamic resource assignement for MC-CDMA with prioritization and QoS constraint," in *Proc. IEEE Asia Pacific Conference on Communications* (APCC 2008), Tokyo, Japan, Oct. 2008.
- [6] W. Bocquet and P. Coupe, "Channel next generation mobile communication system: a systematic user centric approach," in *Proc. International Sympo-*

- sium on Wireless Personal Multimedia Communications* (WPMC 2008), Lapland, Finland, Sept. 2008 (invited paper).
- [7] W. Bocquet and V. Braquet, "Channel estimation for SC-FDE systems based on the RHKS decomposition," in *Proc. IEEE VTS Asia Pacific Wireless Communications Symposium* (APWCS 2008), Sendai, Japan, Aug. 2008.
 - [8] W. Bocquet, K. Hayashi, and H. Sakai, "On the systematic block size adaptation for coded single carrier overlap frequency domain equalization systems," in *Proc. IEEE International Symposium on Image and Video Communications over Fixed and Mobile Networks* (ISIVC 2008), Bilbao, Spain, July 2008 (invited paper).
 - [9] W. Bocquet, K. Hayashi, and H. Sakai, "Combined frequency and spatial domains power distribution for MIMO-OFDM transmission," in *Proc. IEEE International Symposium on Personal, Indoor and Mobile Radio Communications* (PIMRC 2007), pp. 1-5, Athens, Greece, Sept. 2007.
 - [10] W. Bocquet, K. Hayashi, and H. Sakai, "Parallel interference canceller with adaptive MMSE equalization for MIMO-OFDM transmission," in *Proc. International OFDM Workshop 2007*, pp. 261-265, Hamburg, Germany, Aug. 2007.
 - [11] W. Bocquet, K. Hayashi, and H. Sakai, "On the SIC detection with adaptive MMSE equalization for MIMO-OFDM transmissions," in *Proc. IEEE VTS Asia Pacific Wireless Communications Symposium* (APWCS 2007), Hsinchu, Taiwan, Aug. 2007.
 - [12] W. Bocquet, K. Hayashi, and H. Sakai, "On the block size design for single carrier overlap frequency domain equalization," in *Proc. IEEE VTS Asia Pacific Wireless Communications Symposium* (APWCS 2007), Hsinchu, Taiwan, Aug. 2007.
 - [13] W. Bocquet, K. Hayashi, and H. Sakai, "Power allocation scheme for MIMO MC-CDMA with two dimensional spreading," in *Proc. IEEE Vehicular Tech-*

- nology Conference Spring (VTC-Spring 2007), pp. 3145-3149, Dublin, Ireland, Apr. 2007.
- [14] W. Bocquet, K. Hayashi, and H. Sakai, "Frequency domain power adaptation scheme for coded OFDM transmissions," in *Proc. European Wireless 2007*, Paris, France, Apr. 2007.
- [15] W. Bocquet, K. Hayashi, and H. Sakai, "A power allocation scheme for M-QAM modulated MIMO-OFDM systems," in *Proc. International Symposium on Wireless Personal Multimedia Communications* (WPMC 2006), pp. 322-325, San Diego, USA, Sept. 2006.
- [16] W. Bocquet, K. Hayashi, and H. Sakai, "Frequency domain power adaptation scheme for multi-carrier systems," in *Proc. IEEE International Symposium on Personal, Indoor and Mobile Radio Communications* (PIMRC2006), pp. 1-5, Helsinki, Finland, Sept. 2006.
- [17] W. Bocquet, K. Hayashi, and H. Sakai, "A power allocation scheme for coded MIMO multi-carrier systems," in *Proc. International OFDM Workshop 2006*, pp. 96-100, Hamburg, Germany, Aug. 2006.
- [18] W. Bocquet, K. Hayashi, and H. Sakai, "A combined phase compensation and power distribution for multi-carrier modulation," in *Proc. International OFDM Workshop 2006*, pp. 283-287, Hamburg, Germany, Aug. 2006.
- [19] A. Ben Hadj Alaya, A. Ben Jemaa, E. Villebrun, P. Cordier, W. Bocquet, and E. Moulines, "La radio cognitive," *Journes Scientifiques du CNFRS 2006 - Vers les Radiocommunications Reconfigurables et Cognitives*, Paris, France, Mar. 2006 (in French).
- [20] W. Bocquet, K. Hayashi, and H. Sakai, "A power allocation scheme for MIMO-OFDM systems," in *Proc. IEEE-EURASIP International Symposium on Control, Communications, and Signal Processing* (ISCCSP 2006), Marrakech, Morocco, Mar. 2006 (Invited Paper).

- [21] Y. Gong, W. Bocquet, P. Coupe, and R. Lenglet, "Implementation of an integration of rerouting-based micro-mobility and traffic engineering in wireless access networks," in *Proc. IEICE Technical Report*, vol. 108, no. 31, NS2008-6, pp. 31-36, Hokaido, Japan, May 2008.
- [22] V. Braquet and W. Bocquet, "On the channel estimation for OFDM systems based on pilot block transmission," in *Proc. IEICE Technical Report*, vol. 107, no. 518, RCS2007-224, pp. 229-232, YRP, Japan, Mar. 2008.
- [23] W. Bocquet, K. Hayashi, and H. Sakai, "A simple power distribution scheme for MC-CDMA with two dimensional spreading," in *Proc. IEICE Technical Report*, vol. 106, no. 476, RCS2006-206, pp. 67-72, Okinawa, Japan, Jan. 2007.